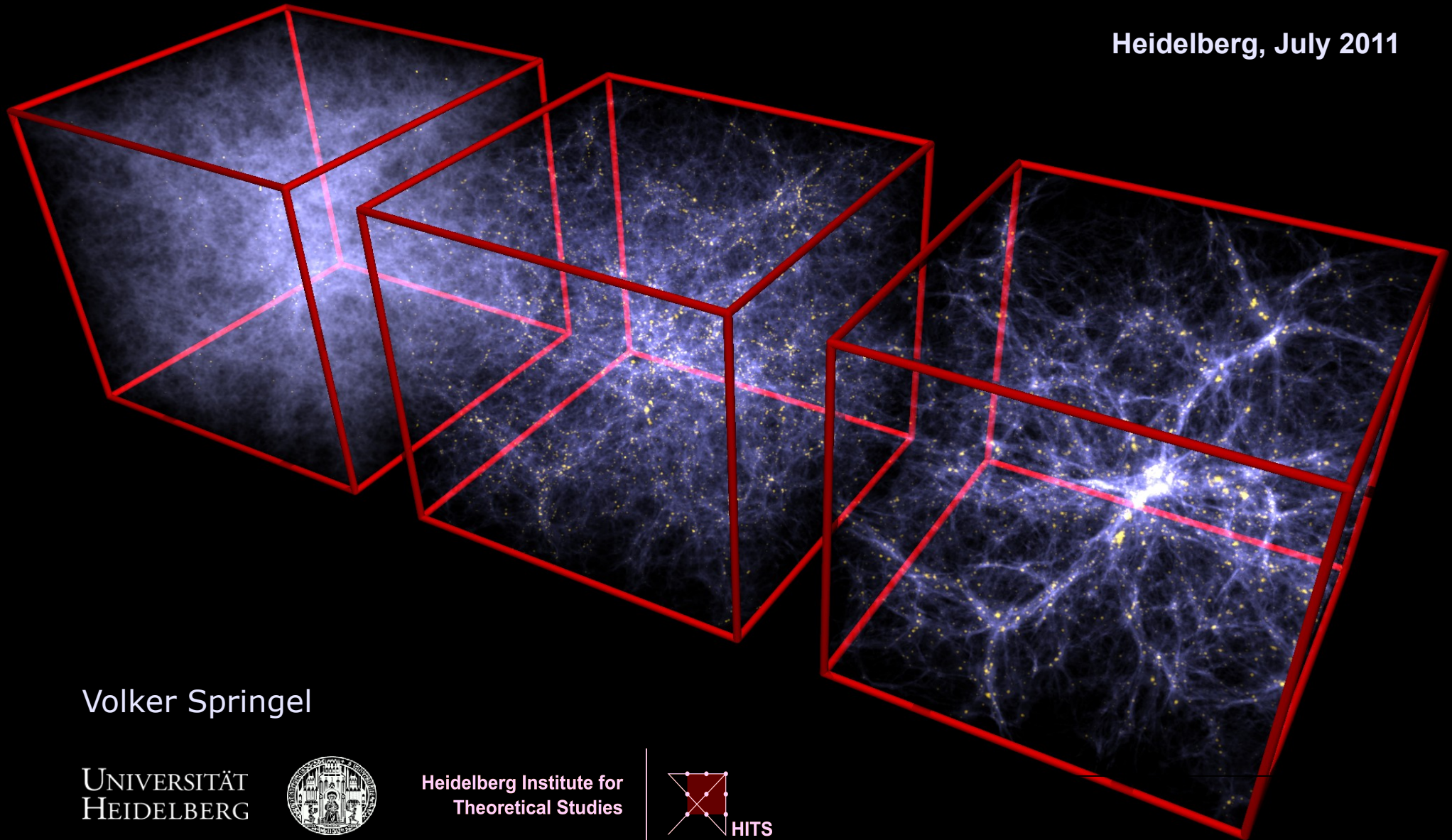


International School on Astro Particle Physics (ISAPP)

Dark Matter, Cosmology & Structure Formation

Heidelberg, July 2011



Volker Springel

UNIVERSITÄT
HEIDELBERG



Heidelberg Institute for
Theoretical Studies



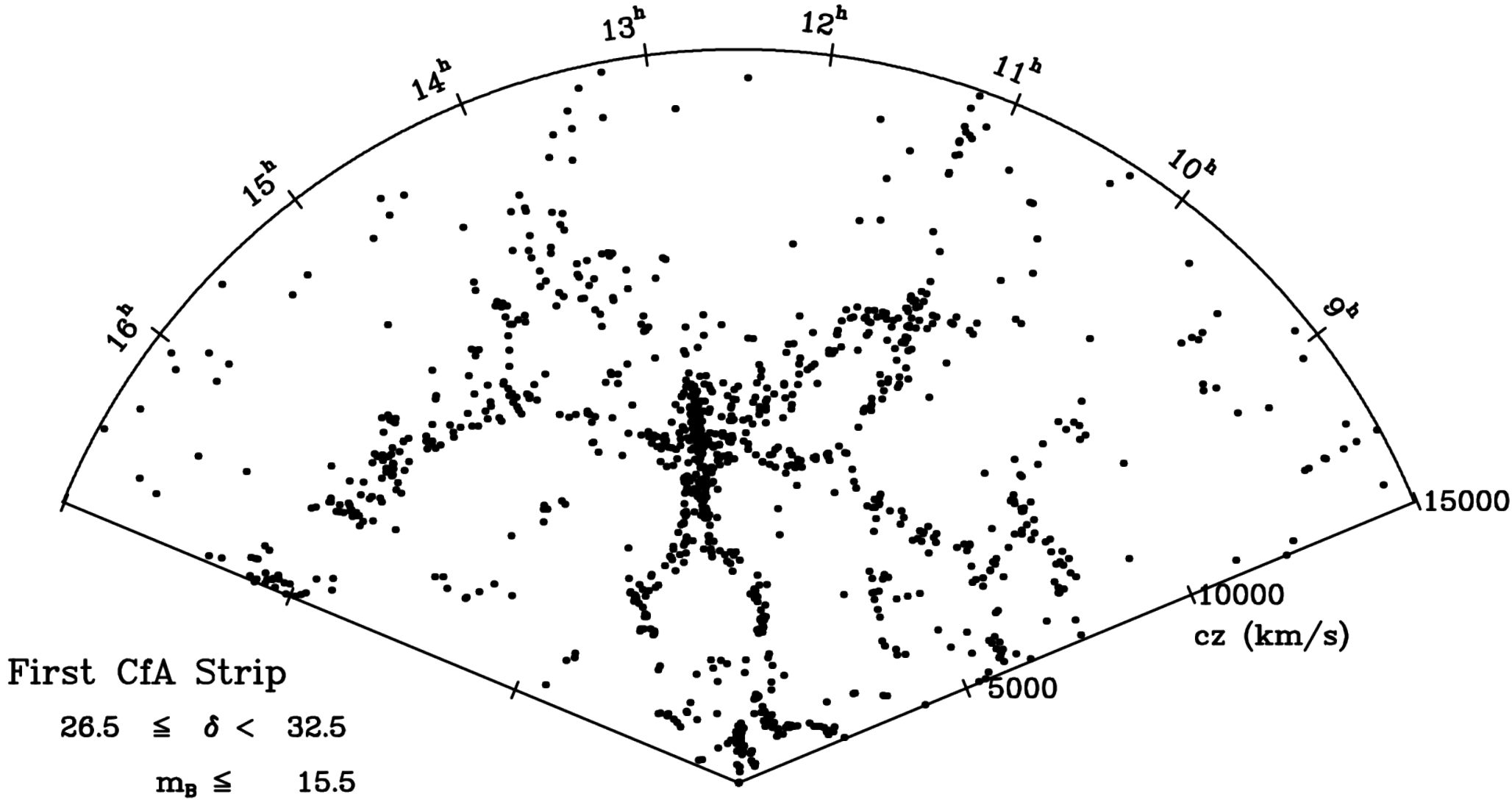
Contents of Lecture

Volker Springel

- ▶ **Basic observations and concepts related to cosmic large-scale structure**
- ▶ **Top-hat collapse and Press-Schechter formalism**
- ▶ **Isothermal spheres, NFW-profile**
- ▶ **Modelling the large-scale galaxy distribution**
- ▶ **Dark matter small-scale structure**
- ▶ **Implications for dark matter annihilation**
- ▶ **Cosmological N-body techniques**

The first slice in the CfA redshift survey

1100 galaxies in a wedge,
6 degrees wide and 110 degrees long



de Lapparent, Geller, Huchra (1986)
Smithsonian Astronomical Observatory

Sloan Digital Sky Survey (SDSS) telescope at Apache Point, New Mexico

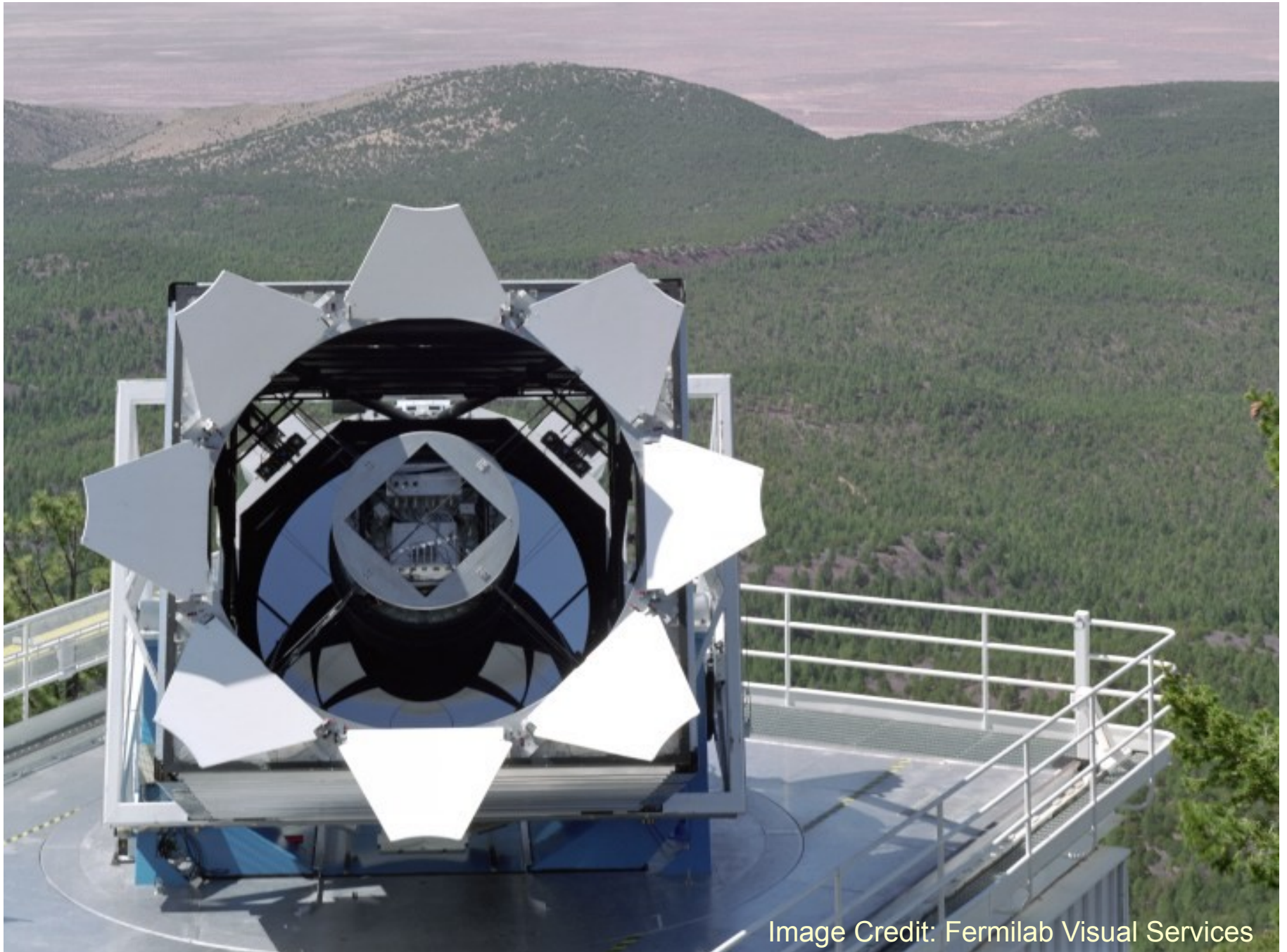
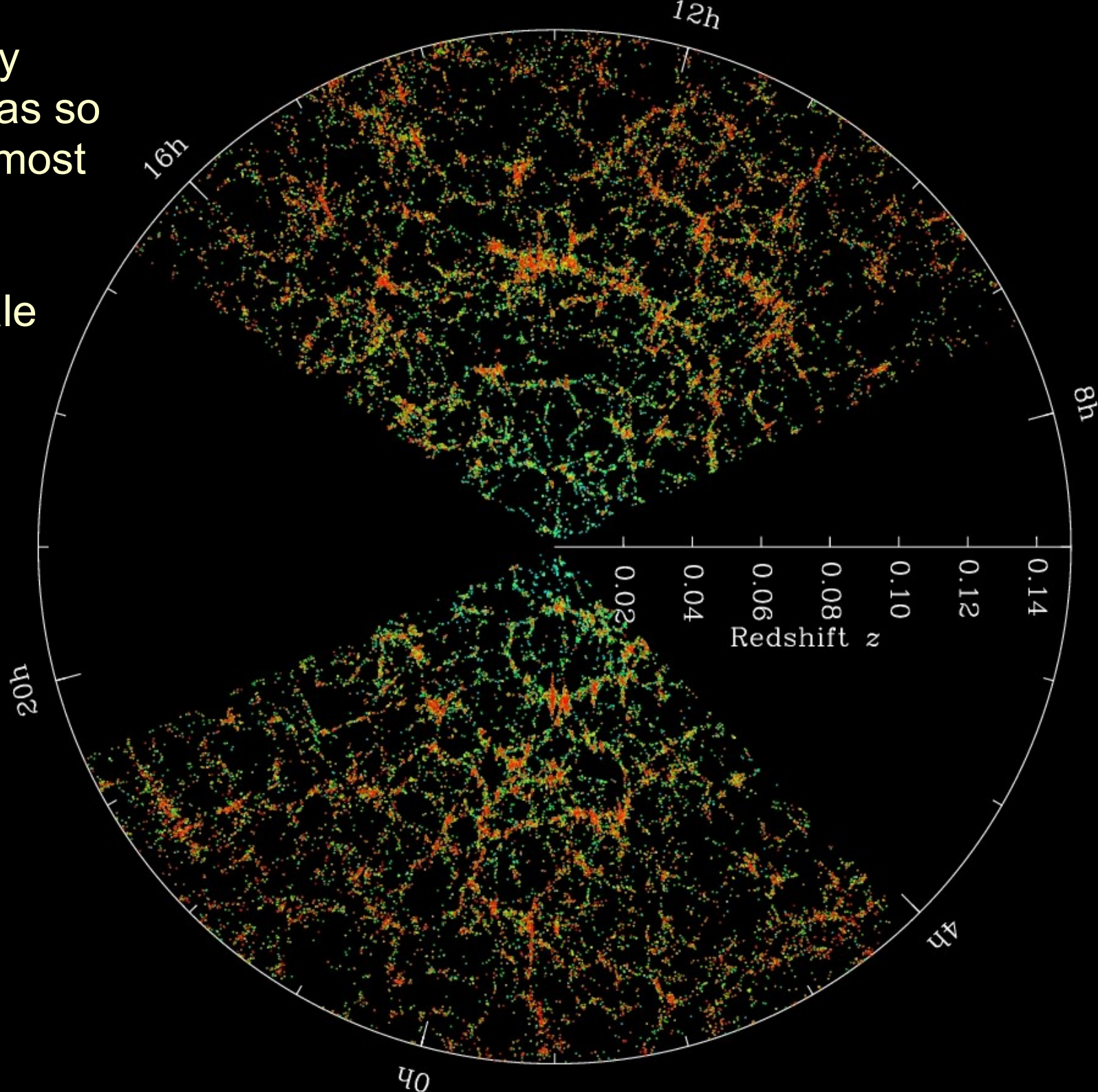


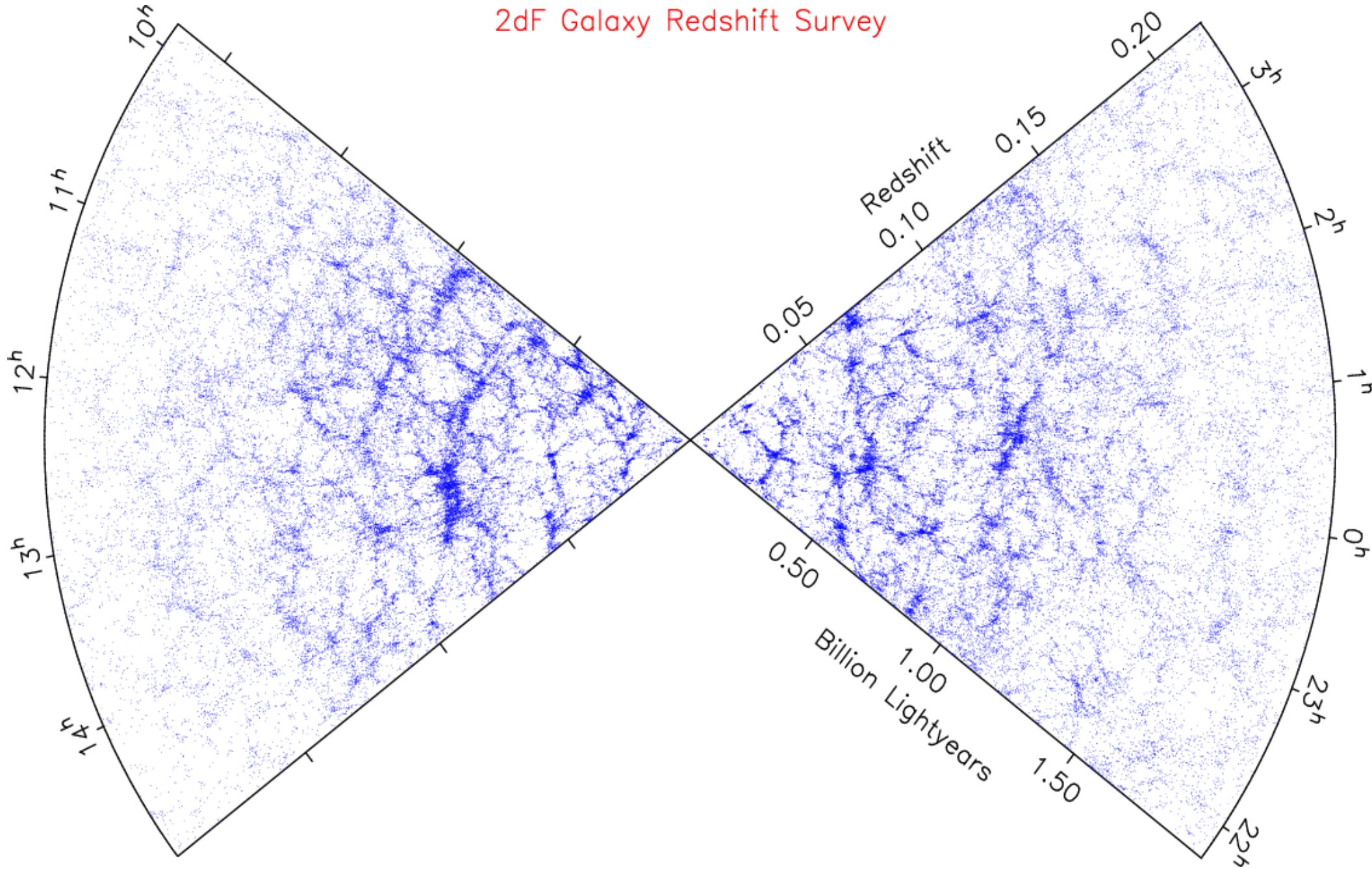
Image Credit: Fermilab Visual Services

The SDSS galaxy redshift survey has so far provided the most comprehensive observations of cosmic large-scale structure



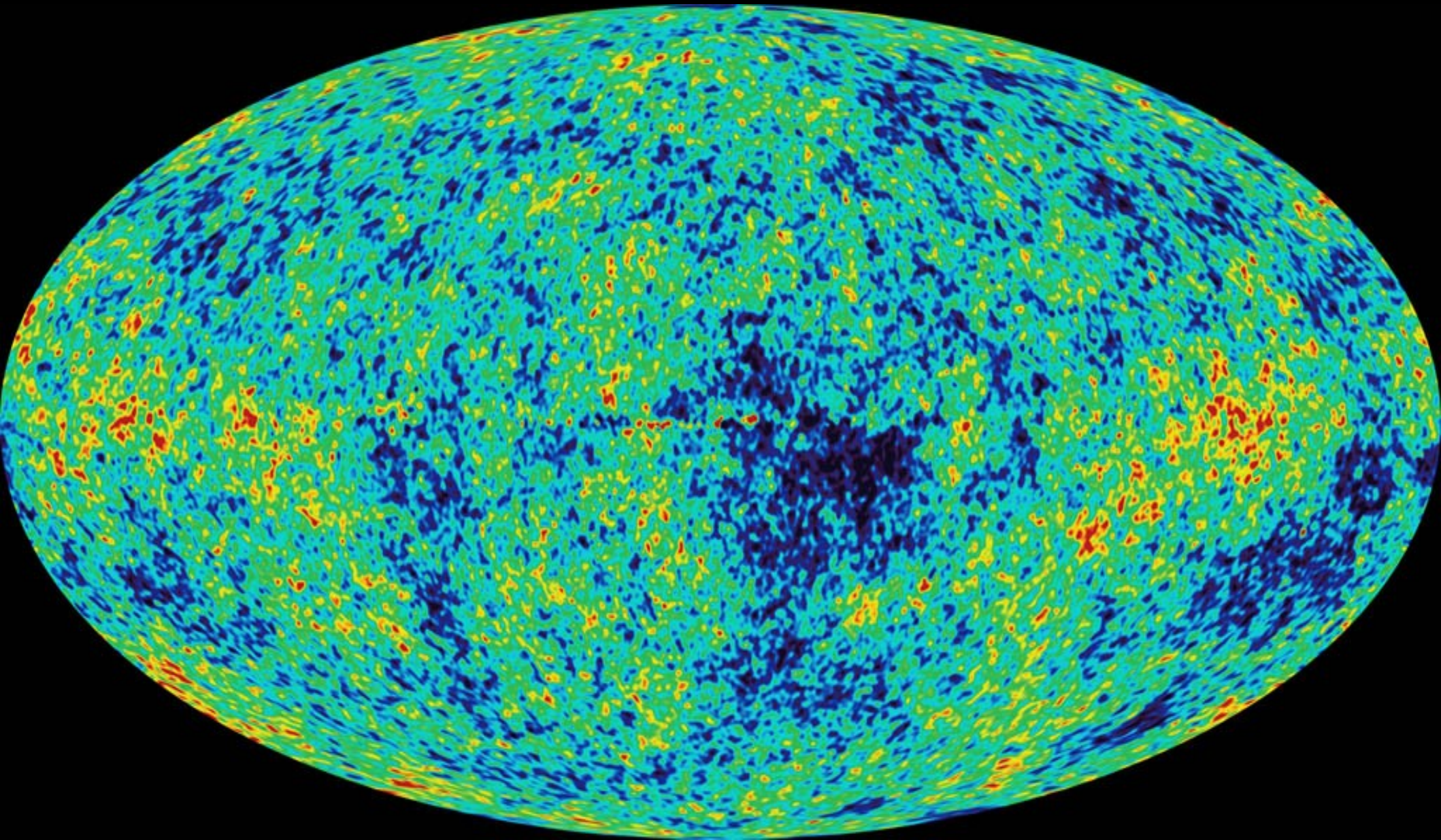
Current galaxy redshift surveys map the Universe with several hundred thousand galaxies

2dF Galaxy Redshift Survey



The initial conditions for cosmic structure formation are directly observable

THE MICROWAVE SKY



WMAP Science Team (2003, 2006, 2008, 2010)

The most important cosmological parameters are well constrained

WMAP-5 CONSTRAINTS, INCLUDING TYPE-IA AND BAO DATA

Minimal, 6-parameter Λ CDM model is a great fit

$$\Omega_c = 0.233 \pm 0.013$$

$$\Omega_b = 0.0462 \pm 0.0015$$

$$\sigma_8 = 0.817 \pm 0.026$$

$$n_s = 0.960^{+0.014}_{-0.013}$$

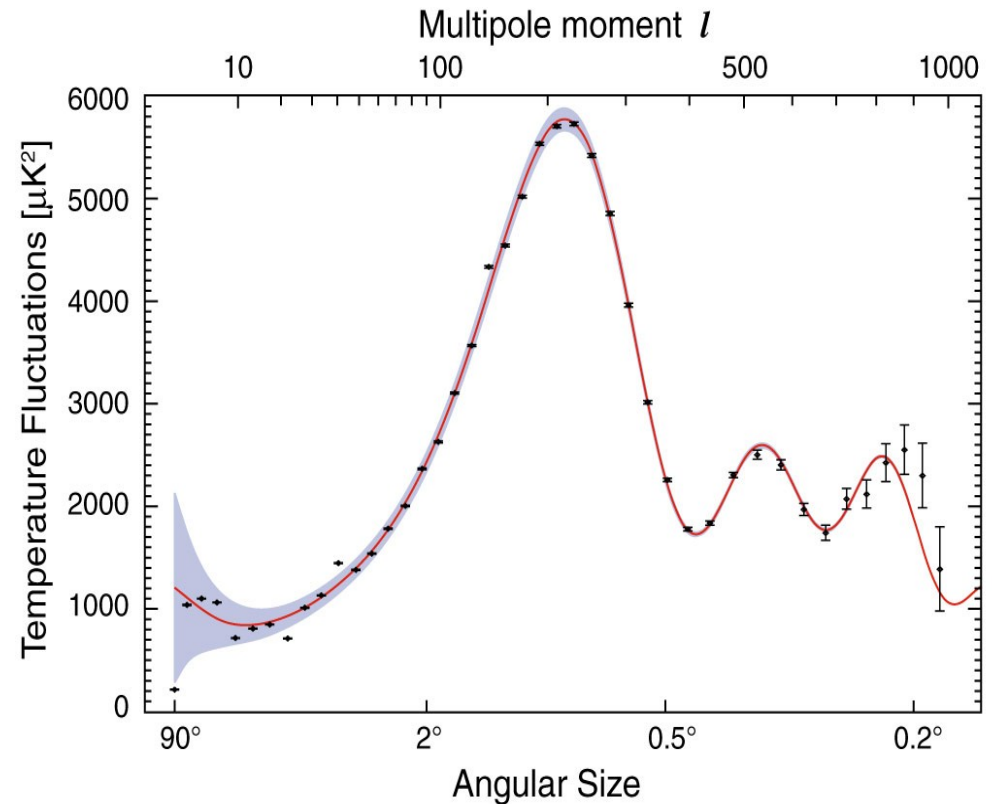
$$H_0 = 70.1 \pm 1.3 \text{ km s}^{-1} \text{ Mpc}^{-1}$$

$$\tau = 0.084 \pm 0.016$$

$$\Omega_\Lambda = 0.721 \pm 0.015$$

$$t_0 = 13.73 \pm 0.12 \text{ Gyr}$$

$$z_{\text{reion}} = 10.8 \pm 1.4$$



Constraints on dark energy equation of state:

$$-0.11 < 1 + w < 0.14$$

(95% CF,
assuming a
constant w)

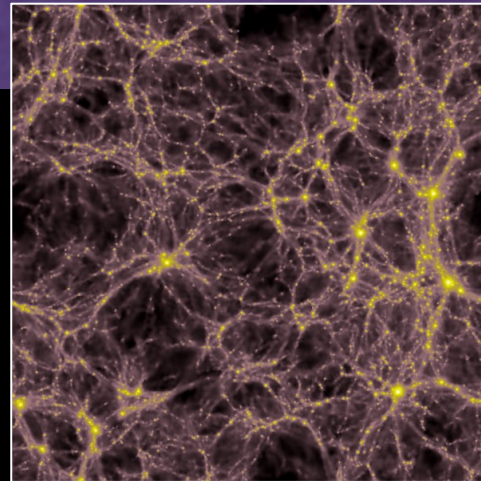
$$-0.0175 < \Omega_k < 0.0085$$

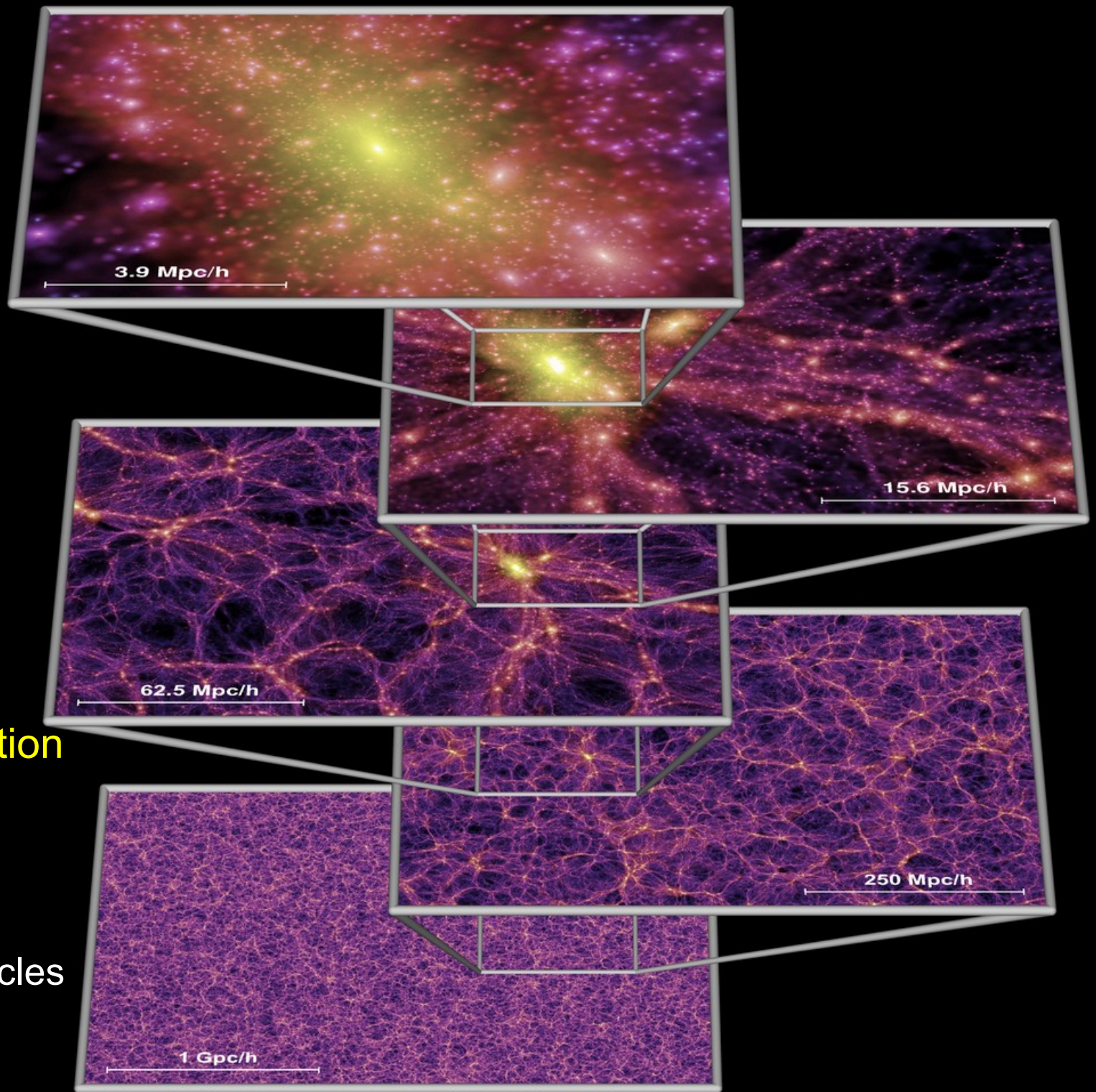
Komatsu et al. (2008)

50 Mpc/h

$z = 20$

~ 13 billion
years





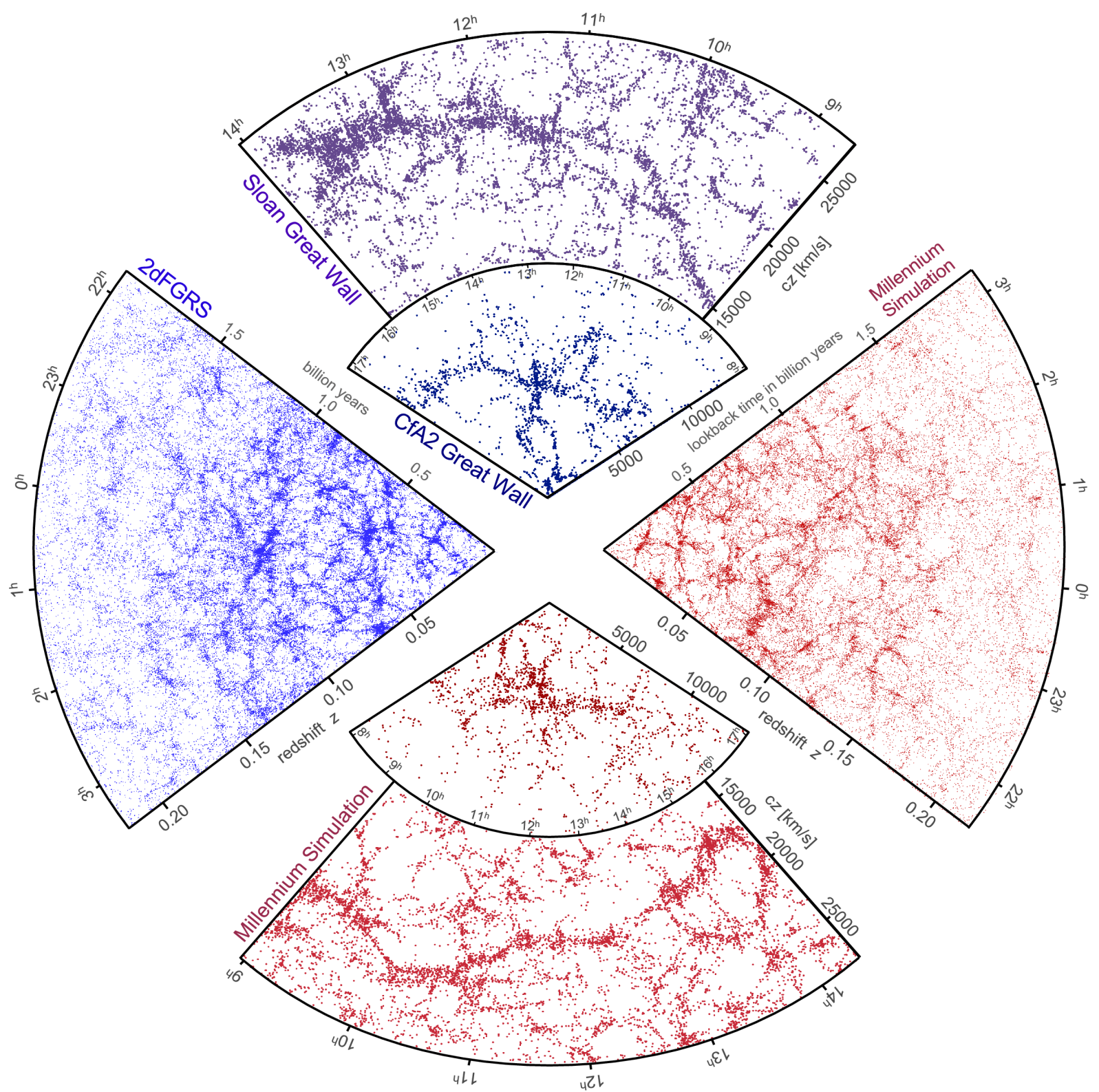
'Millennium' simulation
Springel et al. (2005)

Λ CDM

10,077,696,000 particles
 $m=8.6 \times 10^8 M_{\odot}/h$

Simulated and observed large-scale structure in the galaxy distribution

**MOCK PIE
DIAGRAMS
COMPARED TO
SDSS, 2DFGRS,
AND CFA-2**



Commonly employed mathematical measures of clustering

THE TWO-POINT FUNCTION AND THE POWER SPECTRUM

The **two-point function** gives the excess probability relative to a Poisson distribution to find another point at distance r around a given point:

$$\xi(r) = 1 + \frac{\langle N(r + dr) \rangle}{N_{\text{Poisson}}(r + dr)}$$

With many points, can also define a density field, and discuss the density contrast field:

$$\delta(\mathbf{r}) = \frac{\rho(\mathbf{r}) - \bar{\rho}}{\bar{\rho}} \quad \longrightarrow \quad \xi(r) = \langle \delta(\mathbf{x})\delta(\mathbf{x} - \mathbf{r}) \rangle$$

The clustering can also be conveniently analyzed in Fourier space.

$$\delta(\mathbf{k}) = \frac{1}{(2\pi)^3} \int \delta(\mathbf{x}) e^{-i\mathbf{k}\mathbf{x}} d\mathbf{x}$$

Power spectrum:

$$P(k) = \langle |\delta(\mathbf{k})|^2 \rangle$$

Auto-correlation function and power spectrum contain the same information:

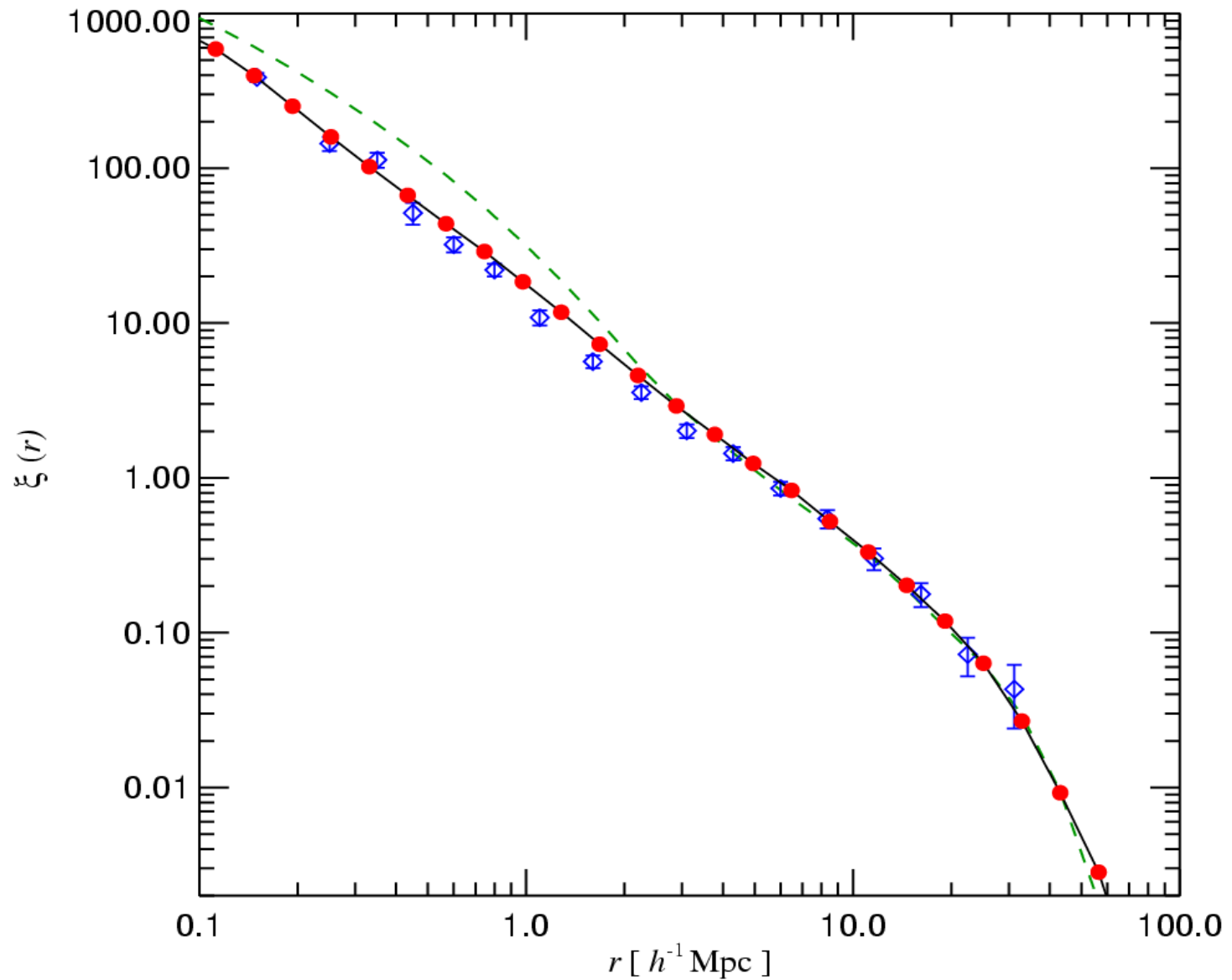
$$\xi(r) = \int P(k) \frac{\sin(kr)}{kr} d^3k$$

A Gaussian random field is fully described by the power spectrum.

Important cosmological question: Did the universe really start from a Gaussian field, or did higher-order correlations exist?

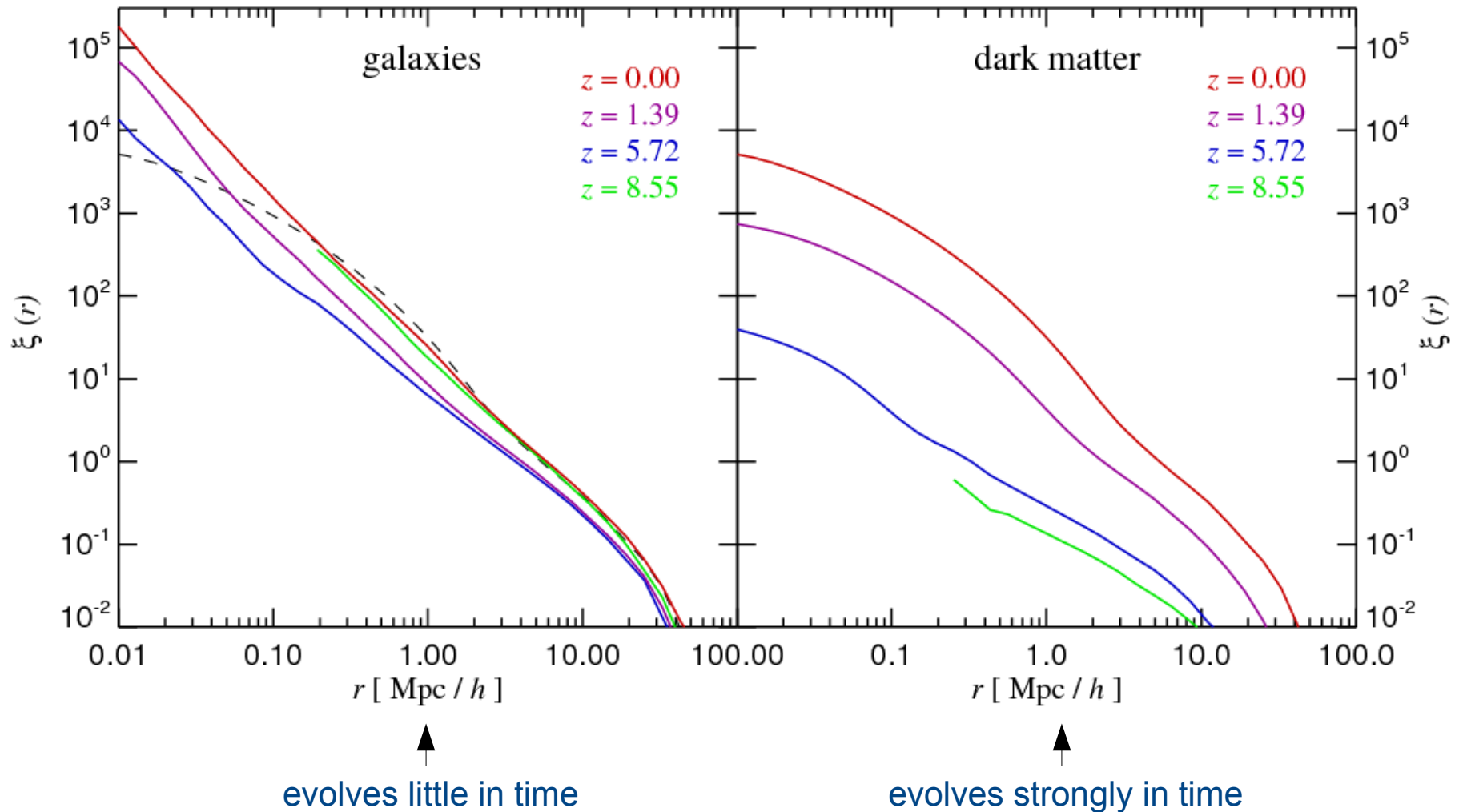
The two-point correlation function of galaxies is a very good power law

GALAXY TWO-POINT FUNCTION COMPARED WITH THE 2dFGRS



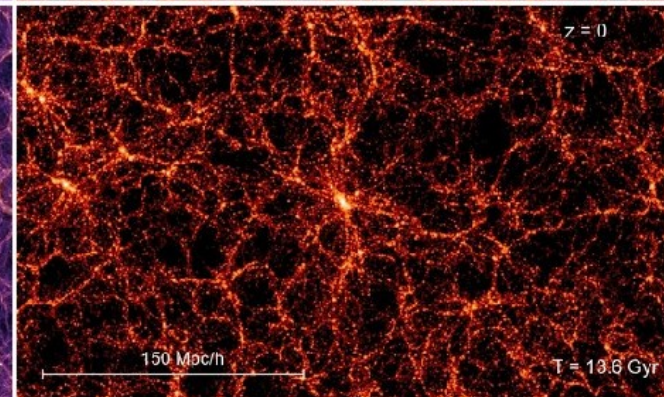
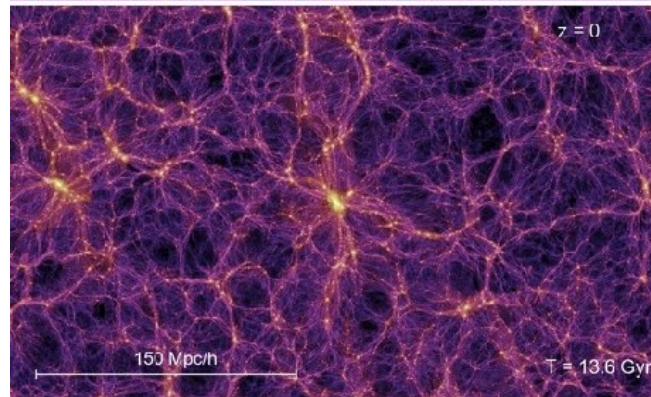
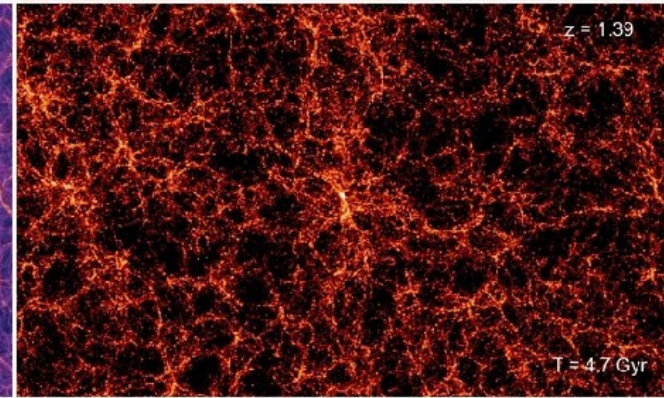
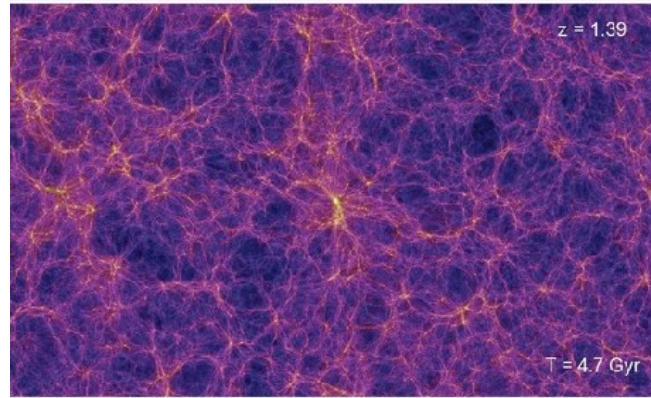
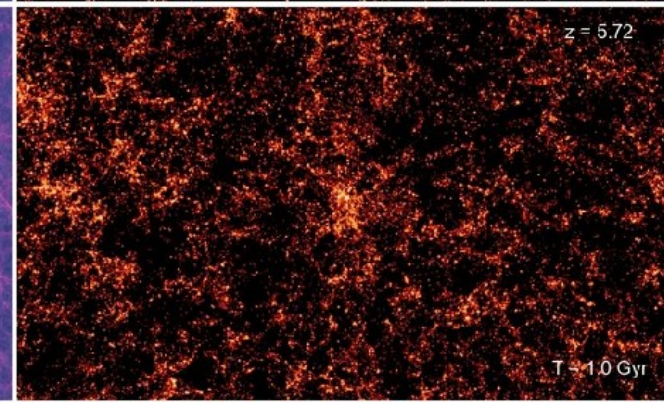
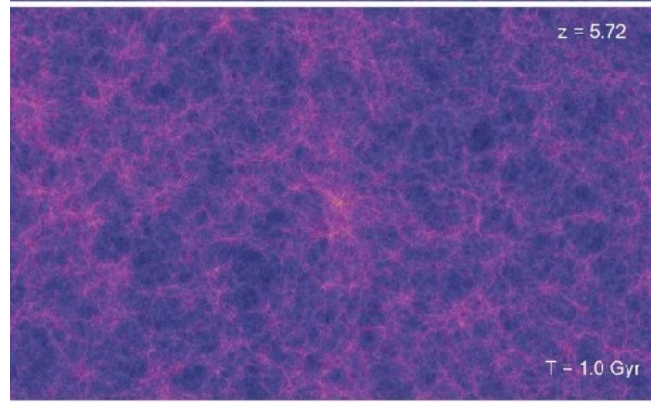
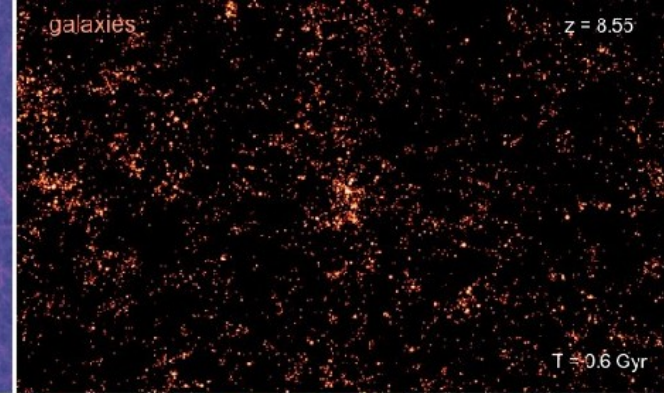
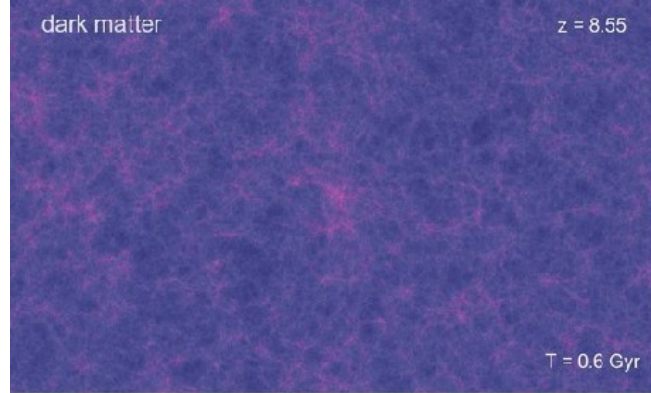
The galaxy distribution is in general biased with respect to the mass distribution

GALAXY AND MASS CLUSTERING AT DIFFERENT EPOCHS



The large-scale clustering pattern of halos and galaxies is already imprinted on the initial conditions

TIME EVOLUTION OF THE MATTER AND GALAXY DISTRIBUTION



If the initial fluctuations are a Gaussian random field, we only need to know the power spectrum and the cosmological parameters to describe the ICs

DIFFERENT PROBES OF THE MASS POWER SPECTRUM

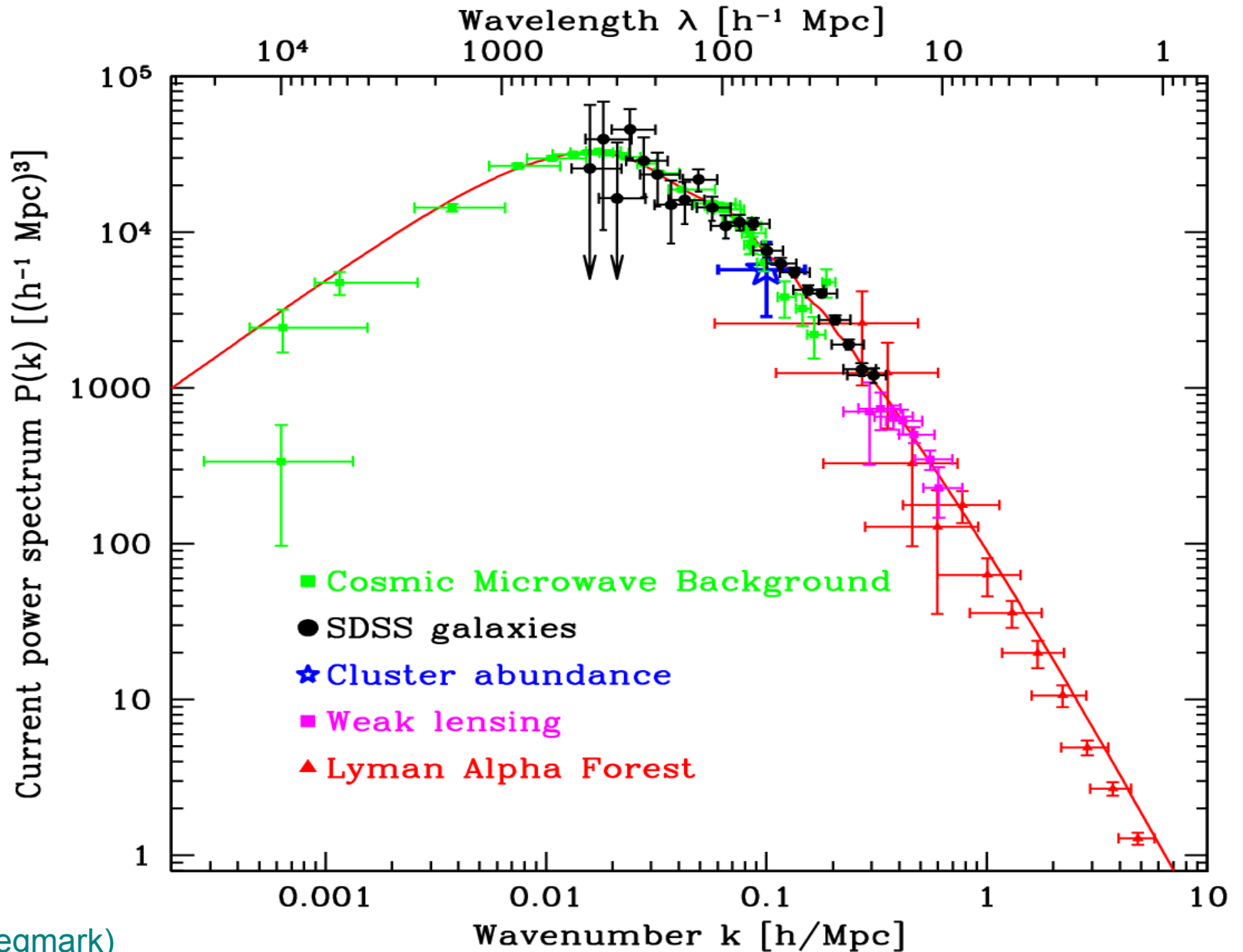
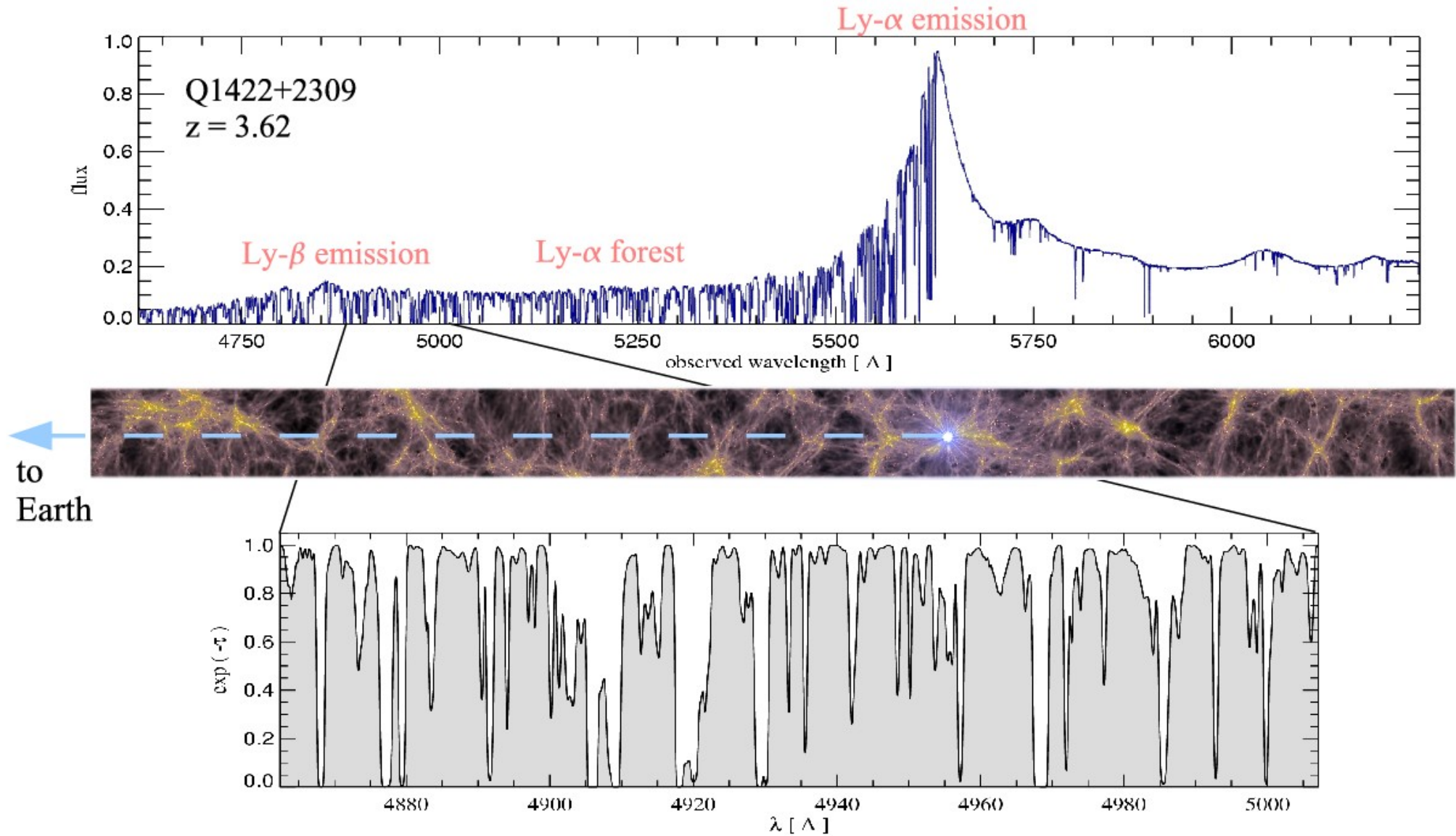


(figure from Max Tegmark)

The Ly- α forest traces the distribution of neutral hydrogen in the cosmic web

ILLUSTRATION OF A QUASAR ABSORPTION SPECTRUM

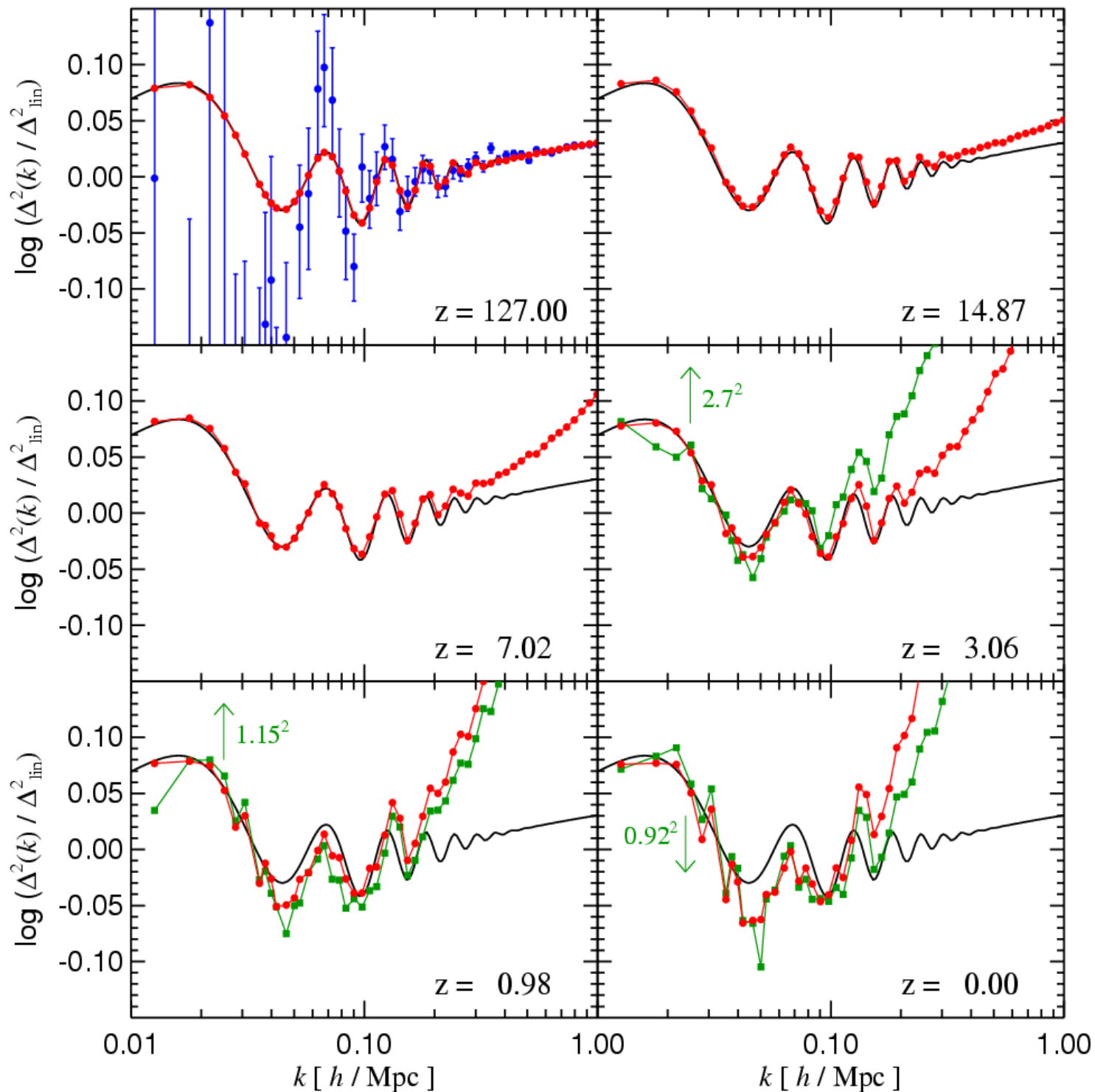


hydrogen spectral series: $\frac{1}{\lambda} = R \left(\frac{1}{n'^2} - \frac{1}{n^2} \right)$

Lyman series: n=1
n'=2(α) $\lambda=122$ nm

The baryonic wiggles remain visible in the galaxy distribution down to low redshift and may serve as a "standard ruler" to constrain dark energy

DARK MATTER AND GALAXY POWER SPECTRA FROM THE MILLENNIUM SIMULATION IN THE REGION OF THE WIGGLES



Higher-order probes for large-scale structure

THE SEARCH FOR DIFFERENCES FROM THE GAUSSIAN PREDICTION

3-point correlation functions, bi-spectrum

Void probability distribution function

Minkowski functionals and other morphological measures

Geometric measures for filamentary, planarity, etc.

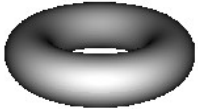
Percolation statistics

Fractal dimension estimators

Genus statistics

Example: Topology of large-scale with the genus statistics

definition of the genus: $G = \text{number of holes} - \text{number of isolated regions}$

torus  $G = 0$

calculation via the
Gauss-Bonnet theorem:

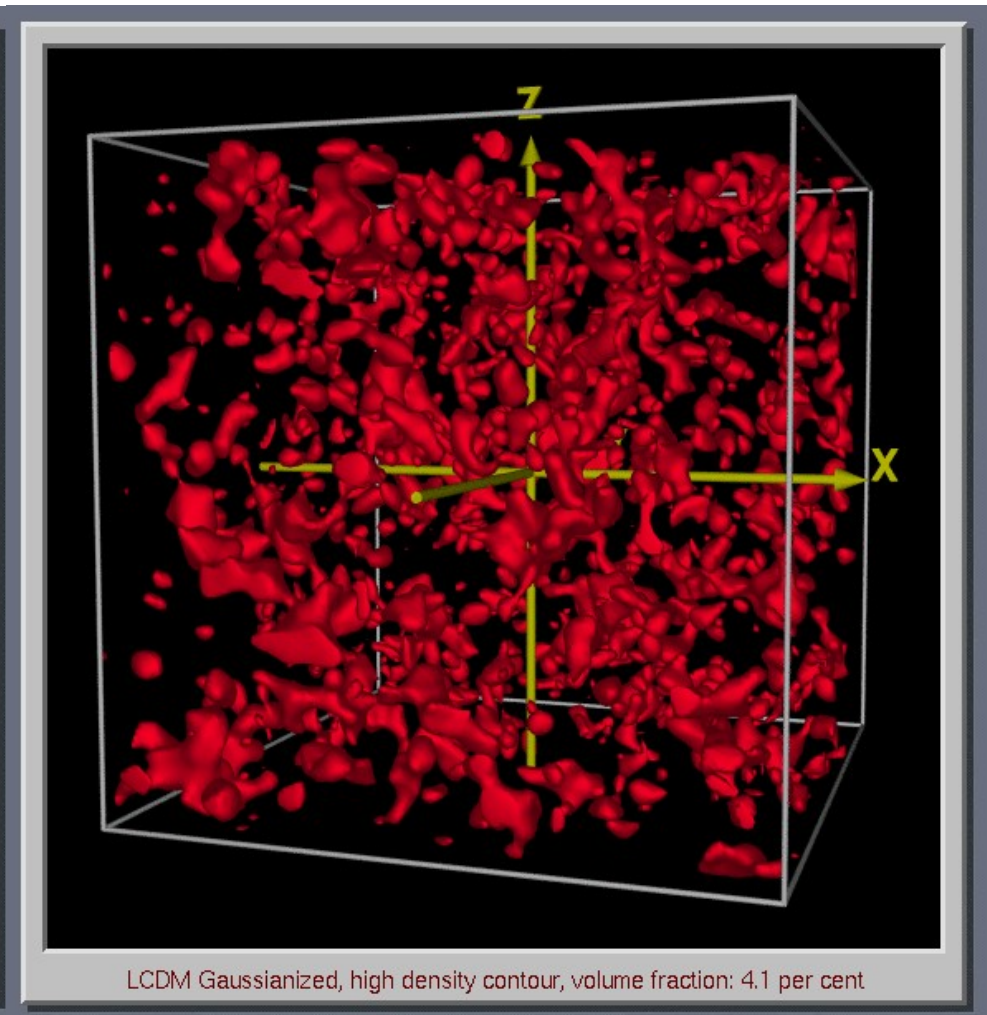
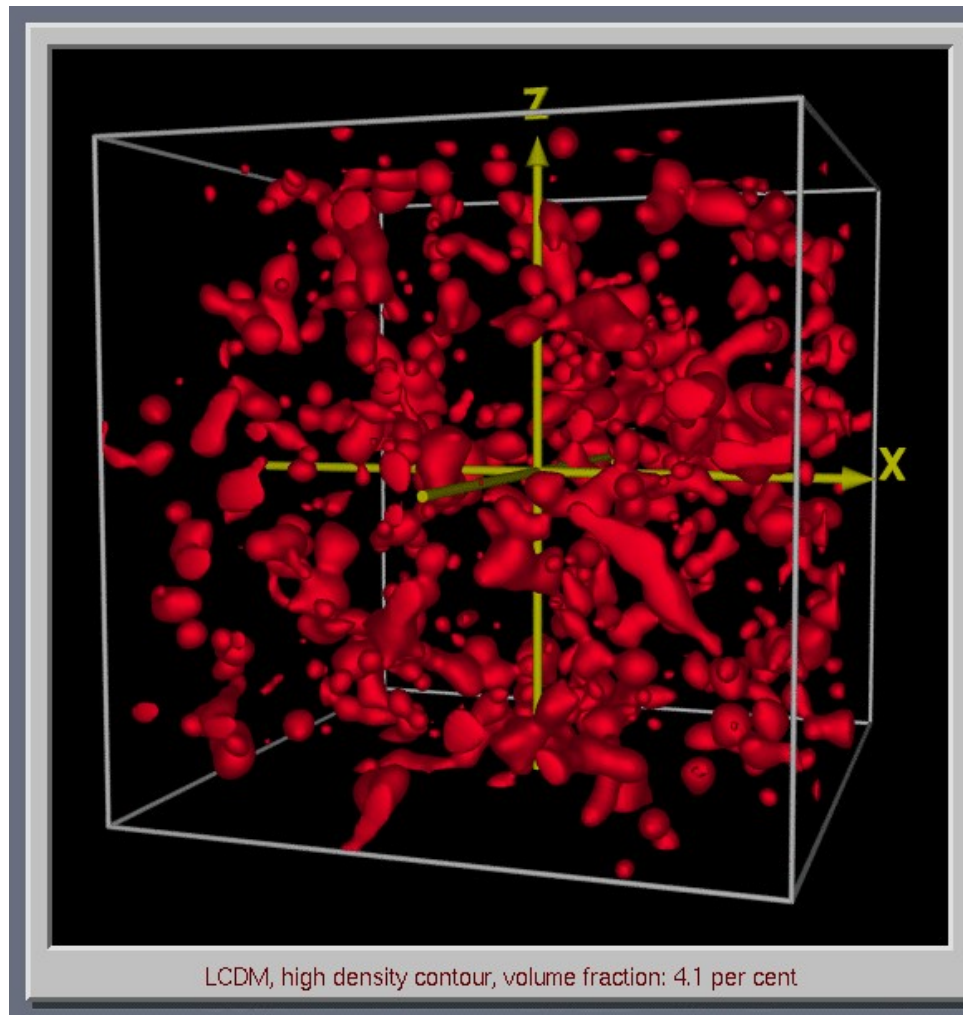
$$G = -\frac{1}{4\pi} \int \kappa dA \quad \kappa = \frac{1}{r_1 r_2}$$

The genus of isodensity contours can reveal non-Gaussian structure in density fields

Identical power spectrum but different genus

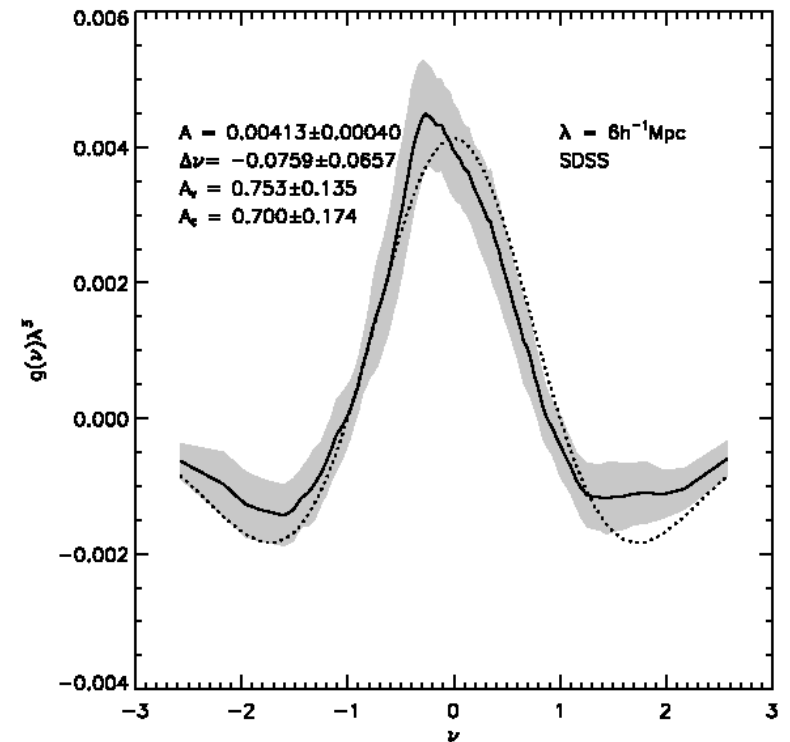
Isodensity surface in a slightly non-linear LCDM density field

Isodensity surface in a Gaussian density field with identical power spectrum

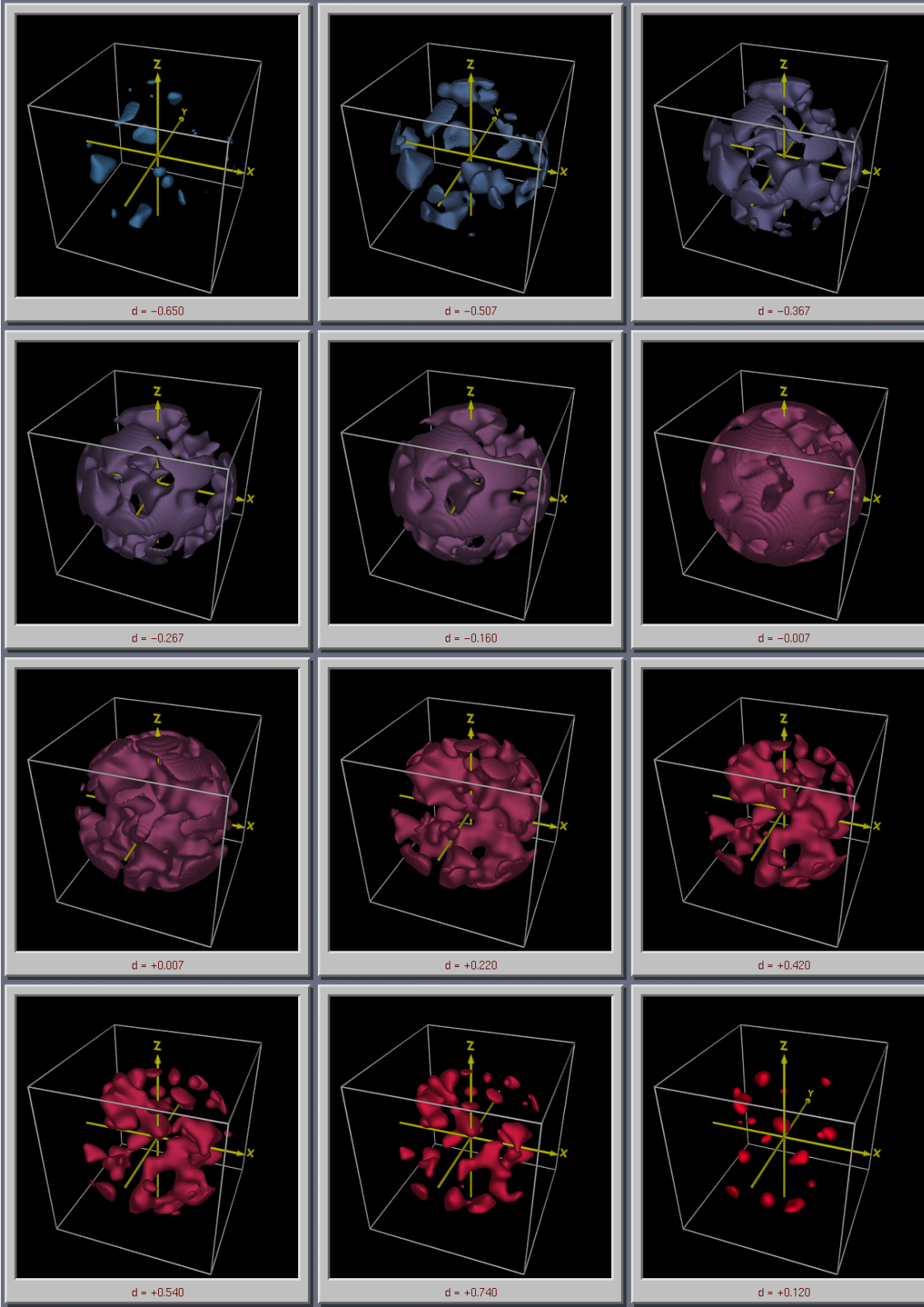


So far, genus results have generally been found to be consistent with the Gaussian expectation

Genus measurement for SDSS galaxies compared to expectation for a Gaussian field



← Isodensity contours for the 1.2-Jy galaxy redshift survey

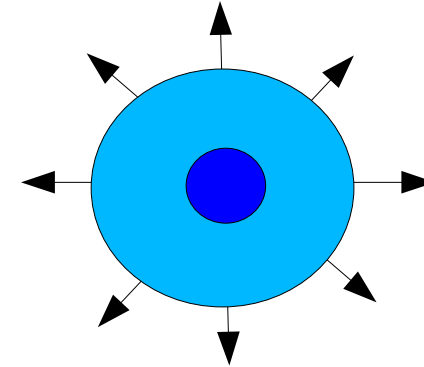


Non-linear models for
structure formation:
Top-hat collapse

The evolution of a spherical overdensity in an infinite background can be followed analytically

THE TOP-HAT COLLAPSE MODEL

Consider a spherically symmetric, slightly overdense perturbation in a critical-density universe



Evolution in linear theory:

$$\delta_{\text{lin}} = \delta_0 a(t) = \delta_0 \left(\frac{3H_0}{2} t \right)^{2/3}$$

$$a(t) = \left(\frac{3H_0}{2} t \right)^{2/3}$$

According to Birkhoff's theorem, the spherical perturbation evolves independently of the outside. Since it is slightly overdense, it behaves like a closed universe.

Cyclic evolution of a closed universe in parametric form:

$$r(\theta) = A(1 - \cos \theta)$$

$$t(\theta) = B(\theta - \sin \theta)$$

$$A^3 = GM B^2$$

At early times, the non-linear evolution of the top-hat can be matched to the solution of linear perturbation theory

MATCHING LINEAR AND NON-LINEAR THEORY

For small times/angles, a series expansion can be used to eliminate the parameter θ . This results in:

$$r \simeq \frac{A}{2} \left(\frac{6t}{B} \right)^{2/3} \left[1 - \frac{1}{20} \left(\frac{6t}{B} \right)^{2/3} \right]$$

This allows to read-off the first order growth rate of the density contrast in the top-hat evolution:

$$\delta(t) \simeq \frac{3}{20} \left(\frac{6t}{B} \right)^{2/3}$$

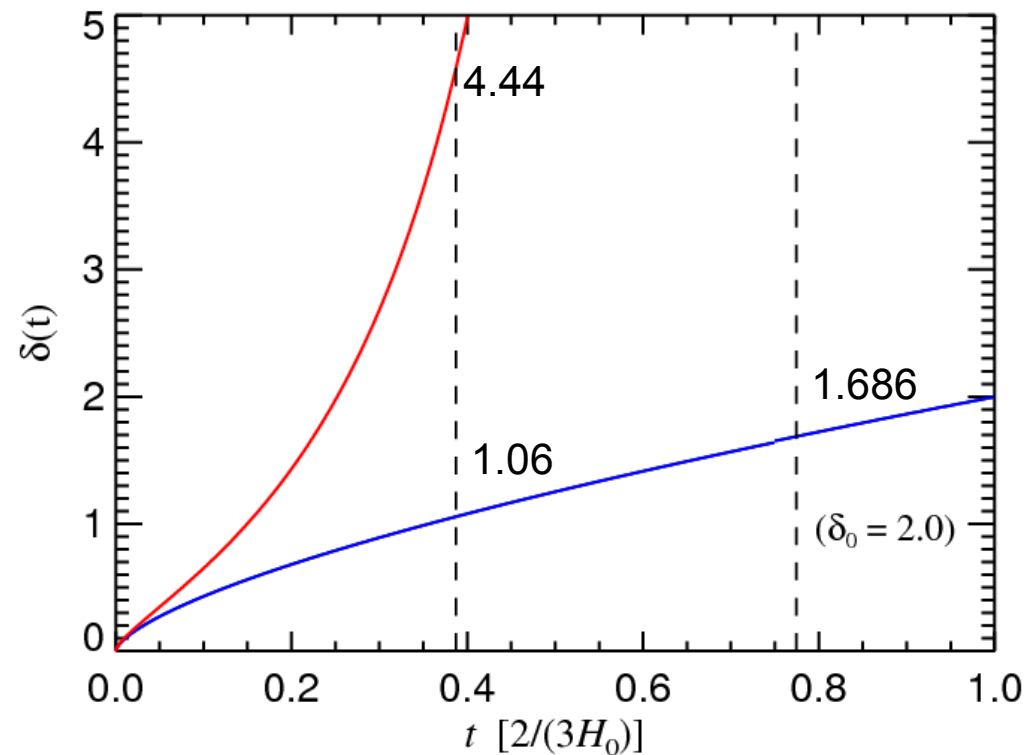
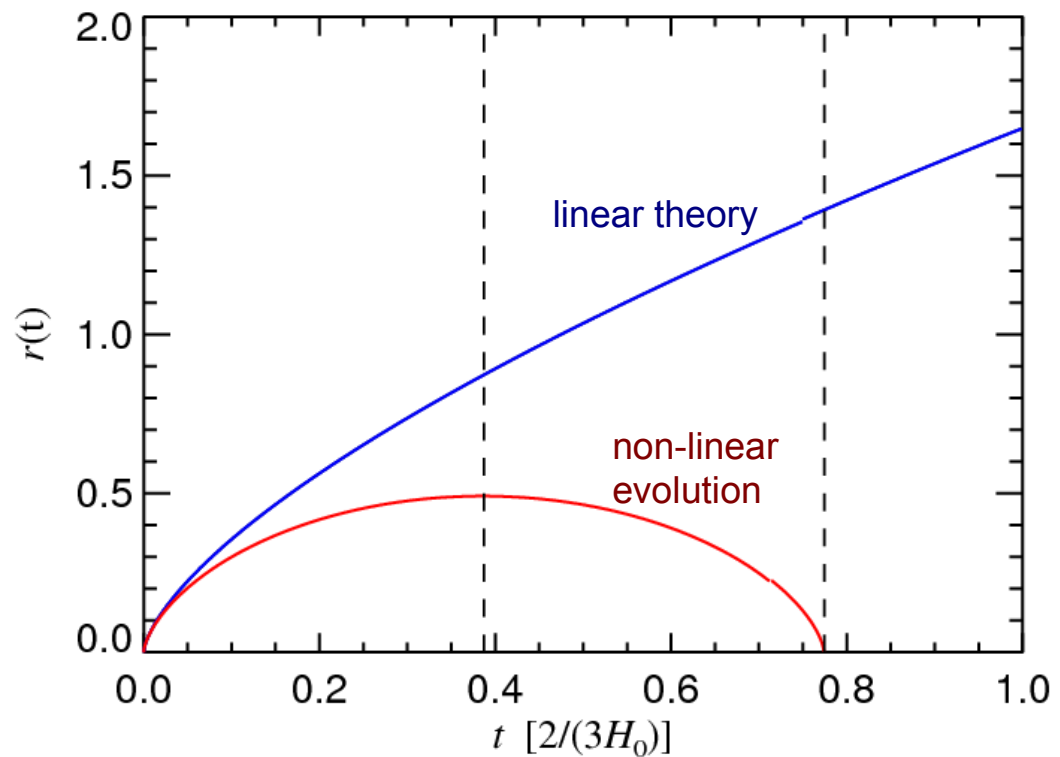
Comparison with the corresponding linear theory growth rate allows a determination of the constants B and A:

$$B = \frac{1}{2 H_0} \left(\frac{3}{5 \delta_0} \right)^{3/2}$$
$$A = \left(\frac{3 M}{4 \pi \rho_0} \right)^{1/3} \left(\frac{3}{10 \delta_0} \right) = \left(\frac{2 M G}{H_0^2} \right)^{1/3} \left(\frac{3}{10 \delta_0} \right)$$

We now know the exact non-linear time evolution of the top-hat perturbation.

When the density contrast reaches about unity in linear theory, the top-hat perturbation goes non-linear and collapses

TIME EVOLUTION OF THE TOP-HAT PERTURBATION IN LINEAR AND NON-LINEAR THEORY



$$\delta_{\text{lin}} = \delta_0 a(t) = \delta_0 \left(\frac{3H_0}{2} t \right)^{2/3}$$

$$\delta_{\text{tophat}}(\theta) = \frac{9}{2} \frac{(\theta - \sin \theta)^2}{(1 - \cos \theta)^3} - 1$$

turn-around

$$\theta = \pi$$

$$t_{\text{turn}} = \pi B = \frac{\pi}{2H_0} \left(\frac{3}{5\delta_0} \right)^{3/2}$$

$$\delta_{\text{lin}} = \frac{3}{5} \left(\frac{3\pi}{4} \right)^{2/3} \simeq 1.062$$

$$\delta_{\text{tophat}} = \left(\frac{3\pi}{4} \right)^2 - 1 \simeq 4.44$$

collapse

$$\theta = 2\pi$$

$$t_{\text{coll}} = 2\pi B = \frac{\pi}{H_0} \left(\frac{3}{5\delta_0} \right)^{3/2}$$

$$\delta_{\text{lin}} = \frac{3}{5} \left(\frac{3\pi}{2} \right)^{2/3} \simeq 1.686$$

virialization

$$\theta = 3\pi/2$$

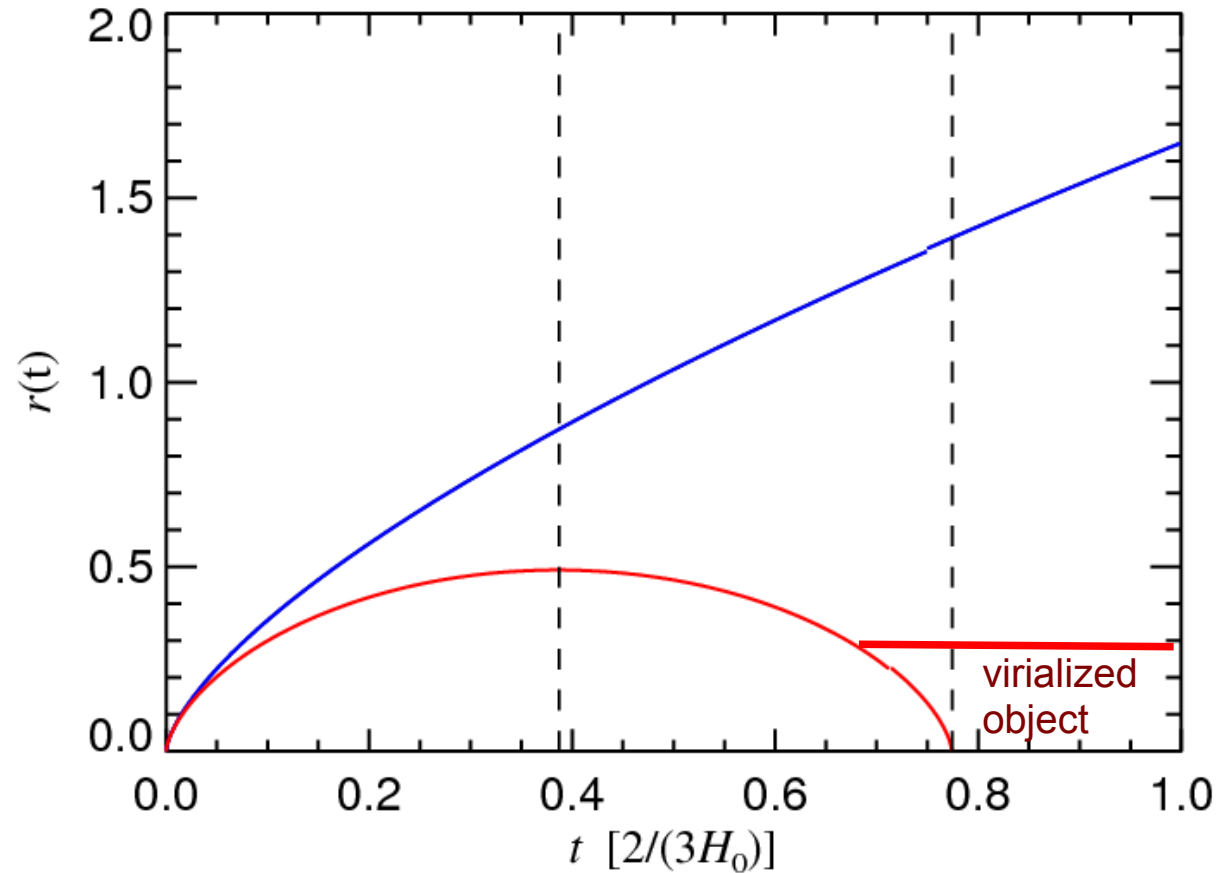
$$r_{\max} = 2A$$

$$E_{\text{tot}} = V_{\text{turn}}$$

At half the turnaround radius, the virial theorem is fulfilled:

$$r_{\text{vir}} = \frac{1}{2} r_{\max}$$

$$E_{\text{kin}} = E_{\text{tot}} - 2V_{\text{turn}} = -E_{\text{tot}}$$



Virial overdensity:

$$\left. \frac{\rho_{\text{vir}}}{\rho_{\text{back}}} \right|_{t_{\text{collapse}}} = \frac{1}{2} (6\pi)^2 \simeq 178$$

Press-Schechter formalism

Using the excursion set approach, a simple model for the abundance of halos of a given mass can be derived

THE PRESS-SCHECHTER FORMALISM

Filtering of the density fluctuations with a top-hat results in a field that is smoothed on a certain “mass scale”:

$$\delta_f(\mathbf{x}) = \int \delta(\mathbf{x}') W_R(|\mathbf{x} - \mathbf{x}'|) d\mathbf{x}'$$

$$\sigma_{M(R)}^2 = \int P(\mathbf{k}) |\hat{W}_R(\mathbf{k})|^2 d\mathbf{k}$$

$$M = \frac{4\pi}{3} \rho_0 R^3$$

$$\hat{W}_R(\mathbf{k}) = \frac{3j_1(kR)}{kR}$$

Press-Schechter's conjecture: The fraction of mass in objects larger than M is given by the probability that a point exceeds the critical linear density contrast for top-hat collapse.

$$\delta_c \equiv 1.686$$

$$F(> M) = \int_{\delta_c}^{\infty} \frac{1}{\sqrt{2\pi}\sigma} \exp\left(-\frac{\delta^2}{2\sigma^2}\right) d\delta$$

This can be rewritten as:

$$\nu \equiv \frac{\delta_c}{\sigma(M)}$$

$$\text{erf}(x) \equiv \frac{2}{\sqrt{\pi}} \int_0^x e^{-y^2} dy$$

$$F(> M) = \frac{1}{2} - \frac{1}{2} \text{erf}\left(\frac{\nu}{\sqrt{2}}\right)$$

Only half of the mass is accounted for – unless one puts in a fudge factor equal to 2...

In Press-Schechter, all mass is assumed to be bound to halos

THE PRESS-SCHECHTER FORMULA

The fraction of mass in objects larger than M is determined by $\sigma(M)$ alone:

$$F(> M) = 1 - \operatorname{erf} \left(\frac{\nu}{\sqrt{2}} \right)$$

For a given mean density of the universe, this immediately gives the number density of objects of a certain mass:

$$n(M) dM = \frac{\left| \frac{dF}{dM} \right| dM \cdot \rho_0}{M}$$
$$n(M) = \sqrt{\frac{\pi}{2}} \frac{\rho_0}{M^2} \left| \frac{d \ln \sigma}{d \ln M} \right| \nu \exp(-\nu^2 / 2)$$

The multiplicity function measures the fraction of mass bound to halos per unit log in mass:

$$S(M) = \frac{dF}{d \log M}$$

The standard equations of linear growth combined with the Press-Schechter formula allow a prediction of the halo mass function at all times, and for all CDM cosmologies

REQUIRED LINEAR THEORY RELATIONS

Growing mode solution in linear theory:

$$\delta(a) \propto \tilde{D}(a) \equiv H(a) \int_0^a \frac{da'}{[a' H(a')]^3}$$

$$H(a) = H_0 \sqrt{\Omega_0/a^3 + (1 - \Omega_0 - \Omega_\Lambda)/a^2 + \Omega_\Lambda}$$

Growth factor:

$$D(a) = \frac{\tilde{D}(a)}{\tilde{D}(1)}$$

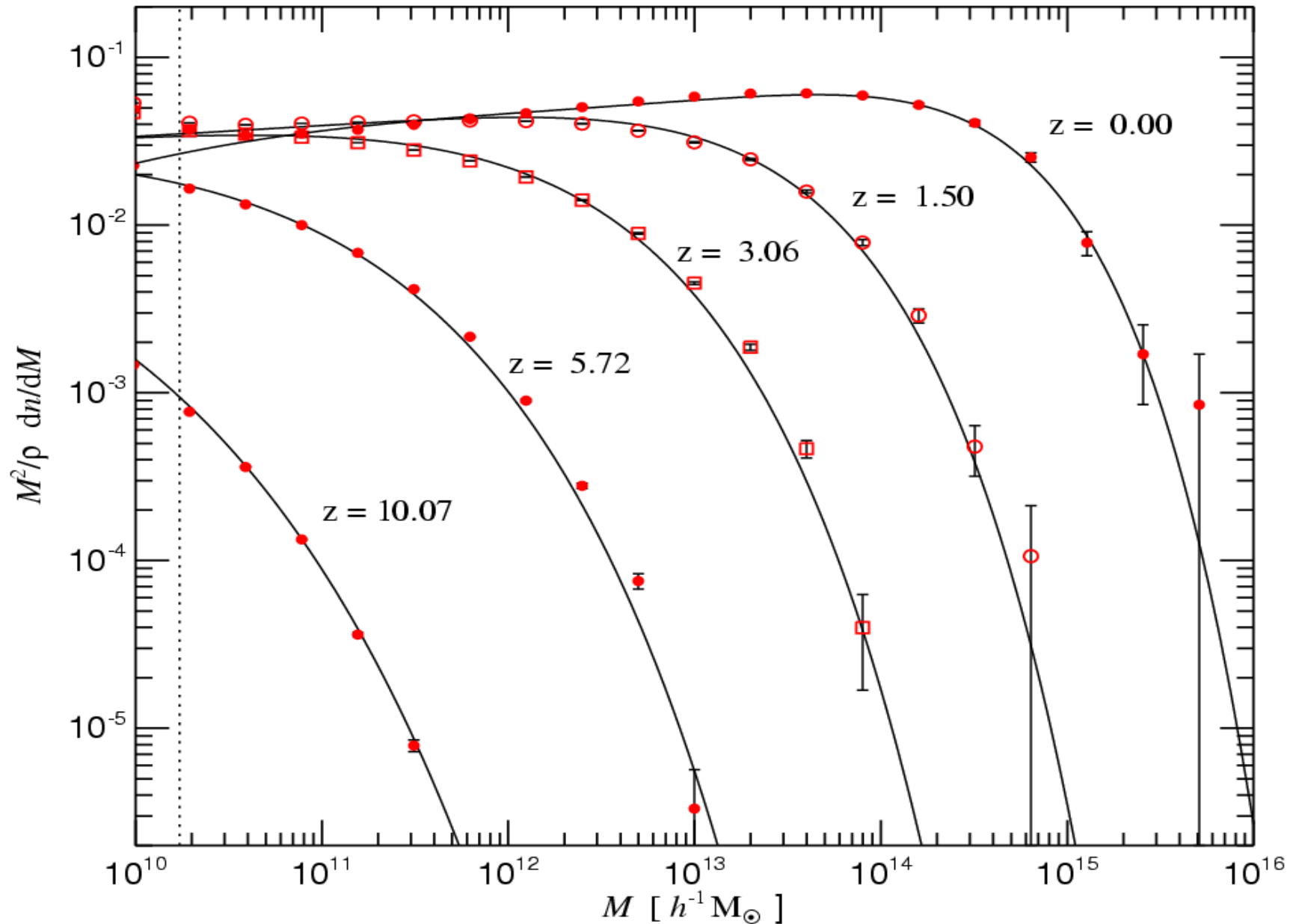
Power spectrum evolution:

$$P_z(k) = [D(k)]^2 P_{z=0}(k)$$

→ Variance $\sigma^2(M)$ can be computed at all times

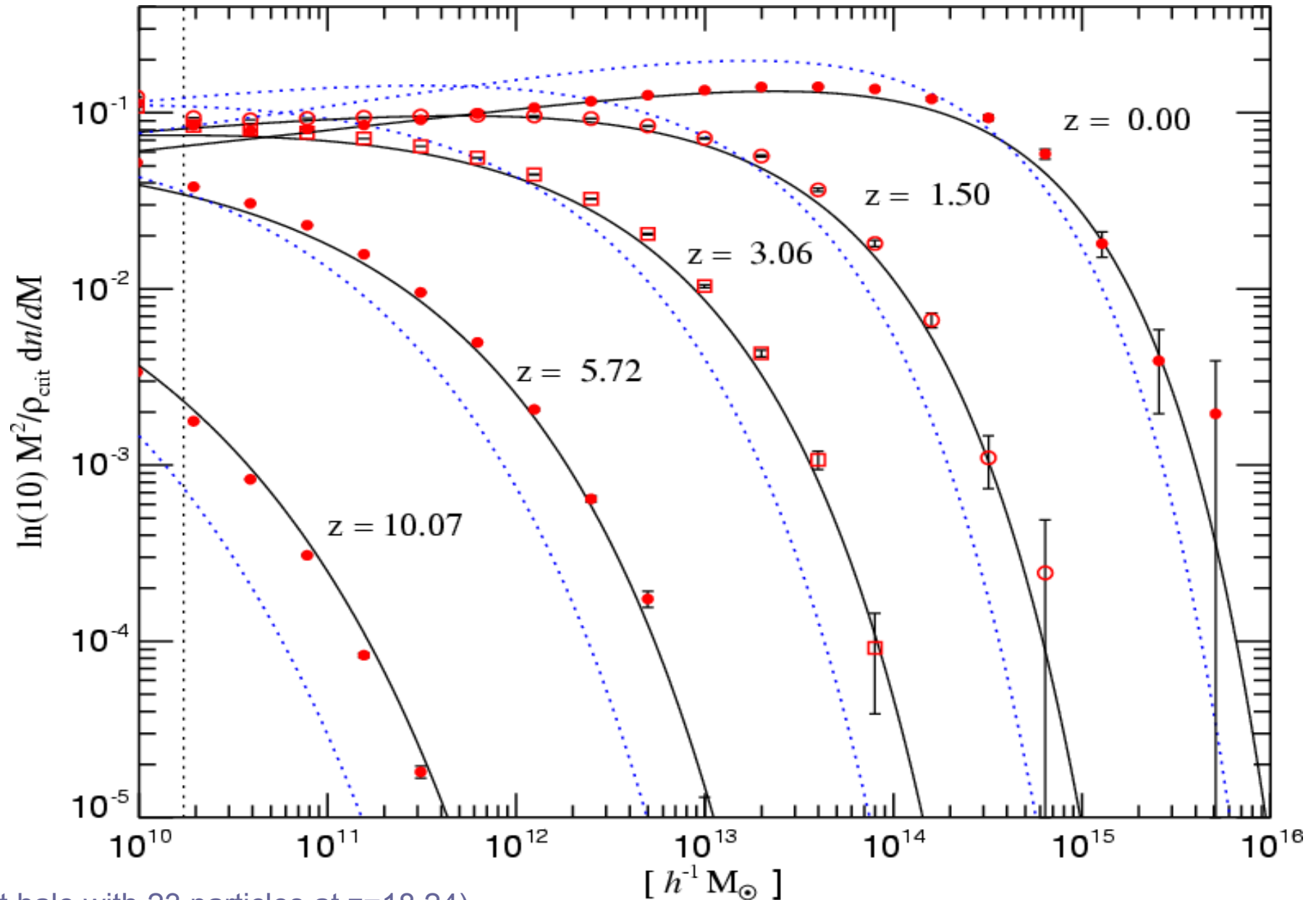
The evolution of the halo mass function is arguably the most fundamental tracer of nonlinear structure growth

HALO MASS FUNCTION OF THE MILLENNIUM COSMOLOGY



The Sheth & Tormen mass function provides a significantly better description than Press & Schechter

MASS MULTIPLICITY FUNCTION



(First halo with 23 particles at $z=18.24$)

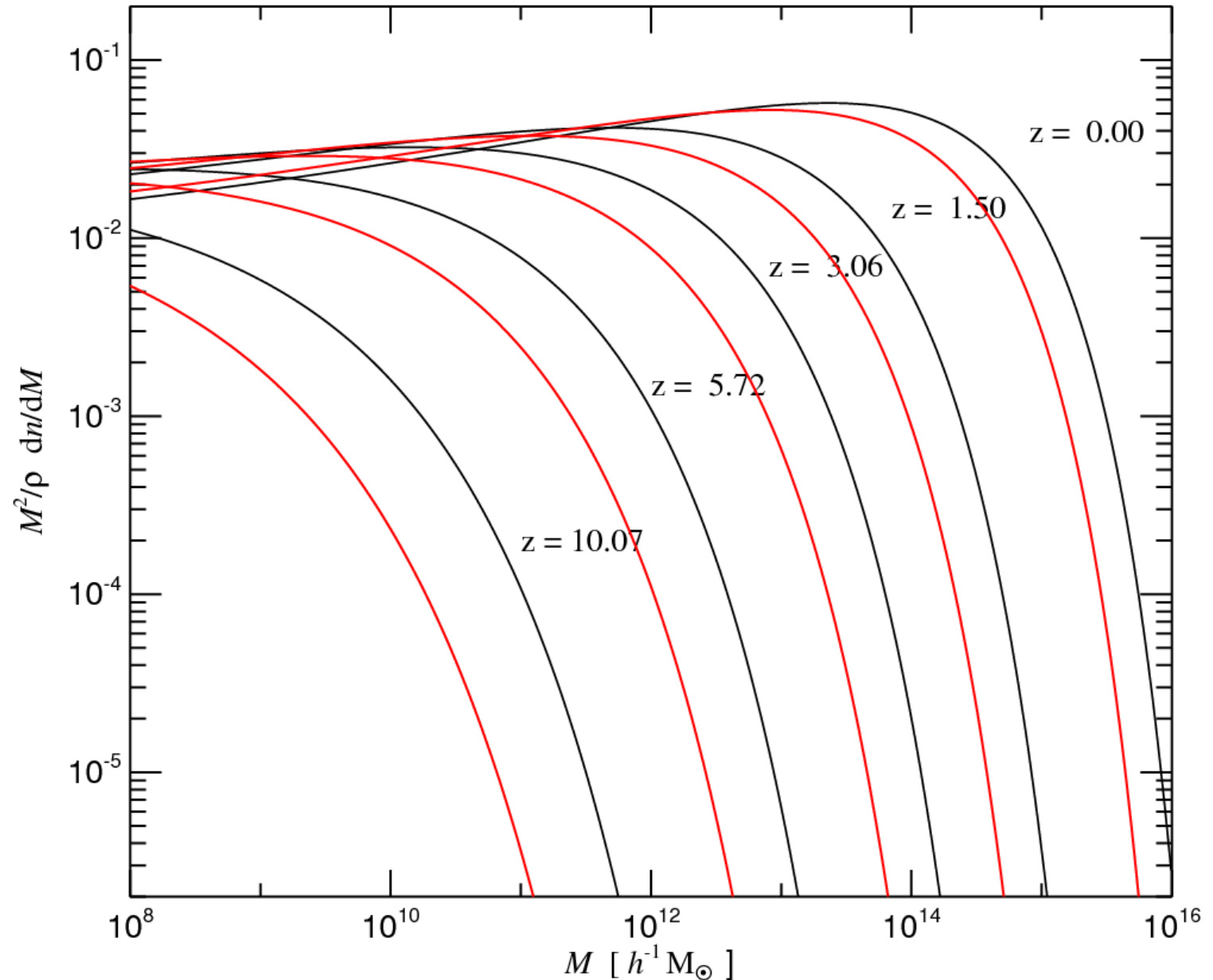
The change in the normalization strongly delays the formation of halos in the exponential tail of the mass function

CHANGES IN THE MASS FUNCTION DUE TO THE SMALLER σ_8

$\sigma_8 = 0.90$



$\sigma_8 = 0.74$



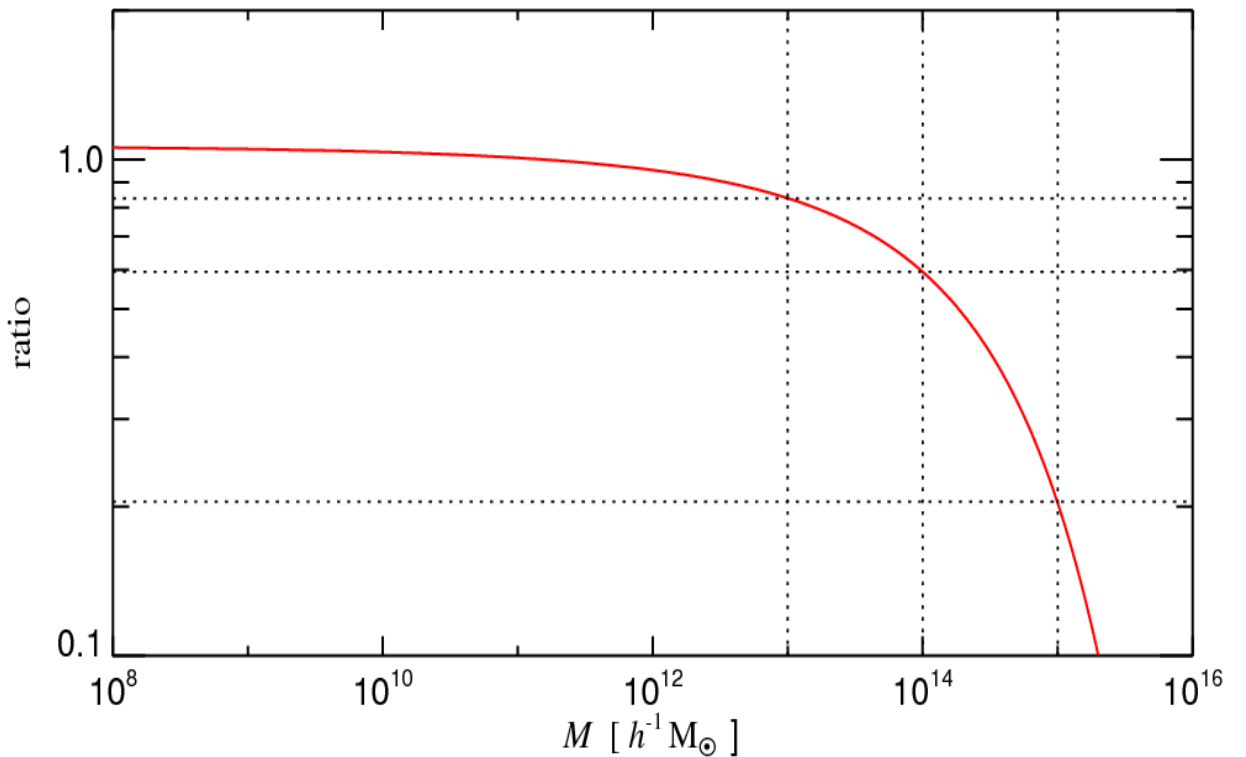
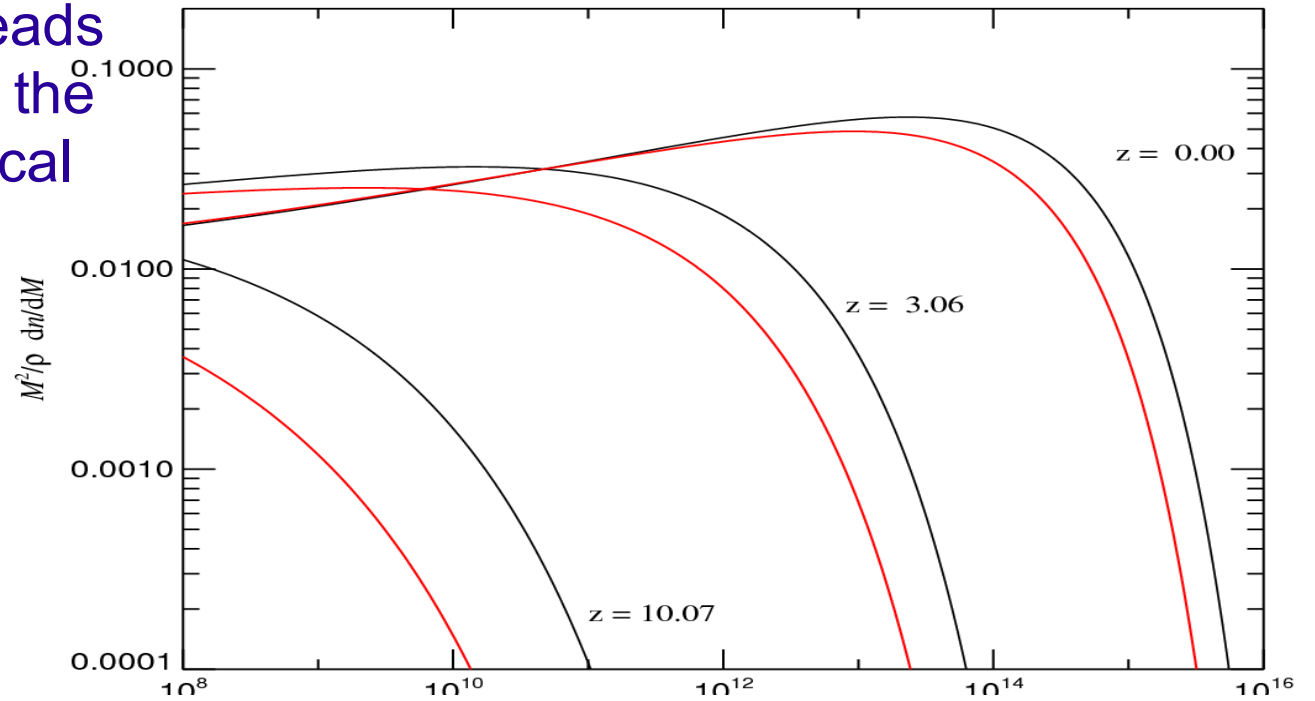
The WMAP3 cosmology leads to a substantial revision of the evolution of the cosmological halo mass function

RELATIVE CHANGE IN THE ABUNDANCE OF HALOS AT Z=0

$\Omega_m = 0.25$
$\Omega_\Lambda = 0.75$
$n = 1.00$
$\sigma_8 = 0.90$
$h = 0.73$
$\Omega_b = 0.045$



$\Omega_m = 0.24$
$\Omega_\Lambda = 0.76$
$n = 0.95$
$\sigma_8 = 0.74$
$h = 0.73$
$\Omega_b = 0.042$



Models for internal halo
structure: self-similar infall,
isothermal spheres,
NFW-profile

The evolution of a point-mass perturbation in a critical density background universe can be treated analytically

BERTSCHINGERS SELF-SIMILAR SOLUTION

Self-similar ansatz for a scale-free collapse solution:

$$\bar{\rho}(r, t) = 5.55 \rho_0(t) f\left(\frac{r}{r_{\text{turn}}(t)}\right)$$

For a point-mass perturbation, the perturbation is a power-law as a function of radius:

$$\bar{\delta}(r) \propto \frac{1}{r^3}$$

Bertschinger has shown that the density profile in the virialized region will then be a power-law as well:

$$\rho(r) \propto r^{-9/4}$$



Close to the slope of an isothermal sphere

Truncated isothermal spheres are often used as a simple model for a halo in approximate dynamical equilibrium

TRUNCATED ISOTHERMAL SPHERES

$$\rho(r) = \frac{\sigma_r^2}{2\pi G r^2} \quad m(r) = M \frac{r}{R} \quad \text{for } r \leq R$$

Let's truncate at the virial overdensity:

$$\frac{M_{\text{vir}}}{\frac{4\pi}{3} R_{\text{vir}}^3} = 200 \rho_{\text{crit}}$$

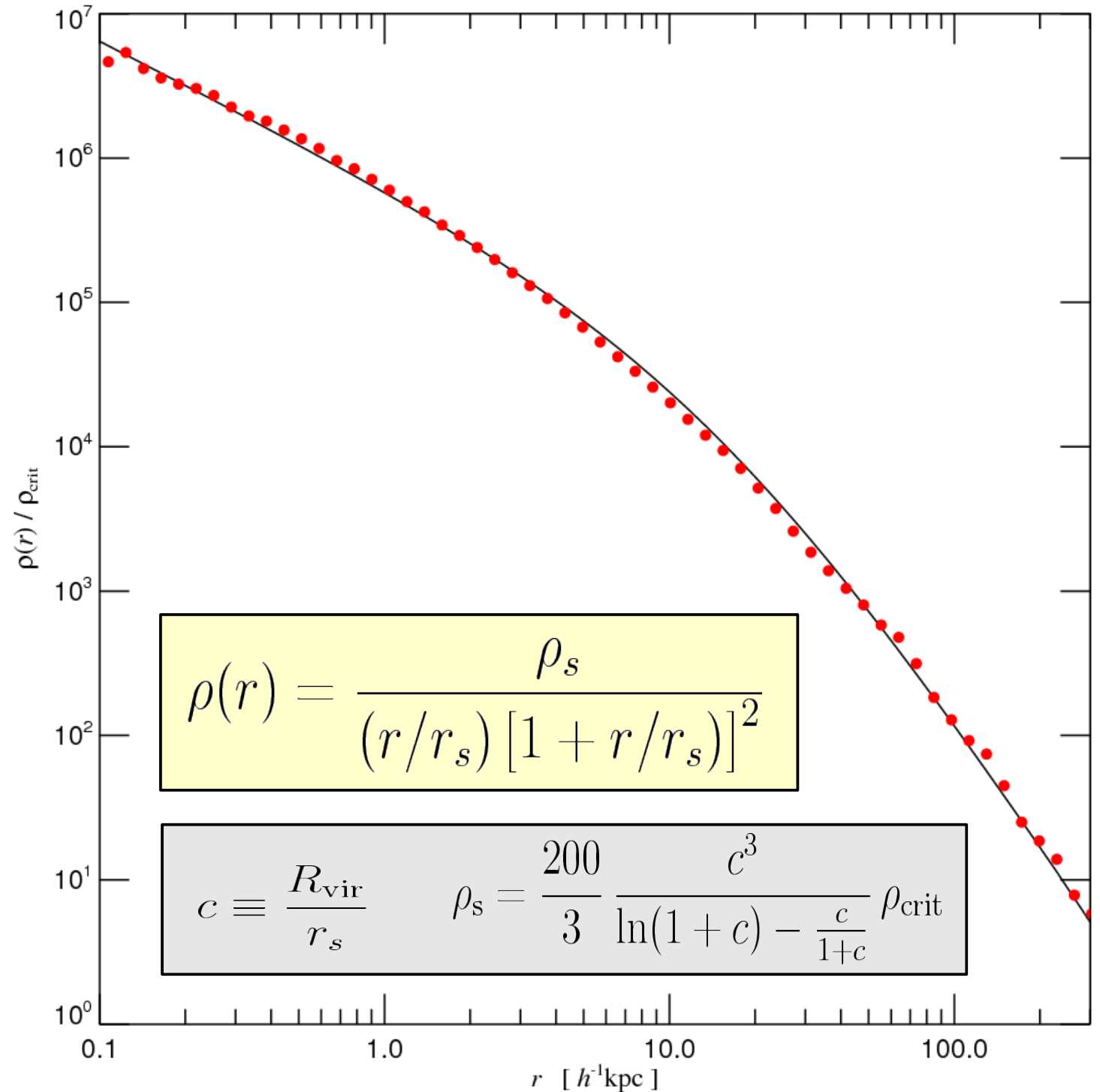
Note: It is a convention to increase the assumed virial overdensity from ~ 178 to 200.

Useful relations between sizes of halos:

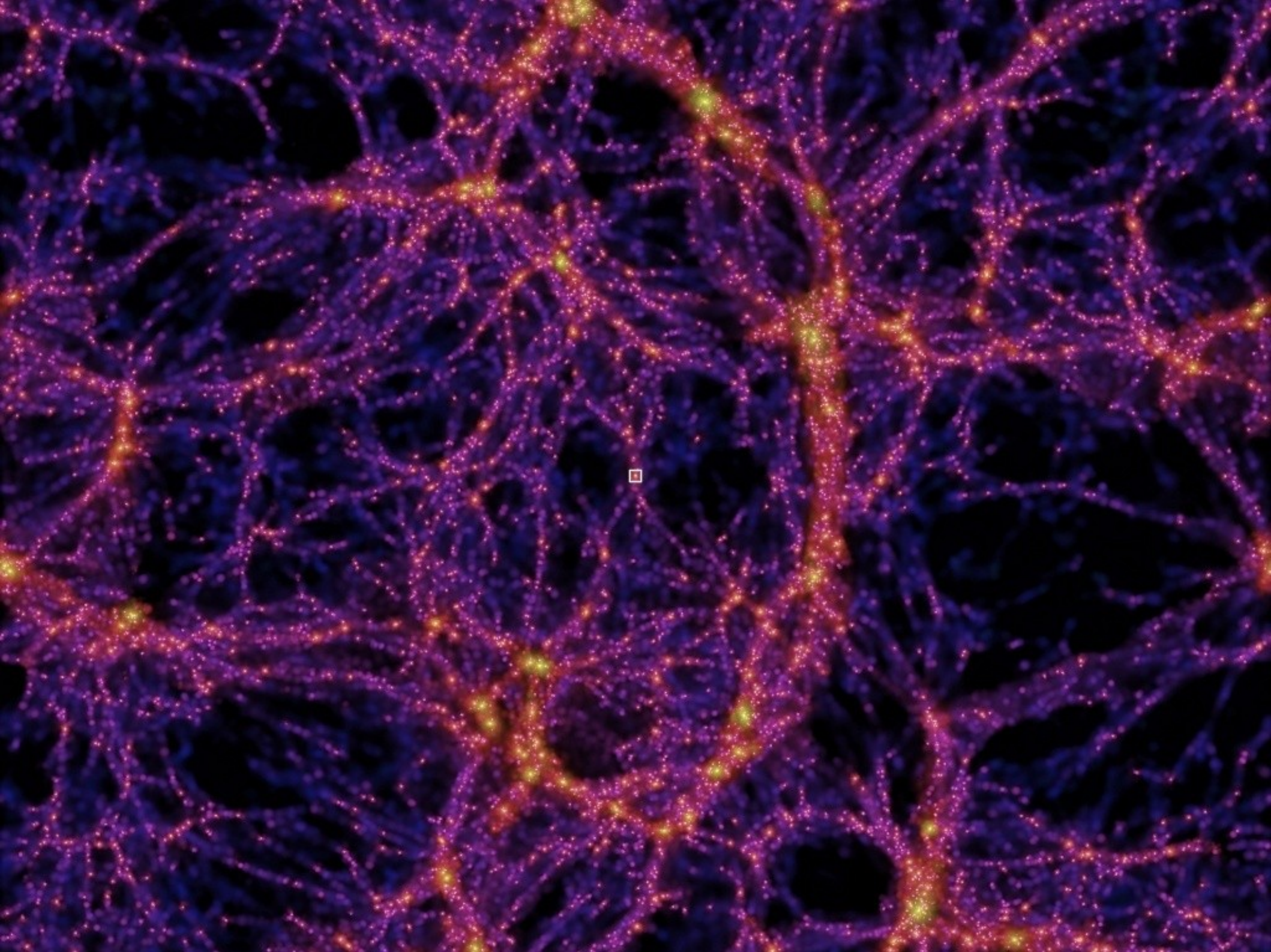
$$V_{\text{vir}}^2 = \frac{G M_{\text{vir}}}{R_{\text{vir}}}$$
$$M_{\text{vir}} = \frac{V_{\text{vir}}^3}{10 G H(z)}$$
$$R_{\text{vir}} = \frac{V_{\text{vir}}}{10 H(z)}$$

N-body
simulations find a
universal profile
that is not a
power-law

THE NFW-PROFILE



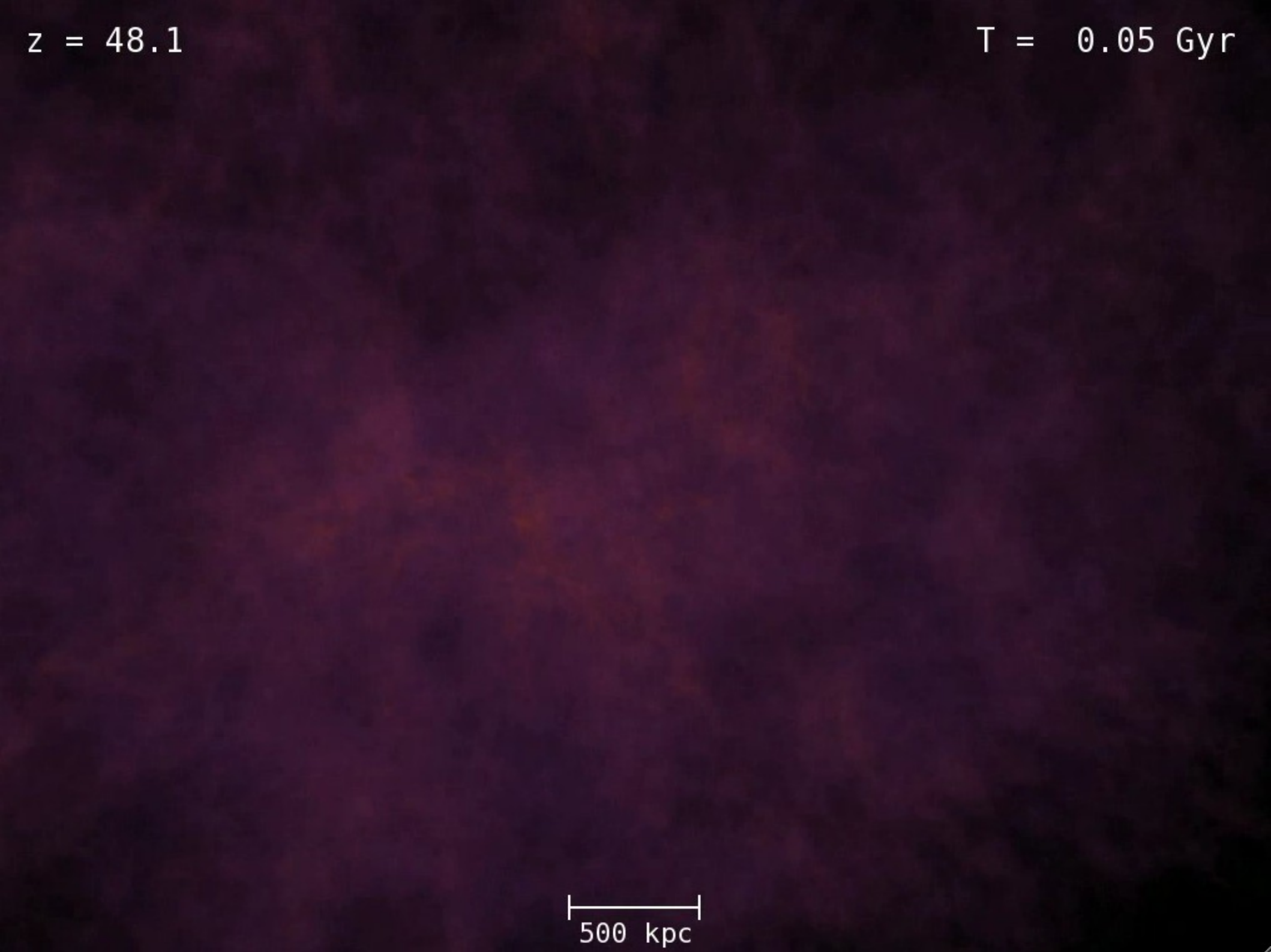
Small-scale dark matter structure



$z = 48.1$

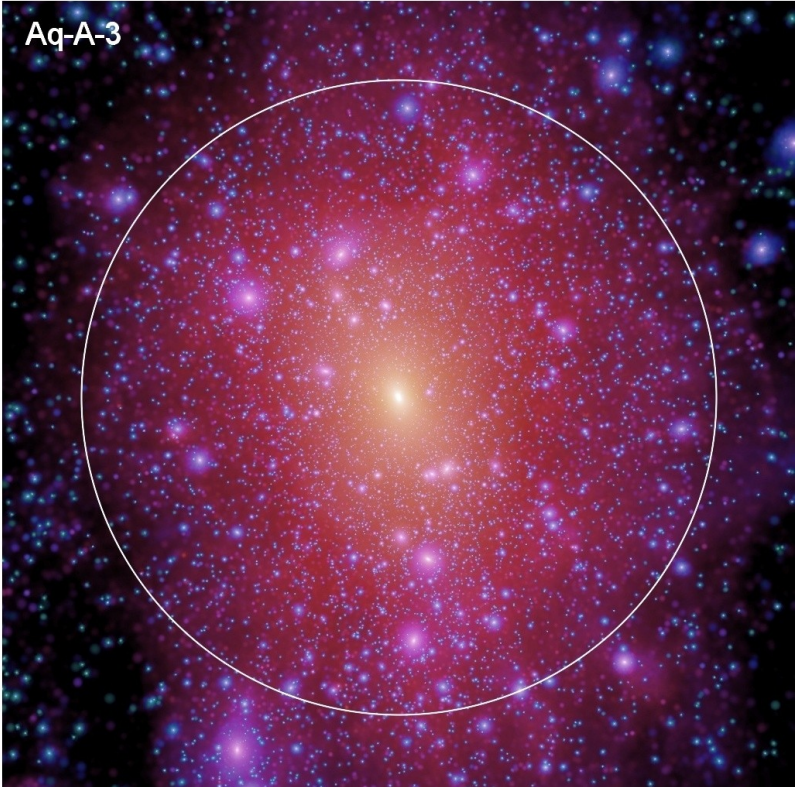
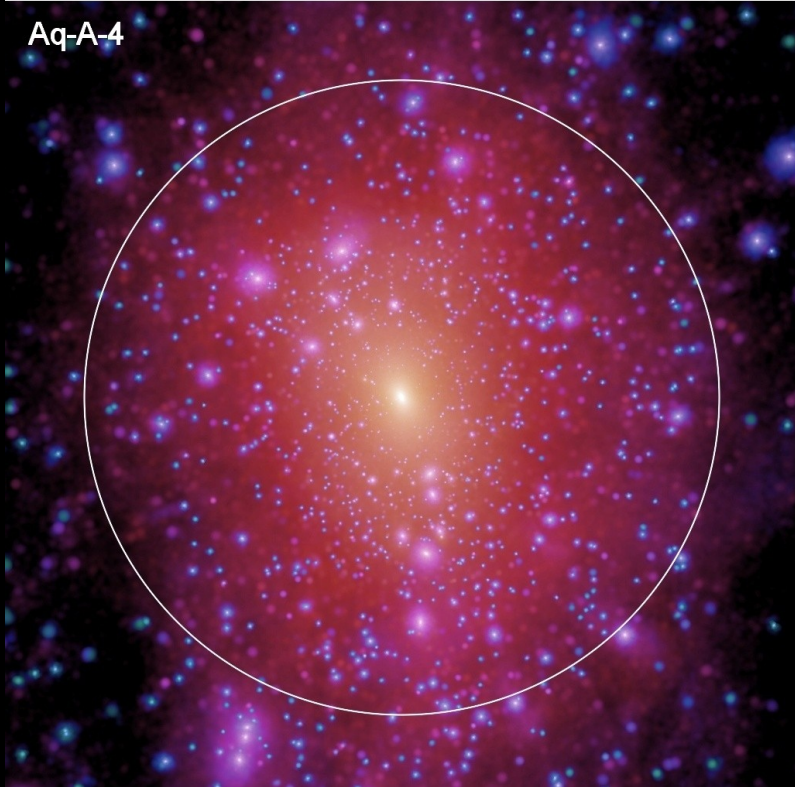
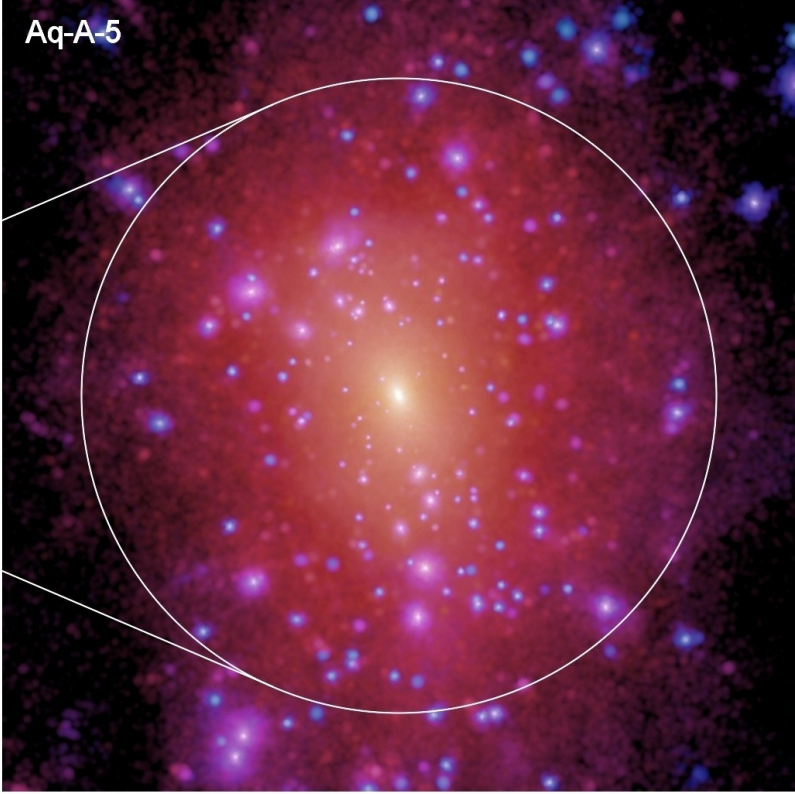
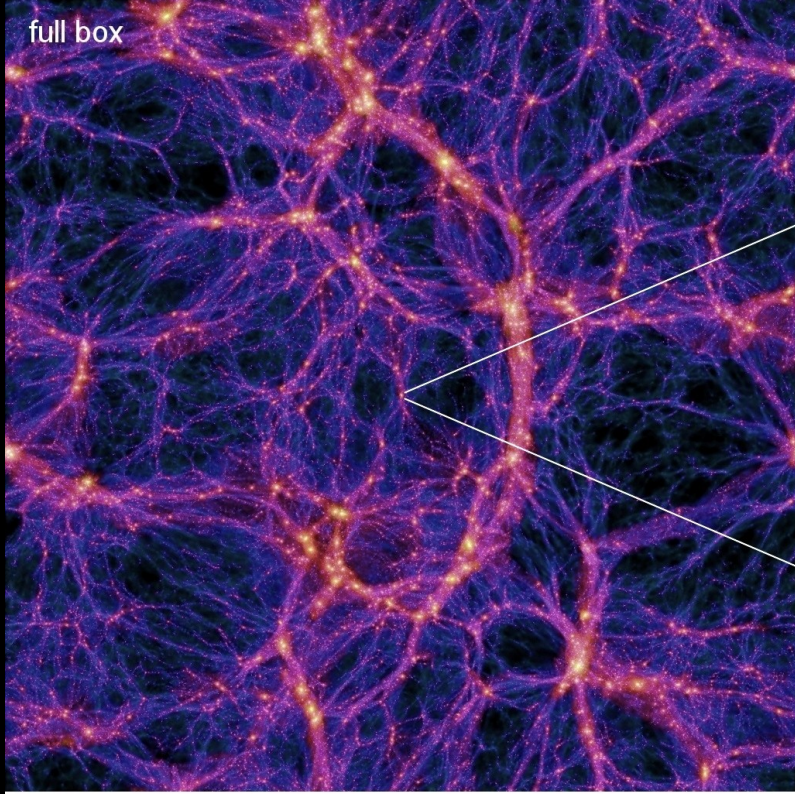
$T = 0.05 \text{ Gyr}$

500 kpc

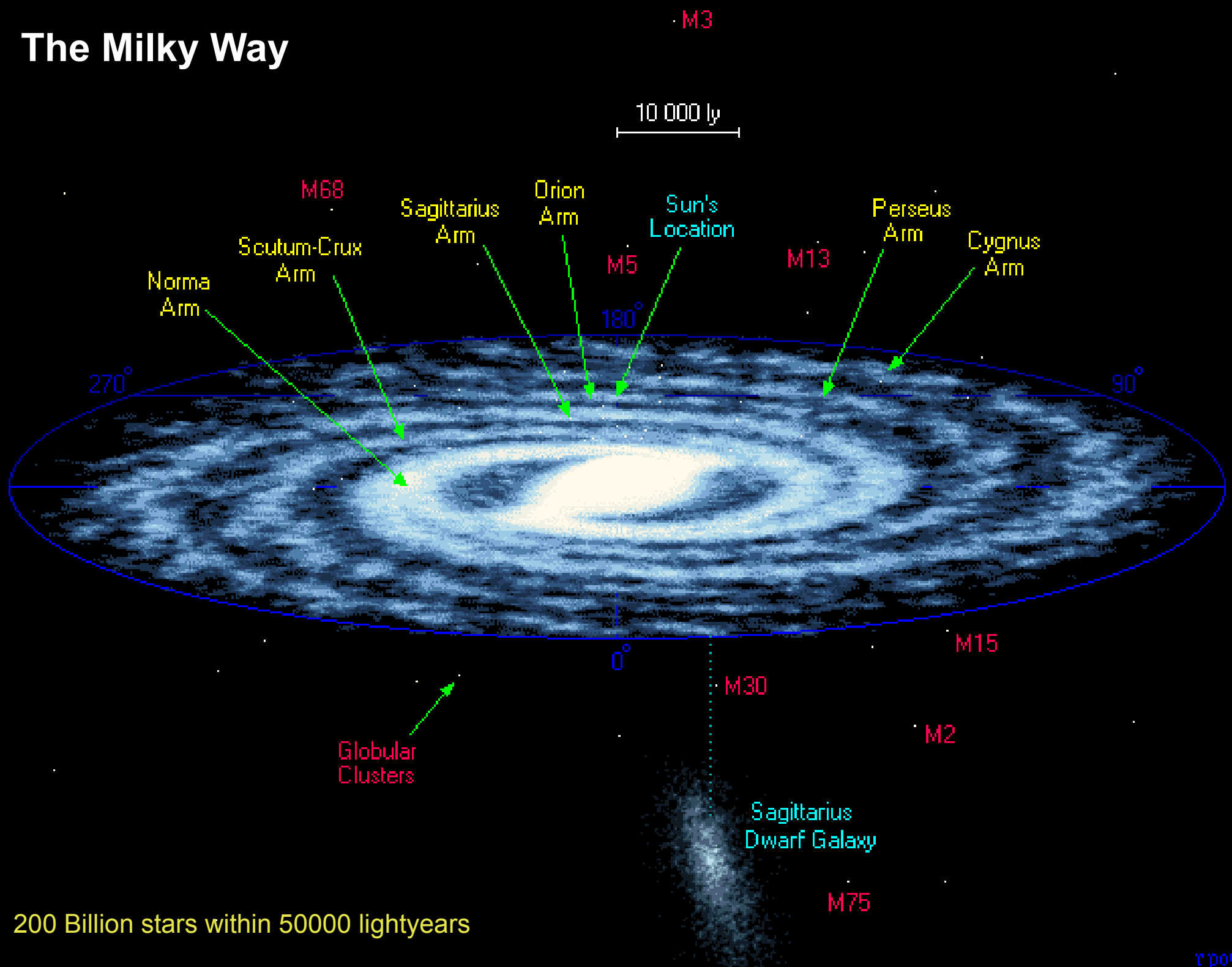


Zooming in on dark matter halos reveals a huge abundance of dark matter substructure

DARK MATTER DISTRIBUTION IN A MILKY WAY SIZED HALO AT DIFFERENT RESOLUTION

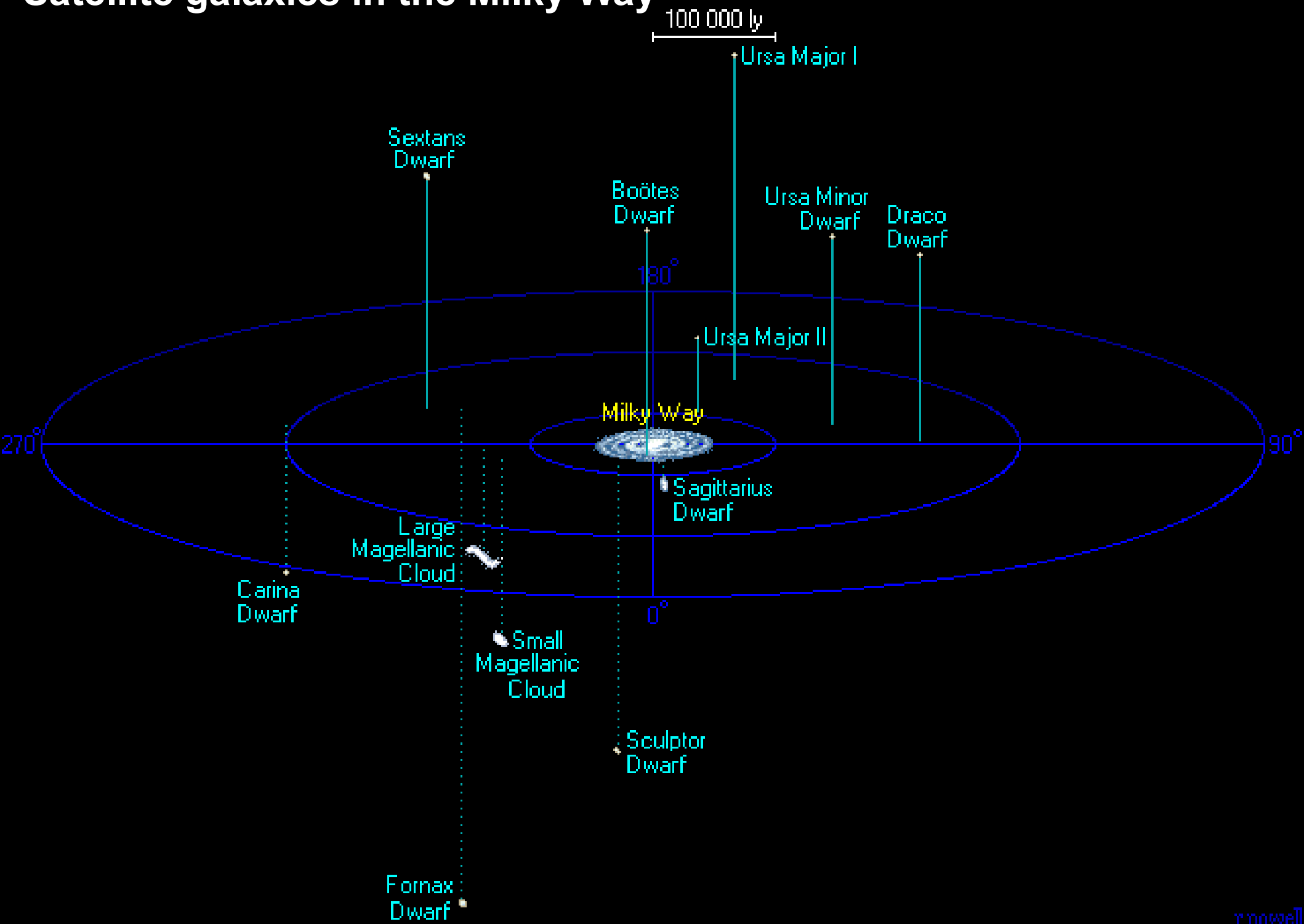


The Milky Way



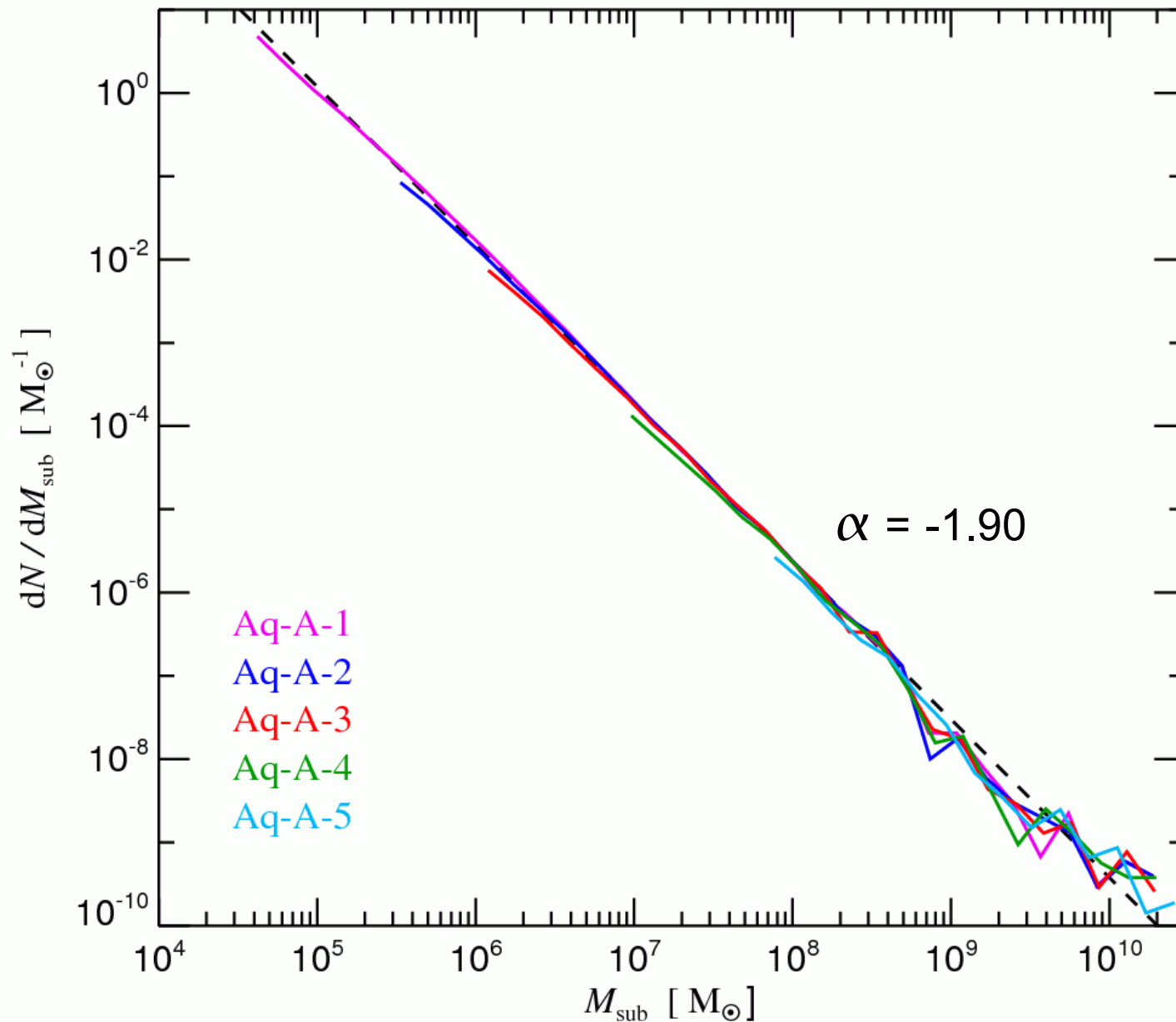
200 Billion stars within 50000 lightyears

Satellite galaxies in the Milky Way



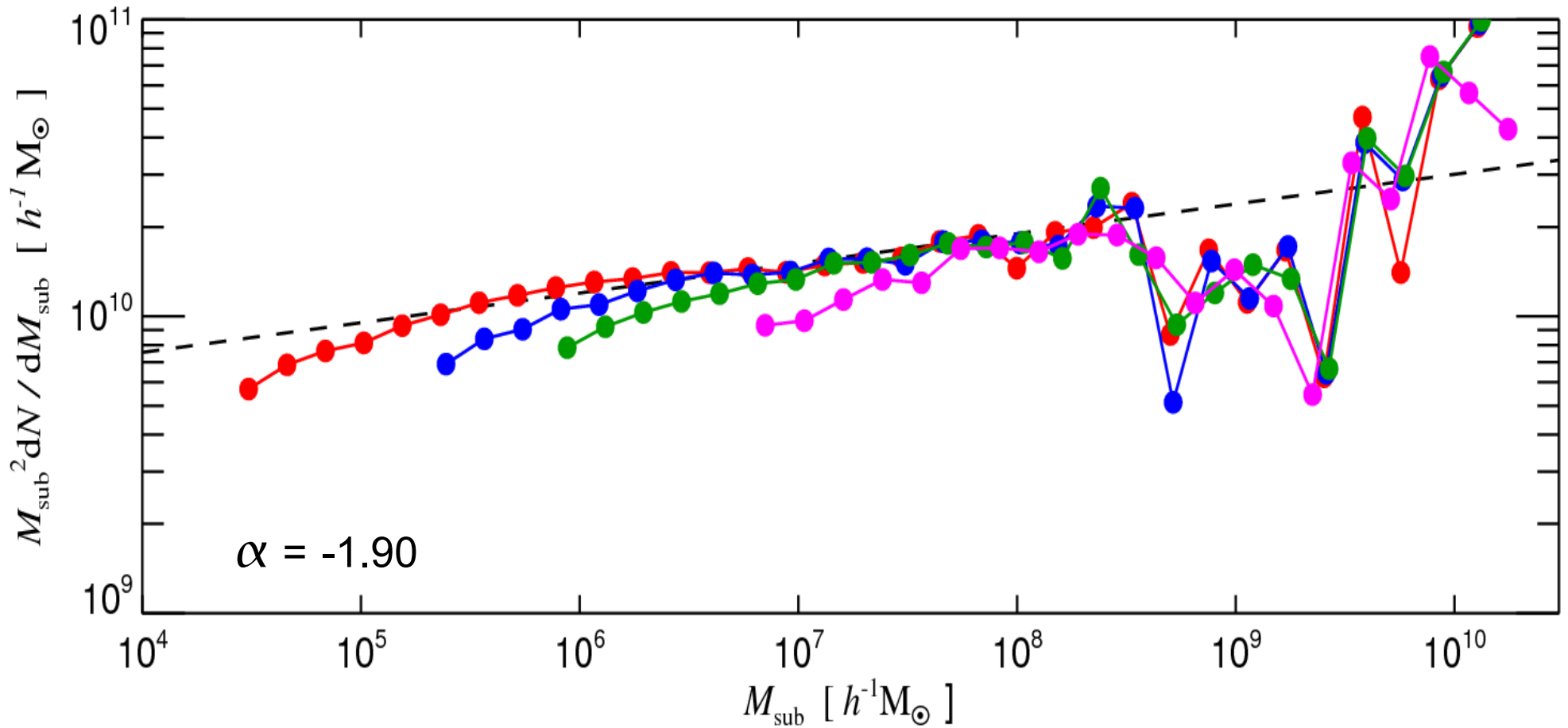
The differential subhalo mass function converges quite well to a power-law

RESULTS FROM A RESOLUTION STUDY OF AQUARIUS HALO AQ-A



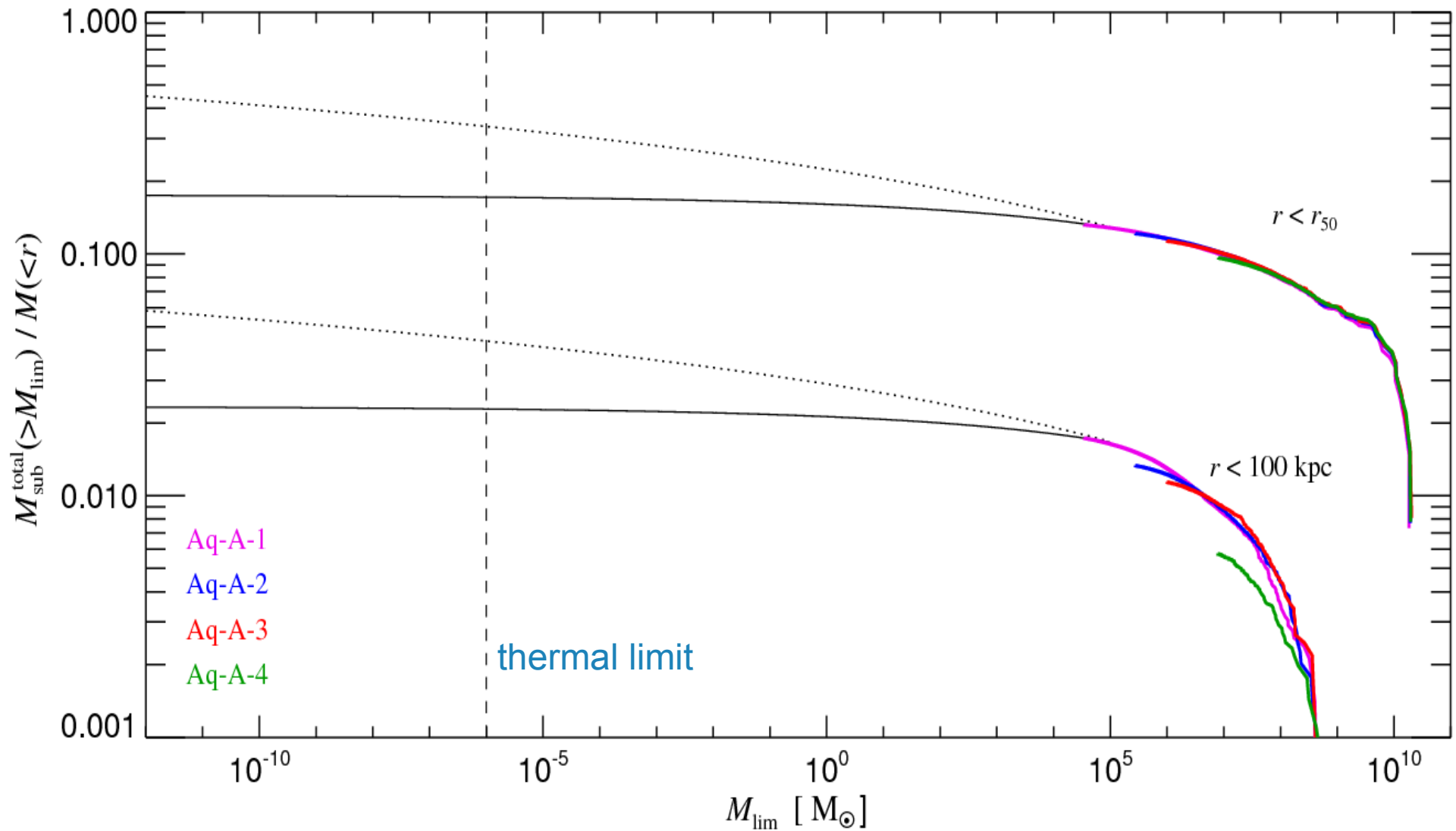
The subcritical slope of the differential subhalo mass function implies that the total mass in substructures converges at the faint end

THE DIFFERENTIAL SUBHALO MASS FUNCTION



The cumulative mass fraction in **resolved substructures** reaches about 12-13%, we expect up to ~18% down to the thermal limit

FRACTION OF MASS IN SUBSTRUCTURES AS A FUNCTION OF MASS LIMIT



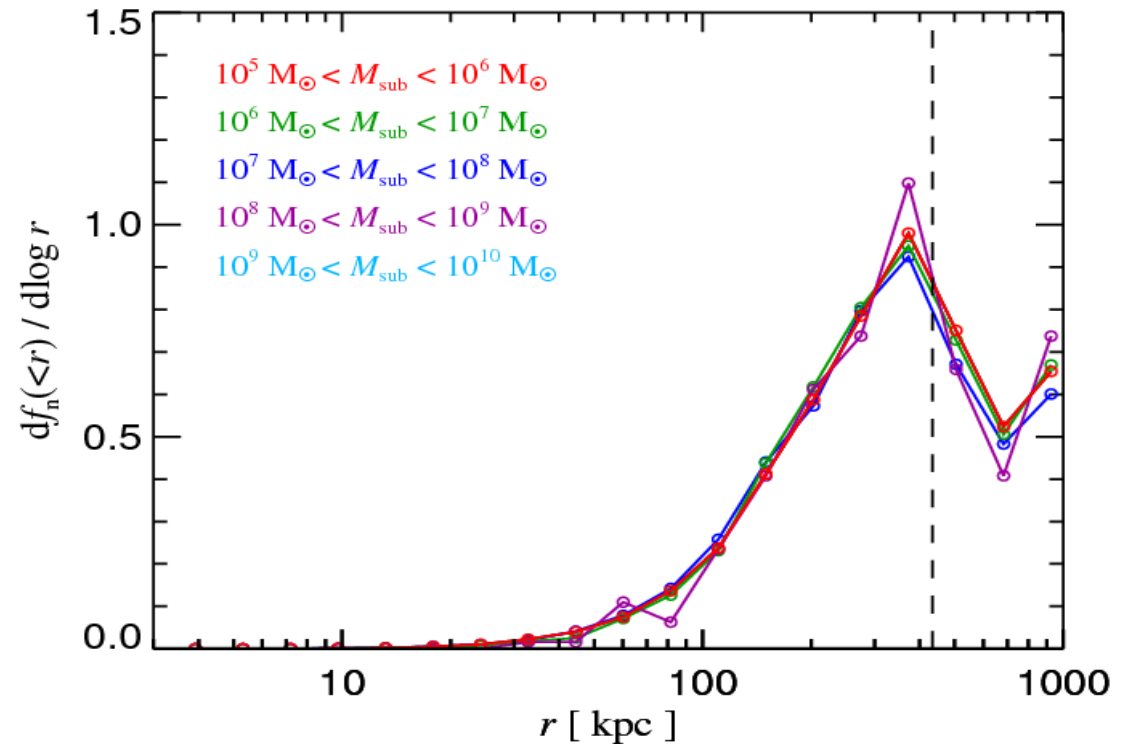
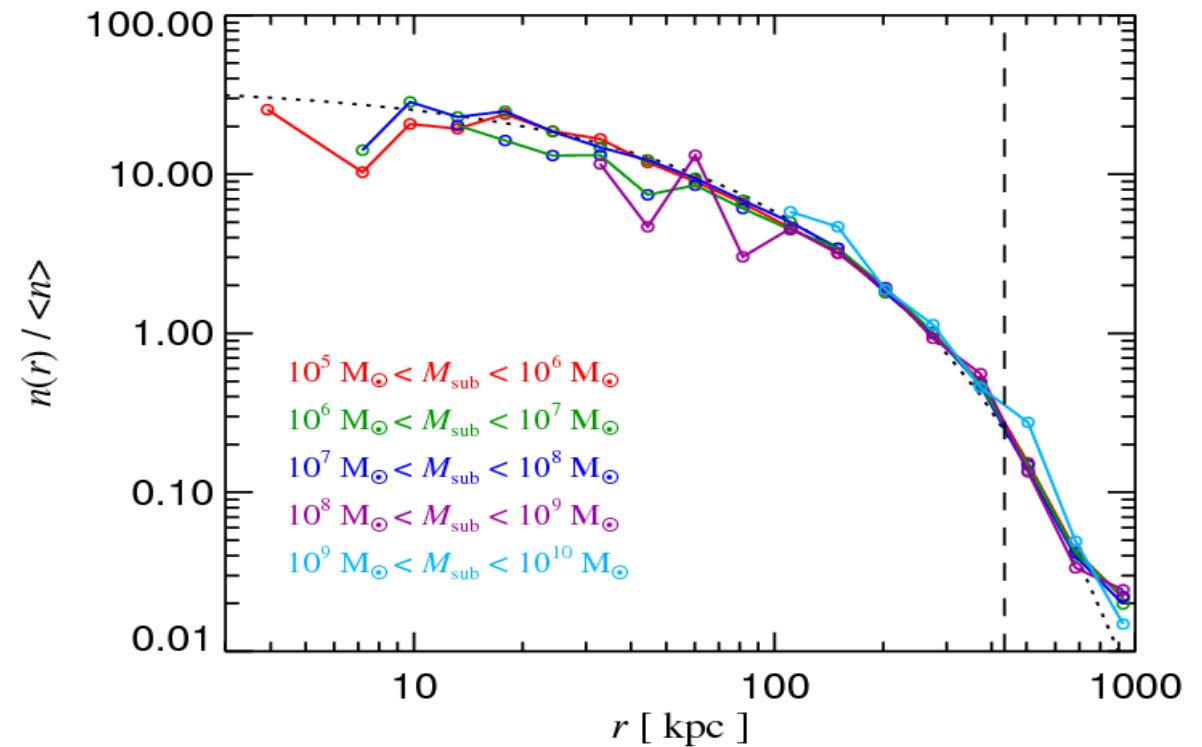
The radial distribution of substructures is strongly antibiased relative to all dark matter, and independent of subhalo mass

RADIAL SUBSTRUCTURE DISTRIBUTION IN Aq-A-1

Most subhalos are at large radii, subhalos are more effectively destroyed near the centre

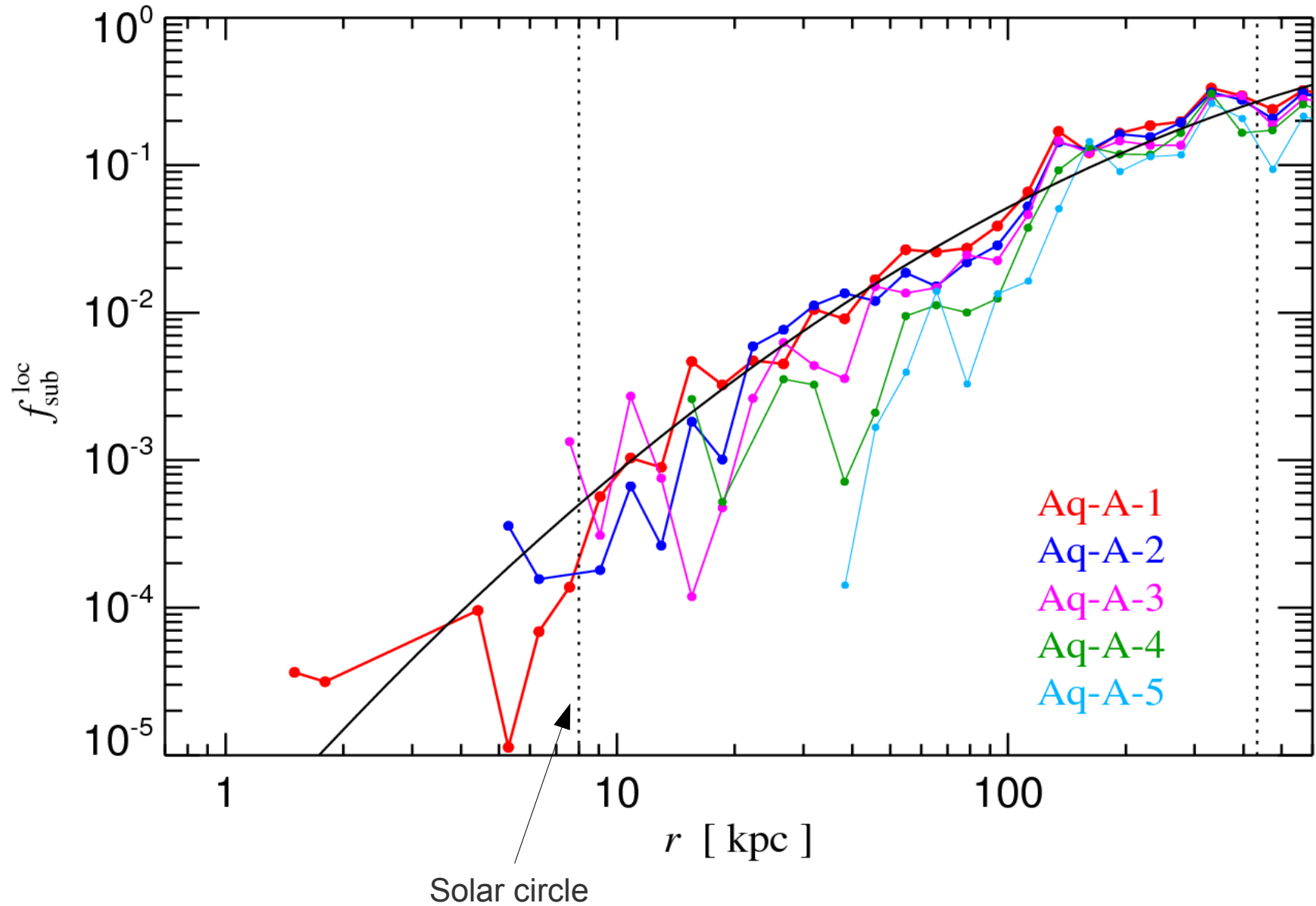
Subhalos are far from the Sun

see also Diemand et al. (2007, 2008)



The local mass fraction in substructures is a strong function of radius

MASS FRACTION IN SUBSTRUCTURES AS A FUNCTION OF RADIUS IN HALO AQ-A

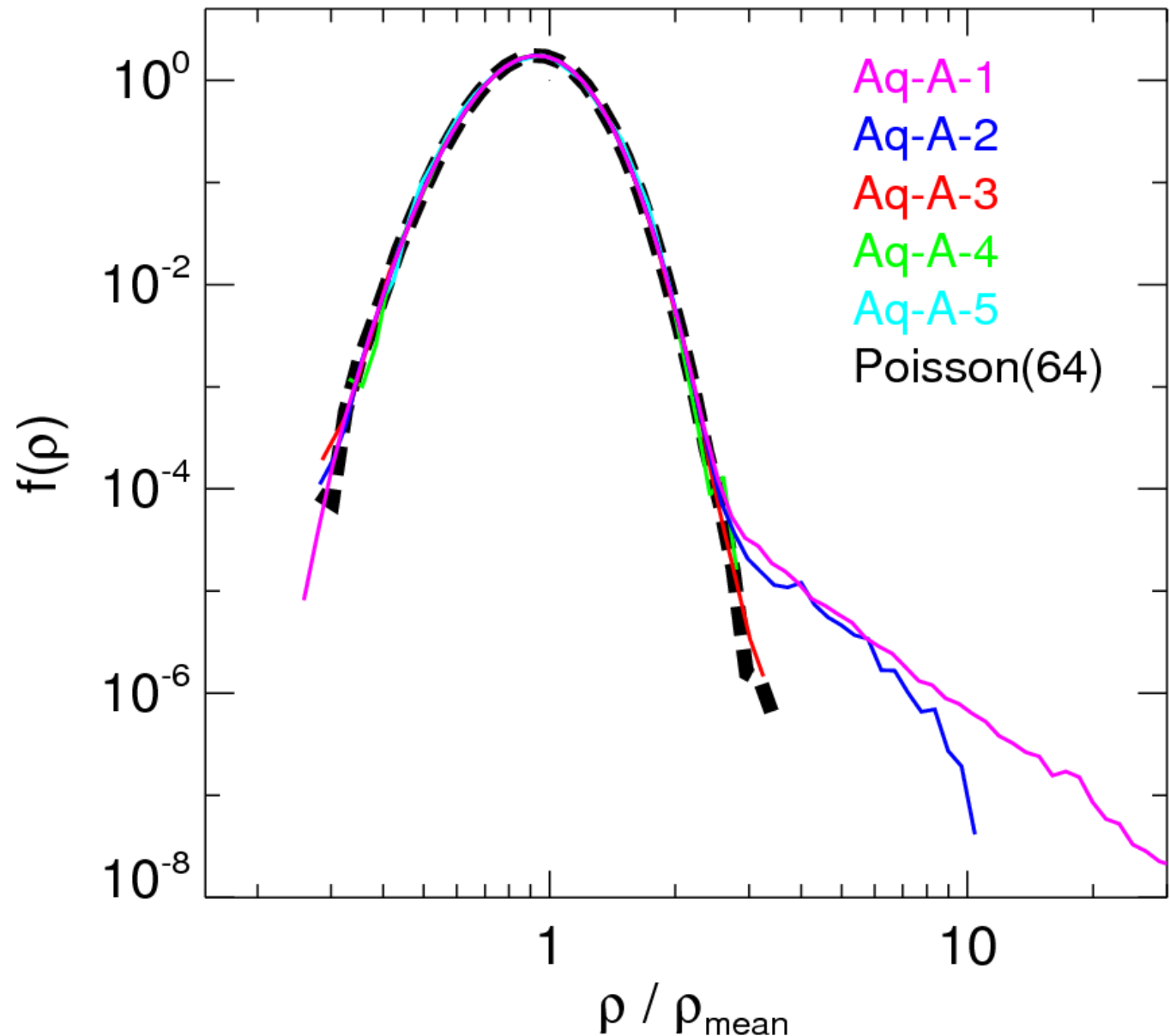


The dark matter distribution at the Solar circle is surprisingly smooth

THE DENSITY PDF AT THE POSITION OF THE SUN

Essentially all of the scatter is due to particle sampling noise.

In fact, the residual intrinsic rms scatter is only 4% around the smooth model



Dark matter annihilation predictions

Dark matter could be self-annihilating, in which case the presence of subhalos should **boost** the expected flux

THE ANNIHILATION SIGNAL DUE TO SUBSTRUCTURES

Annihilation flux:

$$F = \frac{N_\gamma \langle \sigma v \rangle}{2 m_{\text{DM}}^2} \int_V \frac{\rho_{\text{DM}}^2(\mathbf{x})}{4\pi d^2(\mathbf{x})} d^3x$$

Particle physics Astrophysics

Luminosity of a halo with maximum circular velocity $V_c(r_{\text{max}}) = V_{\text{max}}$: $L = \int \rho_{\text{DM}}^2(\mathbf{x}) d^3x$

NFW-Profile: $L = 1.23 \frac{V_{\text{max}}^4}{G^2 r_{\text{max}}}$

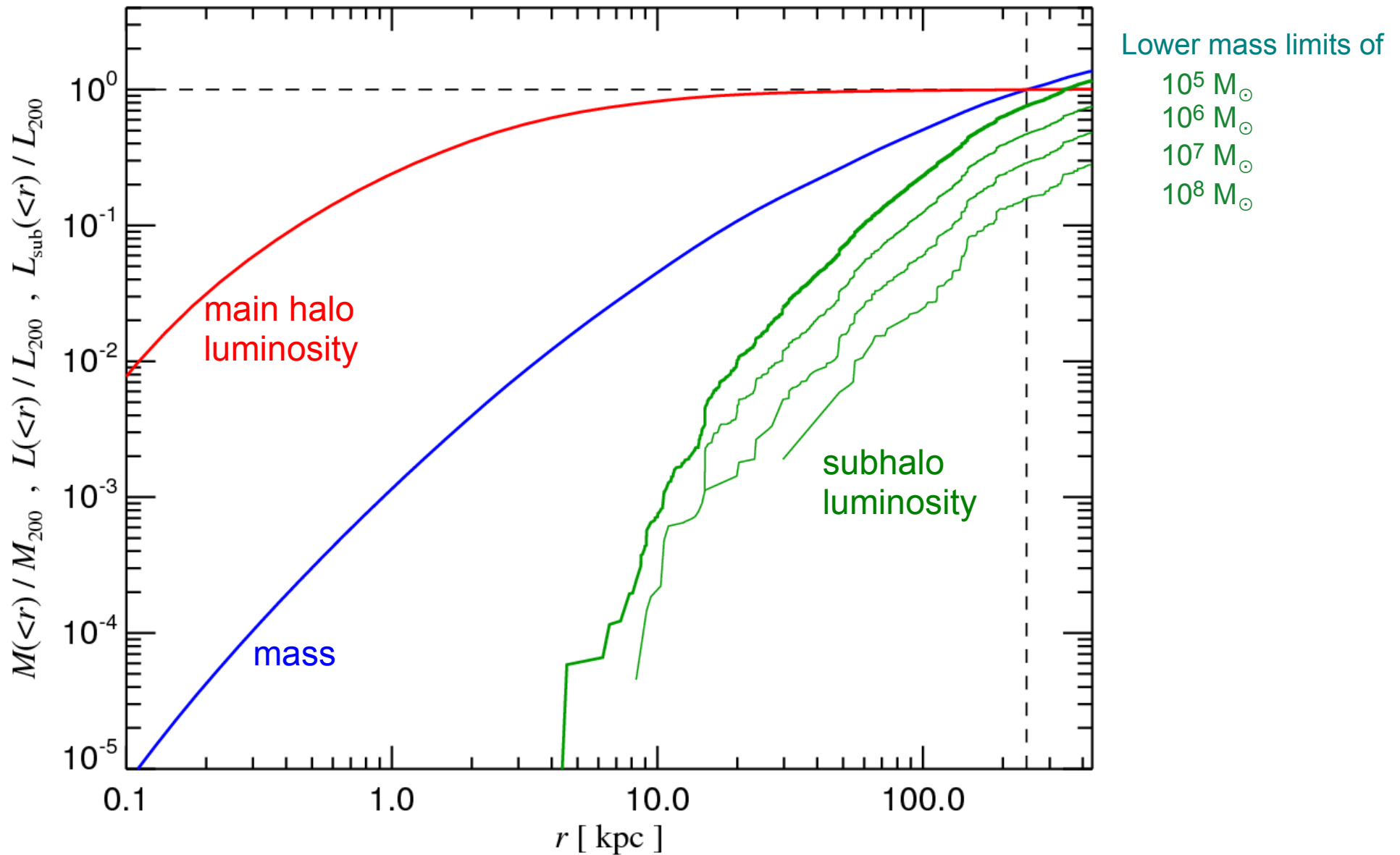
$\alpha = -1.4$ Profile: $L = 3.97 \frac{V_{\text{max}}^4}{G^2 r_{\text{max}}}$

Einasto-Profile: $L = 1.87 \frac{V_{\text{max}}^4}{G^2 r_{\text{max}}}$

Moore-Profile: $L = \infty$

The annihilation luminosity from main halo and subhalos has a very different radial distribution

THE RELATIVE DISTRIBUTION OF MASS, MAIN HALO, AND SUBHALO LUMINOSITY

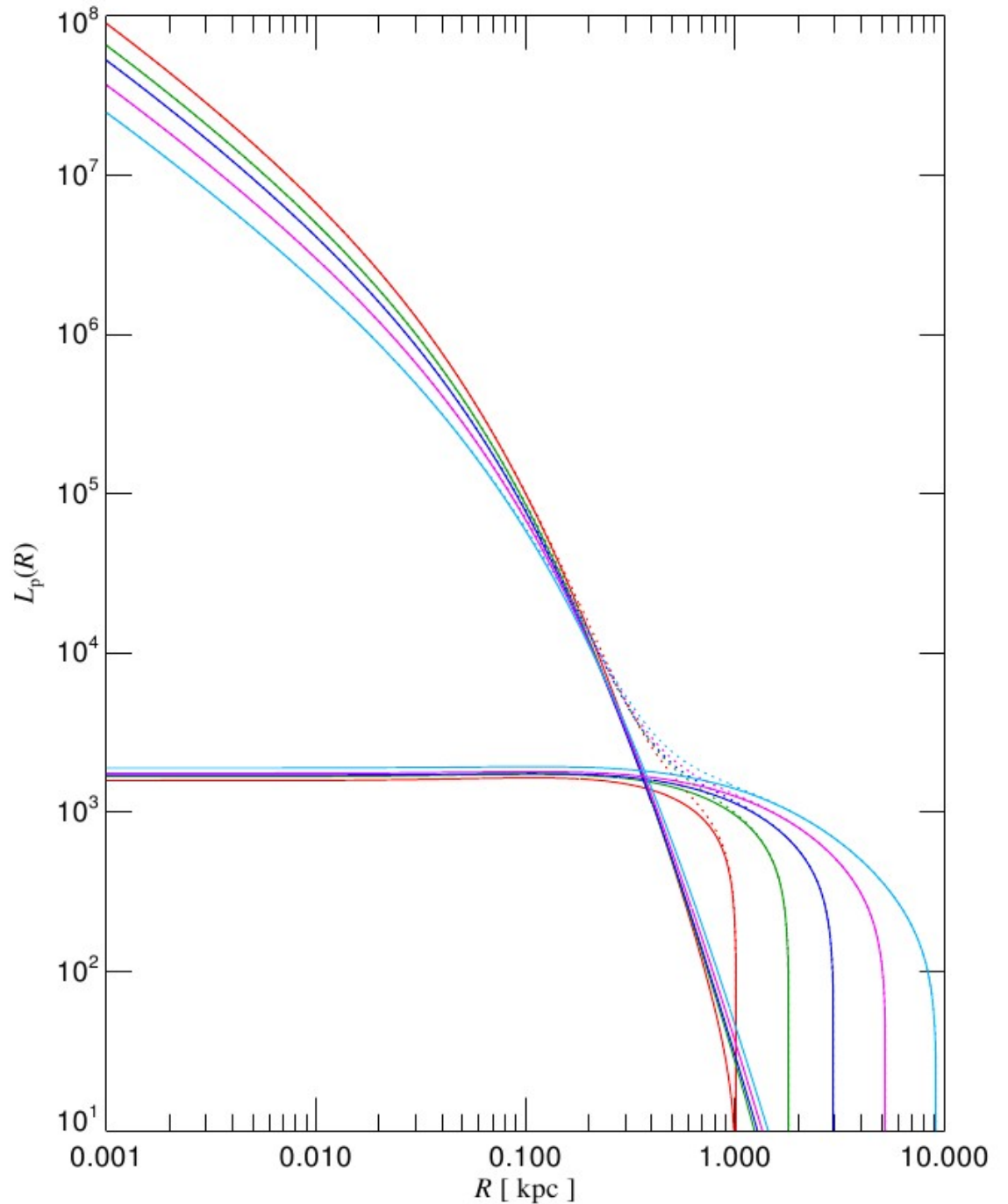


Surface brightness profile of a typical subhalo with $V_{\max}=10$ km/s at different distances from the galactic center

SURFACE BRIGHTNESS PROFILE OF DIFFERENT SUBHALO COMPONENTS

The sub-sub component appears as a (extended) “disk” on the sky

The central surface brightness of the smooth component actually increases with smaller distance (because the concentration increases)

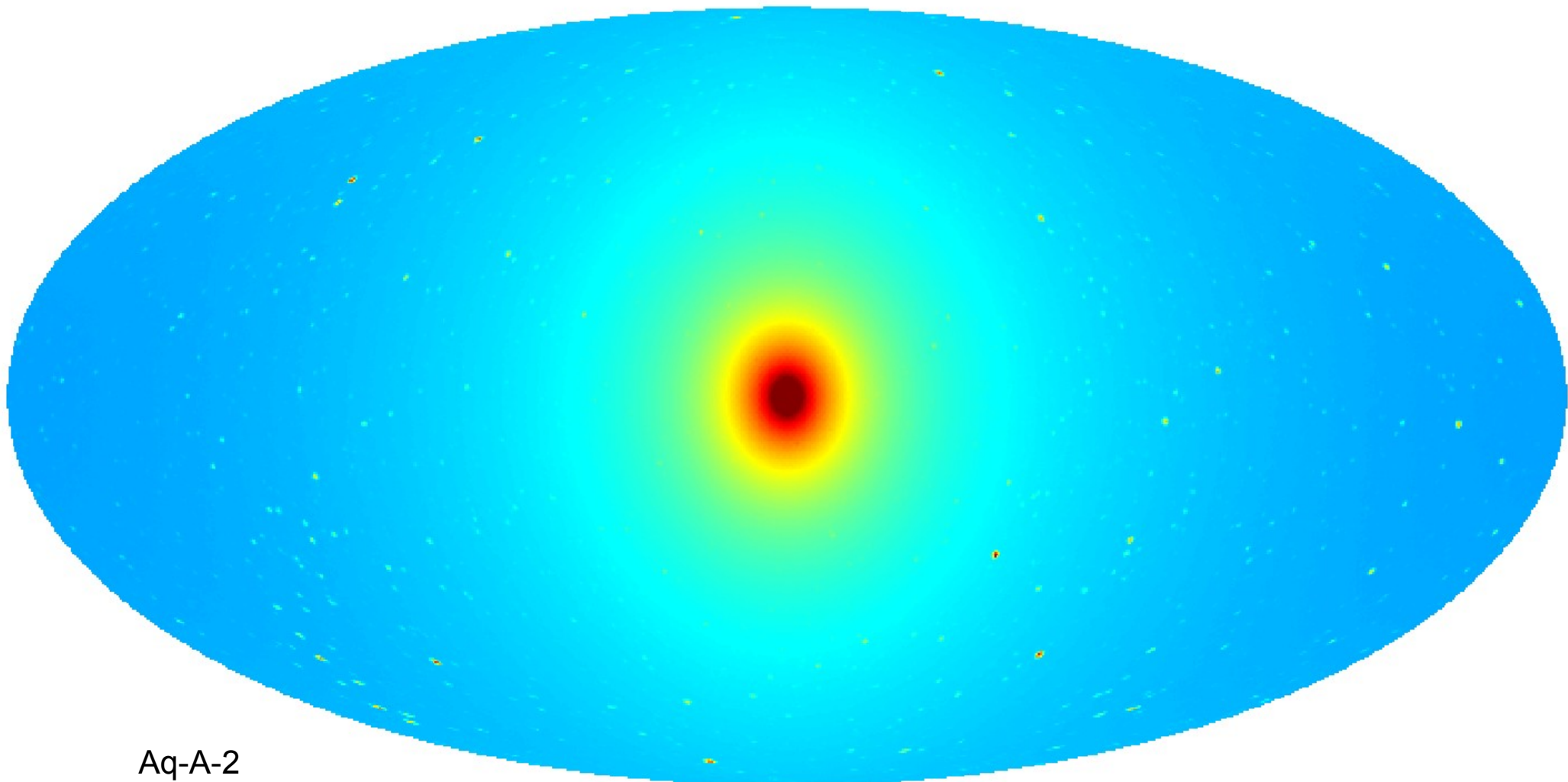


The dark matter annihilation flux is boosted significantly by dark matter substructures

EXTRAPOLATED ALL-SKY MAP OF THE DM ANNIHILATION FLUX FROM THE MILKY WAY

$$L \propto \rho^2 dV$$

total emission



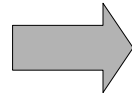
Aq-A-2

-0.50  2.0 *Log(Intensity)*

Dark matter annihilation can be best discovered with an optimal filter against a bright background

THE SIGNAL-TO-NOISE FOR DETECTION WITH AN OPTIMAL FILTER

The optimal filter is proportional to the signal



$$S/N = \sqrt{\tau A_{\text{eff}}} \left[\int \frac{n_{\gamma}^2(\theta, \phi)}{n_{\gamma}(\theta, \phi) + b_{\gamma}(\theta, \phi)} d\Omega \right]^{1/2}$$

signal

background noise

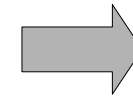
The background dominates, then:

Main halo's smooth component:

$$(S/N)_{\text{MainSm}} = f_{\text{MainSm}} \left[\frac{\tau A_{\text{eff}}}{b_{\gamma}} \right]^{1/2} \frac{F}{\theta_h}$$

Subhalo's smooth component:

$$(S/N)_{\text{SubSm}} = f_{\text{SubSm}} \left(\frac{\theta_h}{\theta_{\text{psf}}} \right) \left[\frac{\tau A_{\text{eff}}}{b_{\gamma}(\vec{\alpha})} \right]^{1/2} \frac{F}{(\theta_h^2 + \theta_{\text{psf}}^2)^{1/2}}$$



$$S/N \sim F / \theta$$

$$S/N \sim L / r_h d$$

Sub-substructure of a subhalo:

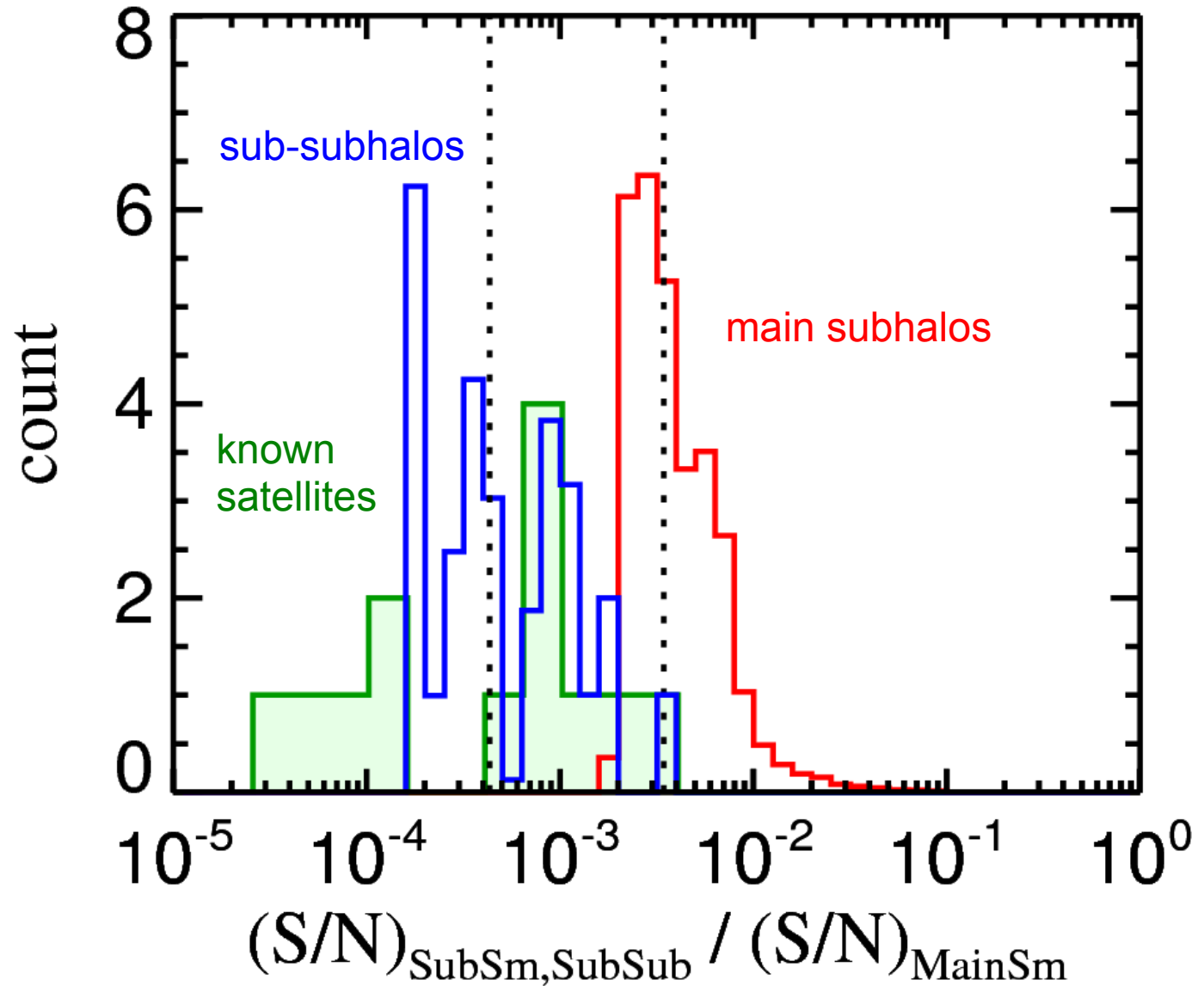
$$(S/N)_{\text{SubSub}} = f_{\text{SubSub}} \left(\frac{\theta_h}{\theta_{\text{psf}}} \right) \left[\frac{\tau A_{\text{eff}}}{b_{\gamma}(\vec{\alpha})} \right]^{1/2} \frac{F}{(\theta_h^2 + \theta_{\text{psf}}^2)^{1/2}}$$

Detectability of different annihilation emission components in the Milky Way

S/N for detecting subhalos in units of that for the main halo

30 highest S/N objects, assuming the use of optimal filters

$$S/N \propto C V_{\max}^4 / (r_{\text{half}}^2 d)$$



Highest S/N subhalos have 1% of S/N of main halo

Highest S/N subhalos have 10 times S/N of known satellites

Substructure of subhalos has no influence on detectability

But what about
other nearby
structures, like
galaxy clusters?



High resolution
“Phoenix” project

Gao et al. (2011)

The nearest massive galaxy clusters are attractive targets for annihilation detection

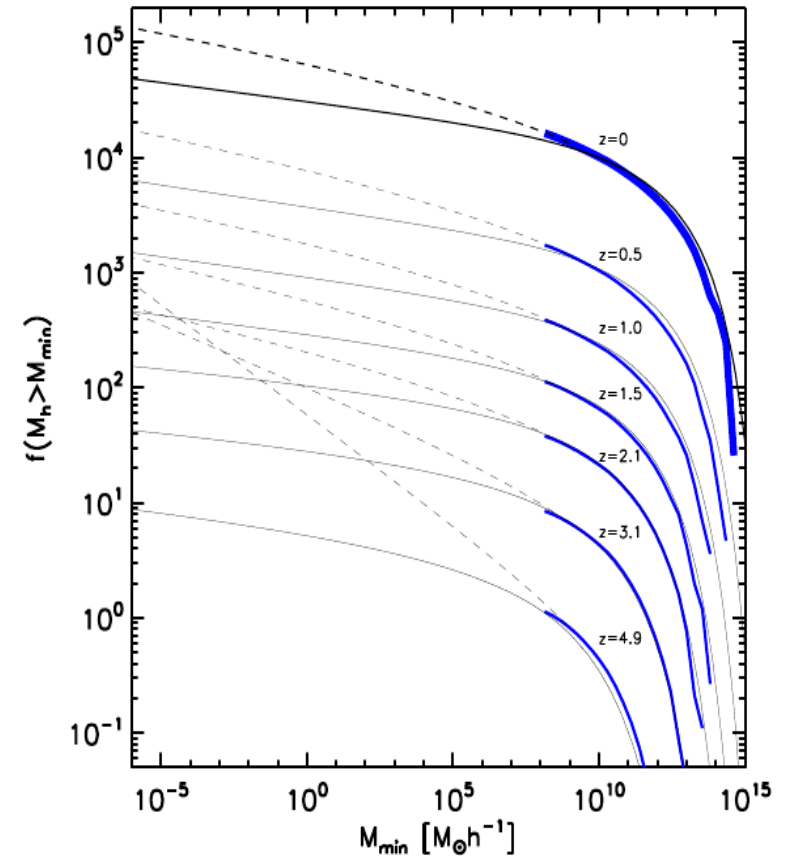
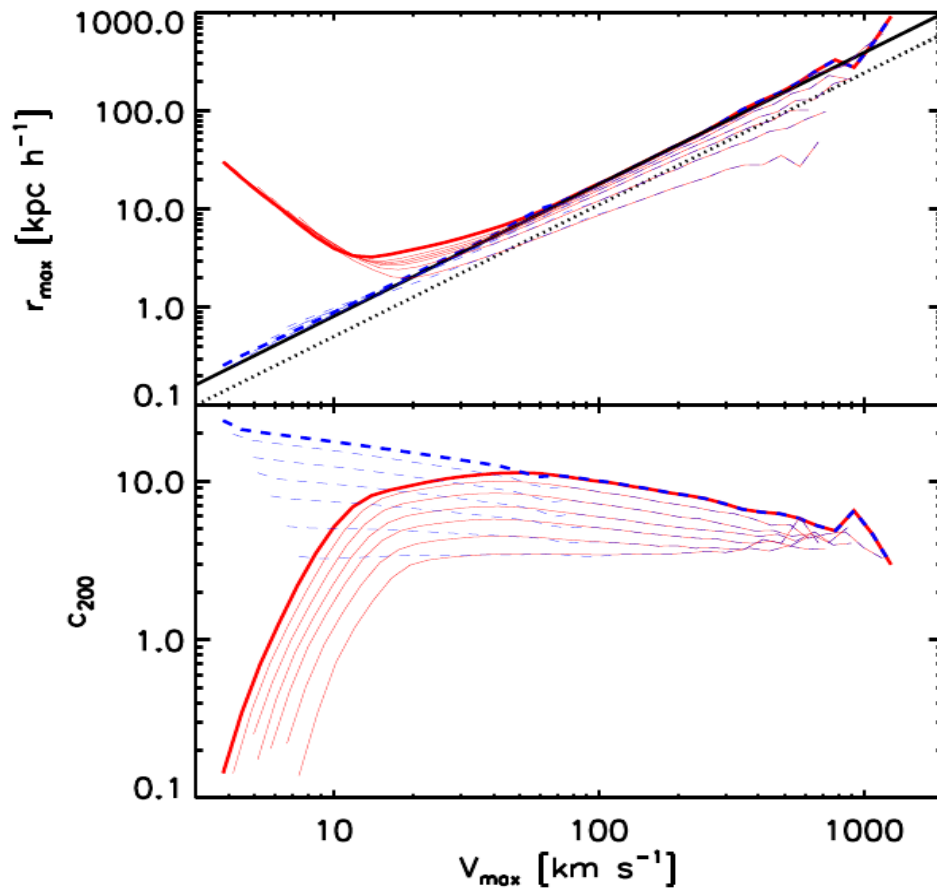
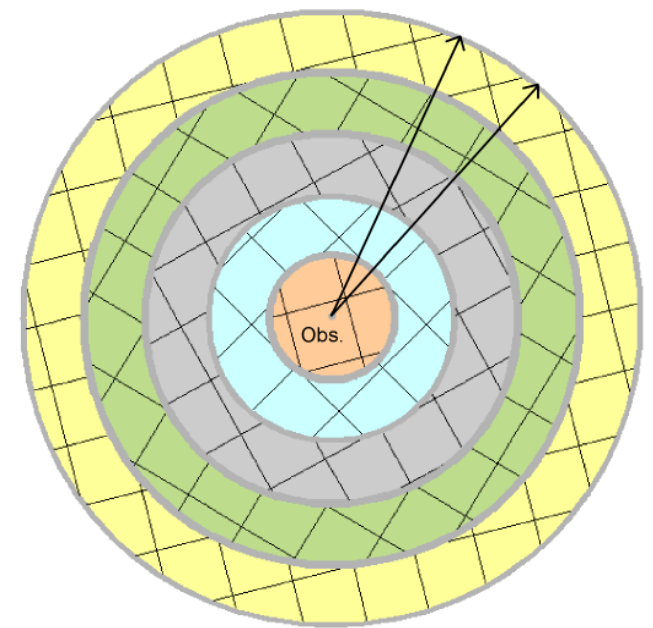
COMPARISON OF SIGNAL-TO-NOISE FOR DETECTION OF NEARBY SOURCES

Object Name	Half-light radius [arcmin]	Distance [Mpc]	M_{200} [M_{\odot}]	L [L_{mw}]	$F = L/(4\pi d^2)$ [F_{mw}]	S/N [$(S/N)_{\text{mw}}$]
AWM 7	35.5	67.0	4.2×10^{14}	7.1×10^4	3.2×10^{-4}	6.8×10^{-3}
Fornax Cluster	84.1	17.5	1.0×10^{14}	1.2×10^4	8.0×10^{-4}	7.3×10^{-3}
M49	59.6	18.2	0.4×10^{14}	3.9×10^3	2.4×10^{-4}	3.1×10^{-3}
NGC 4636	52.6	17.4	0.24×10^{14}	2.1×10^3	1.4×10^{-4}	2.0×10^{-3}
Centaurus (A3526)	40.1	50.5	2.6×10^{14}	3.9×10^4	3.1×10^{-4}	5.8×10^{-3}
Coma	36.1	95.8	1.3×10^{15}	2.9×10^5	6.4×10^{-4}	1.3×10^{-2}
Draco	16.4	0.082	N/A	5.2×10^{-3}	1.6×10^{-5}	6.3×10^{-4}
UMaI	18.4	0.066	N/A	4.3×10^{-3}	2.0×10^{-5}	7.5×10^{-4}
LeoI	4.4	0.25	N/A	3.5×10^{-3}	1.2×10^{-6}	8.2×10^{-5}
Fornax dwarf	5.9	0.138	N/A	2.0×10^{-3}	2.2×10^{-6}	1.5×10^{-4}
LeoII	2.5	0.205	N/A	8.5×10^{-4}	4.1×10^{-7}	3.1×10^{-5}
Carina	4.6	0.101	N/A	7.1×10^{-4}	1.4×10^{-6}	1.0×10^{-4}
Sculpt	13.2	0.079	N/A	3.2×10^{-3}	1.0×10^{-5}	4.9×10^{-4}
Sext	3.3	0.086	N/A	3.0×10^{-4}	8.3×10^{-7}	6.1×10^{-5}
UMaII	28.8	0.032	N/A	2.6×10^{-3}	5.2×10^{-5}	1.3×10^{-3}
Comber	15.9	0.044	N/A	1.6×10^{-4}	1.7×10^{-5}	6.8×10^{-4}
WillI	17.7	0.066	N/A	3.9×10^{-3}	1.8×10^{-5}	7.0×10^{-4}
LMC	82.5	0.049	N/A	3.8×10^{-2}	3.3×10^{-4}	3.1×10^{-3}
SMC	45.5	0.061	N/A	1.9×10^{-2}	1.1×10^{-4}	1.8×10^{-3}
M31	351.5	0.807	1.8×10^{12}	1.3×10^2	4.2×10^{-3}	9.3×10^{-3}

The Millennium-II simulation can be used to construct full backwards lightcones of the expected gamma-ray annihilation background

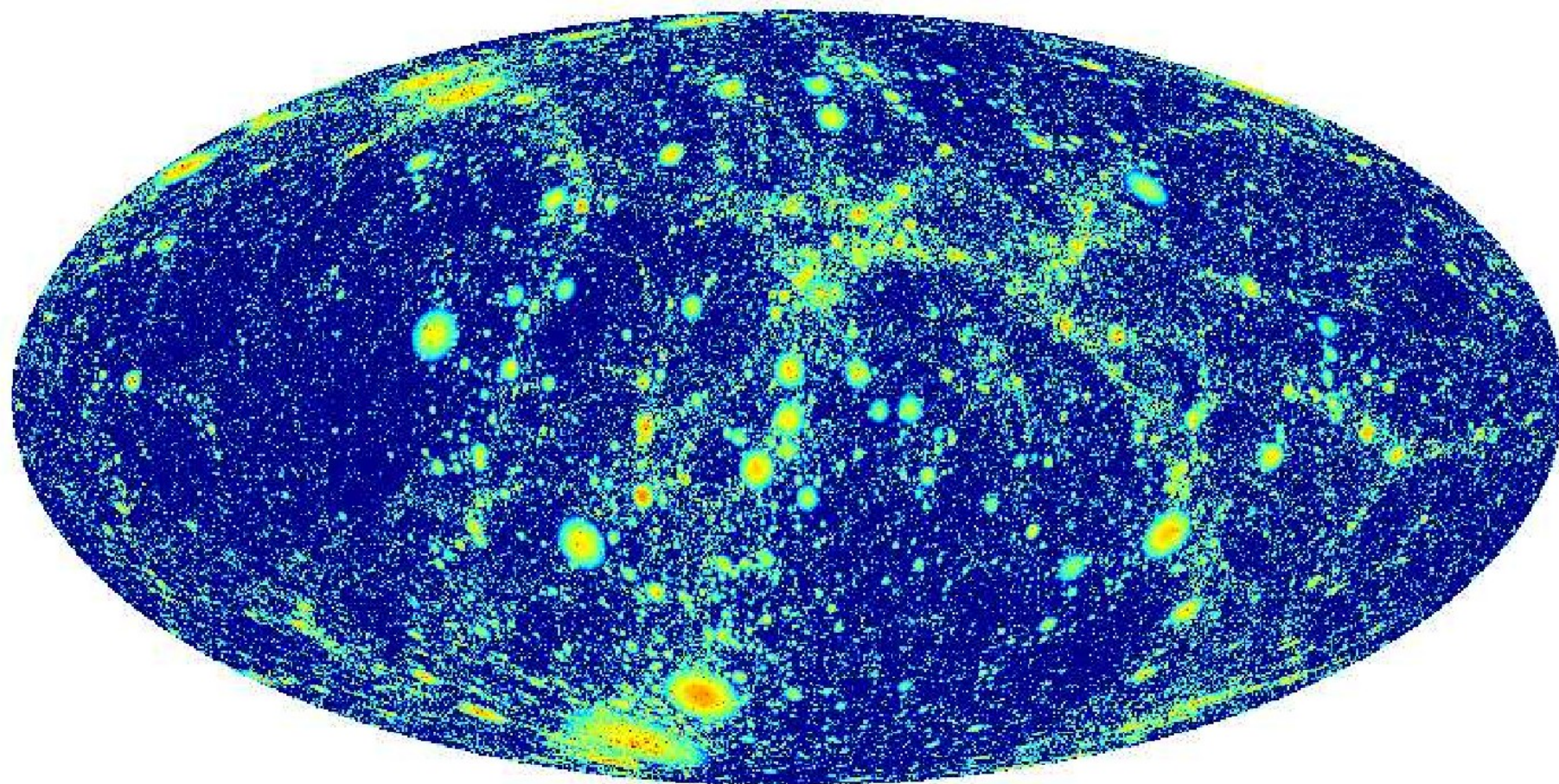
SIMULATION BOX STACKING AND EXTRAPOLATION OF HALO PROPERTIES

Zavala, Springel & Boylan-Kolchin (2010)



Thin redshift slices of the gamma-ray background reveal cosmic large-scale structure

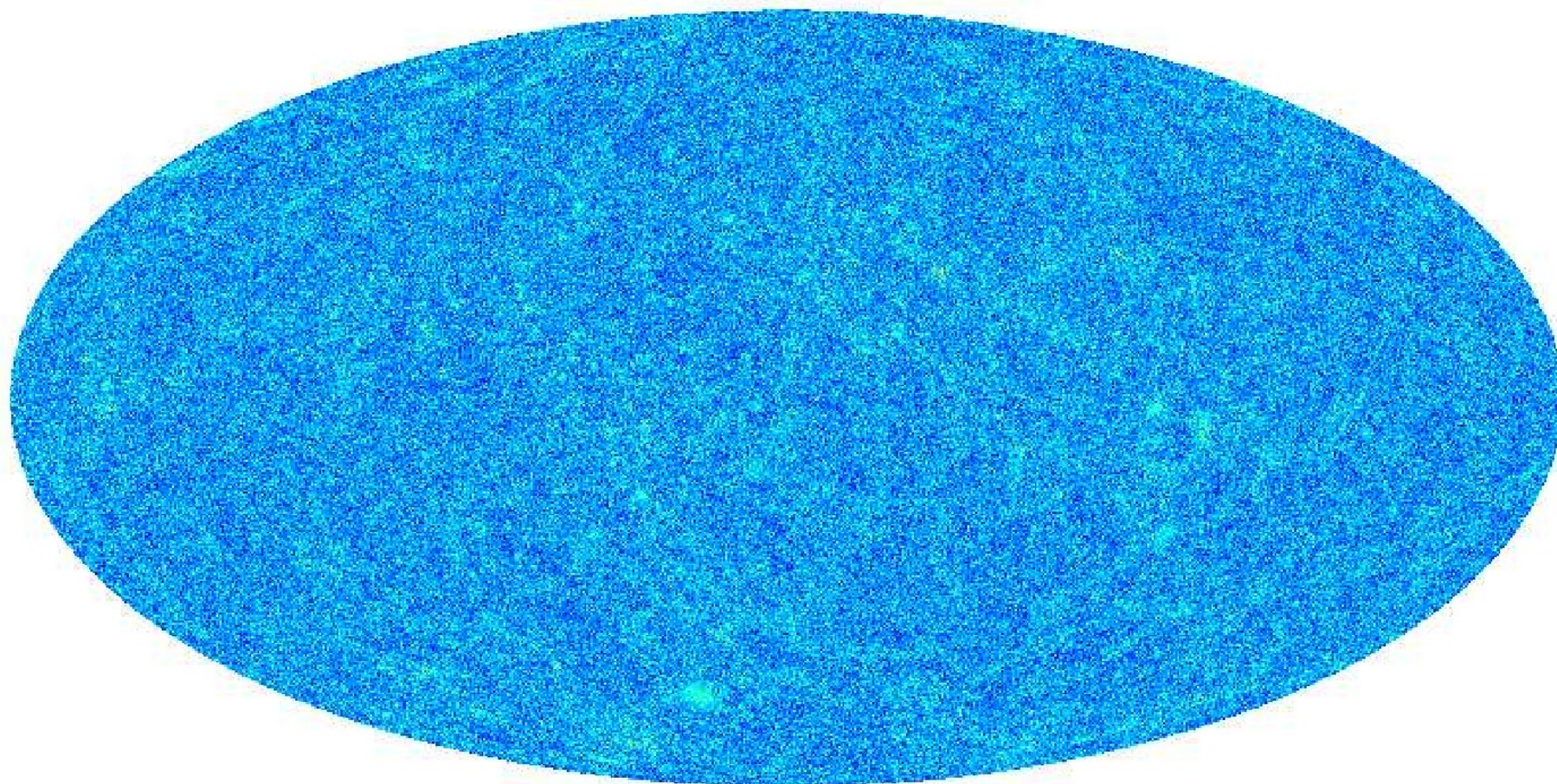
A PARTIAL MAP AT ENERGY 10 GEV NEAR Z~0



-15.1  -8.1 $\text{Log} (I_{\gamma,0})$

In the complete coadded map, individual structures vanish in the high background level except for very near halos

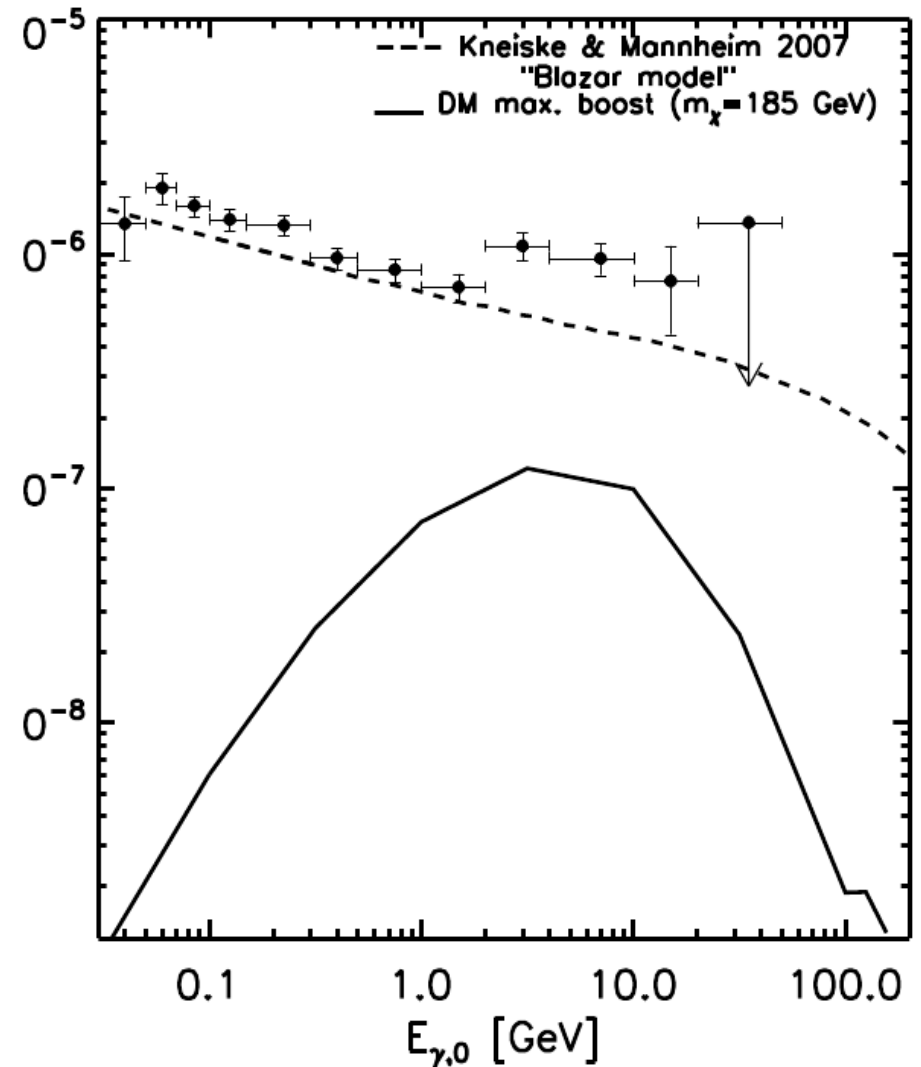
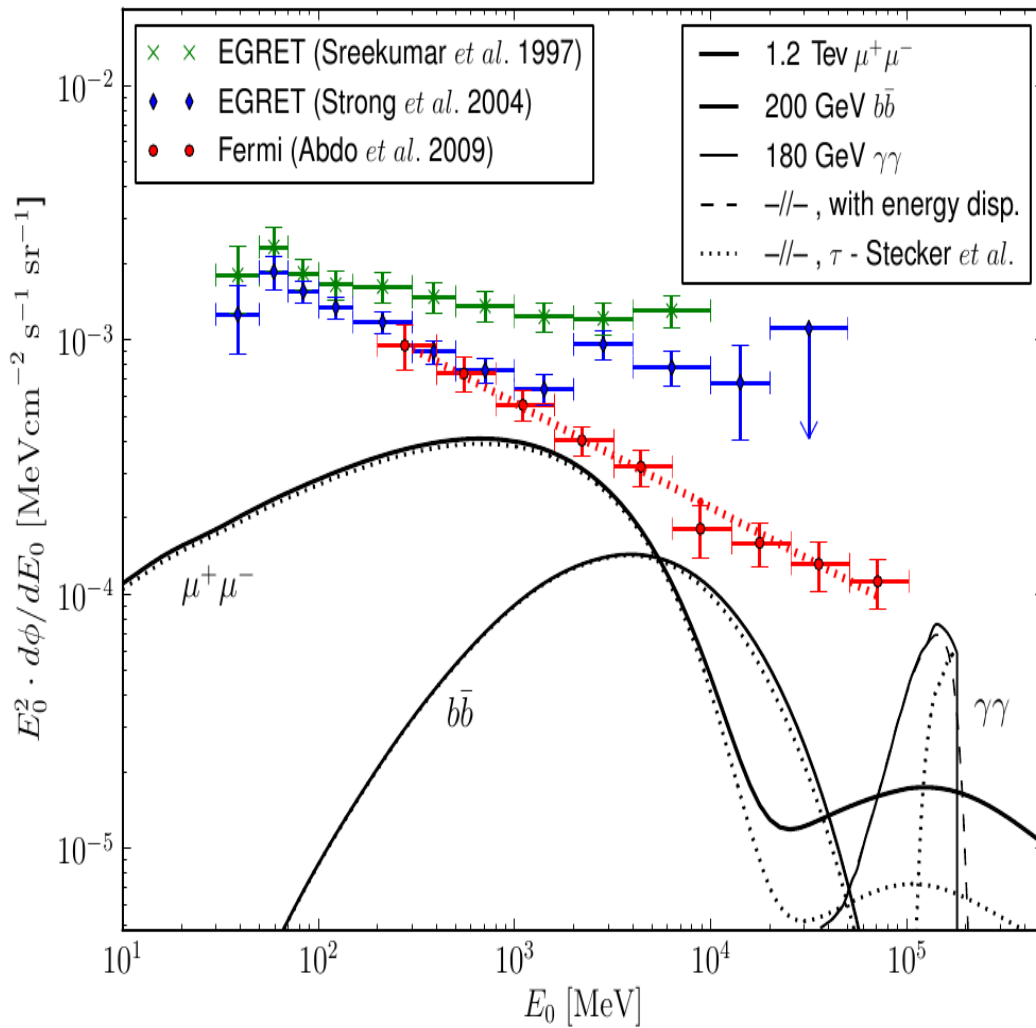
THE FULL BACKGROUND MAP OUT TO REDSHIFT $Z = 10$



-11.0  -8.0 $\text{Log} (L_{\gamma,0})$

The full-sky maps can be used to extract direct predictions for the properties of the background

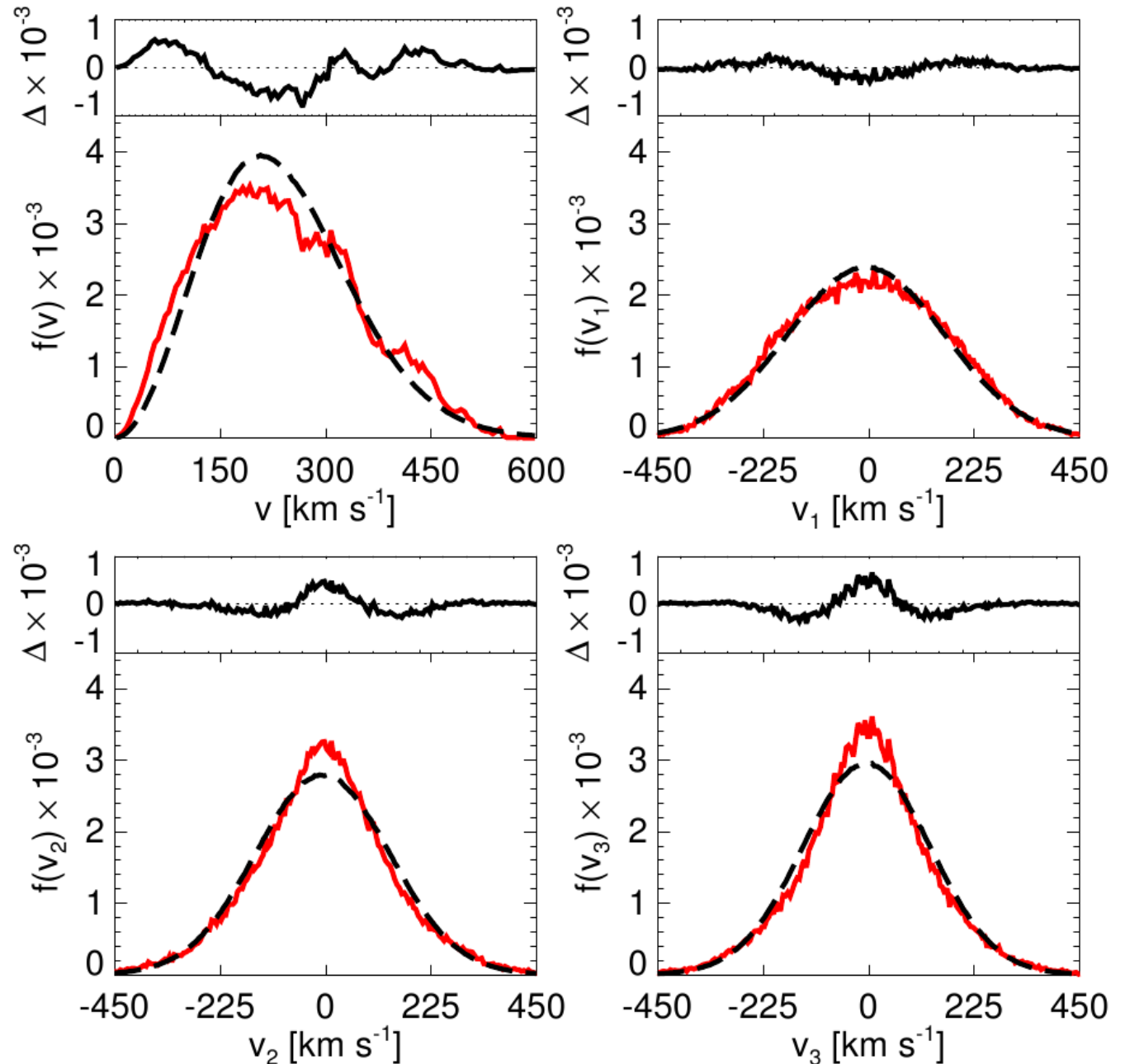
ENERGY SPECTRUM OF THE BACKGROUND



Residual structure in energy space

The velocity distribution of dark matter at the Sun's position shows residual structure

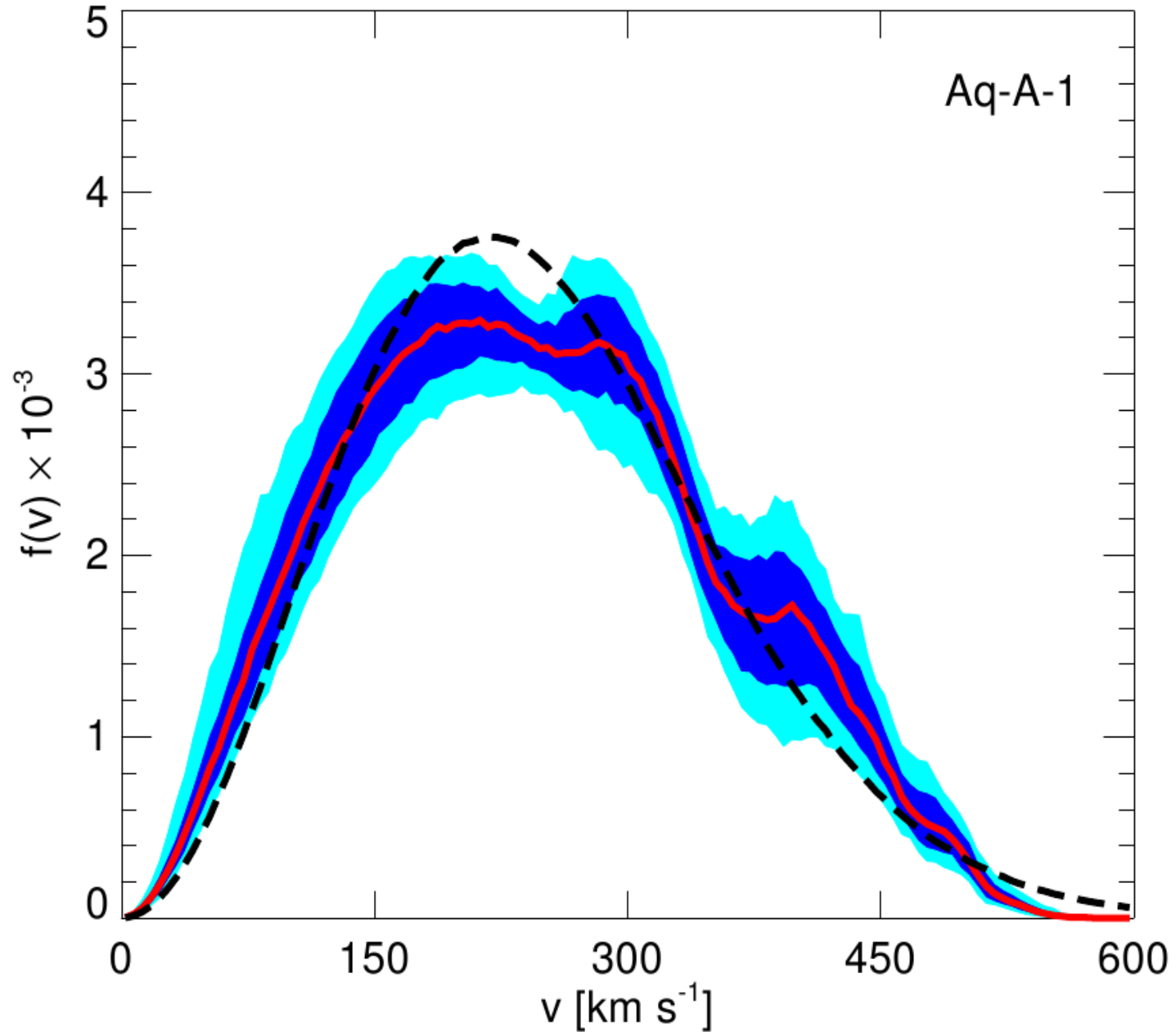
DISTRIBUTION OF VELOCITY COMPONENTS AND VELOCITY MODULUS



Vogelsberger et al. (2009)

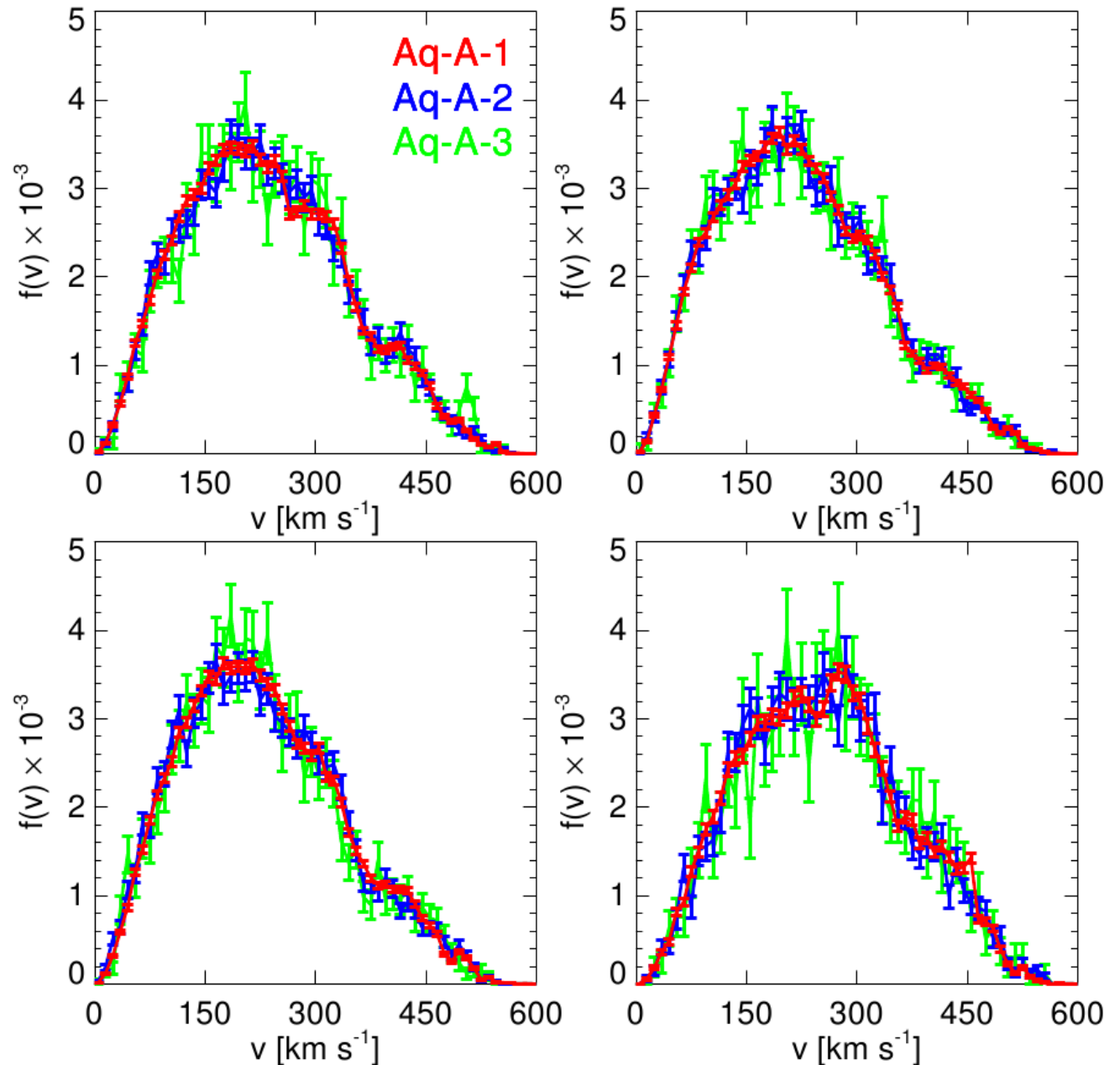
Wiggles in the distribution of the modulus of the velocity point to residual structure in energy space

DISTRIBUTION OF THE VELOCITY MODULUS



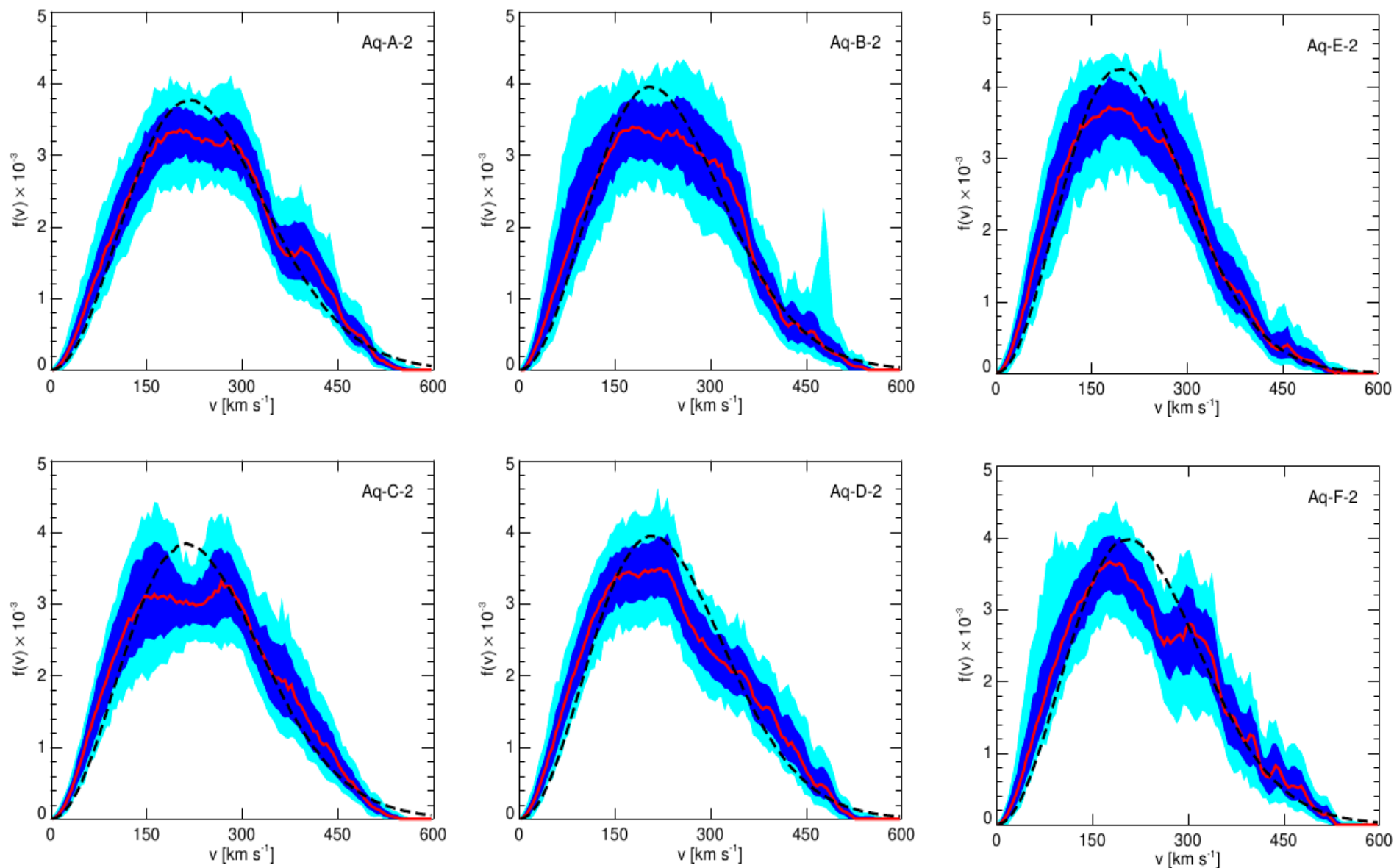
The wiggles are the same in well-separated boxes at the same radial distance, and are reproduced in simulations of different resolution

DISTRIBUTION OF THE VELOCITY MODULUS IN DIFFERENT WELL-SEPARATED BOXES



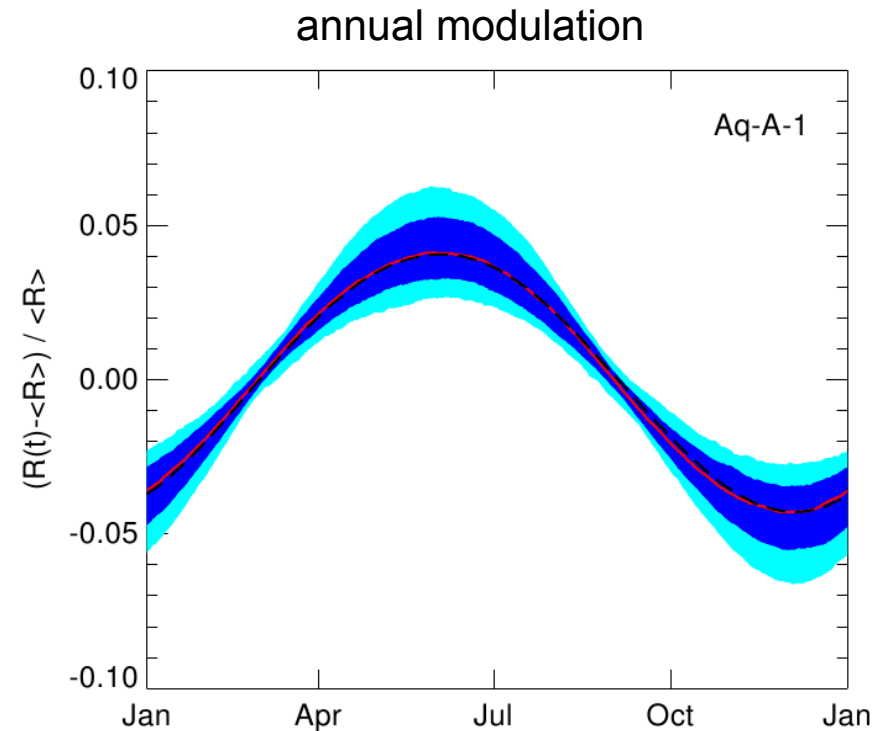
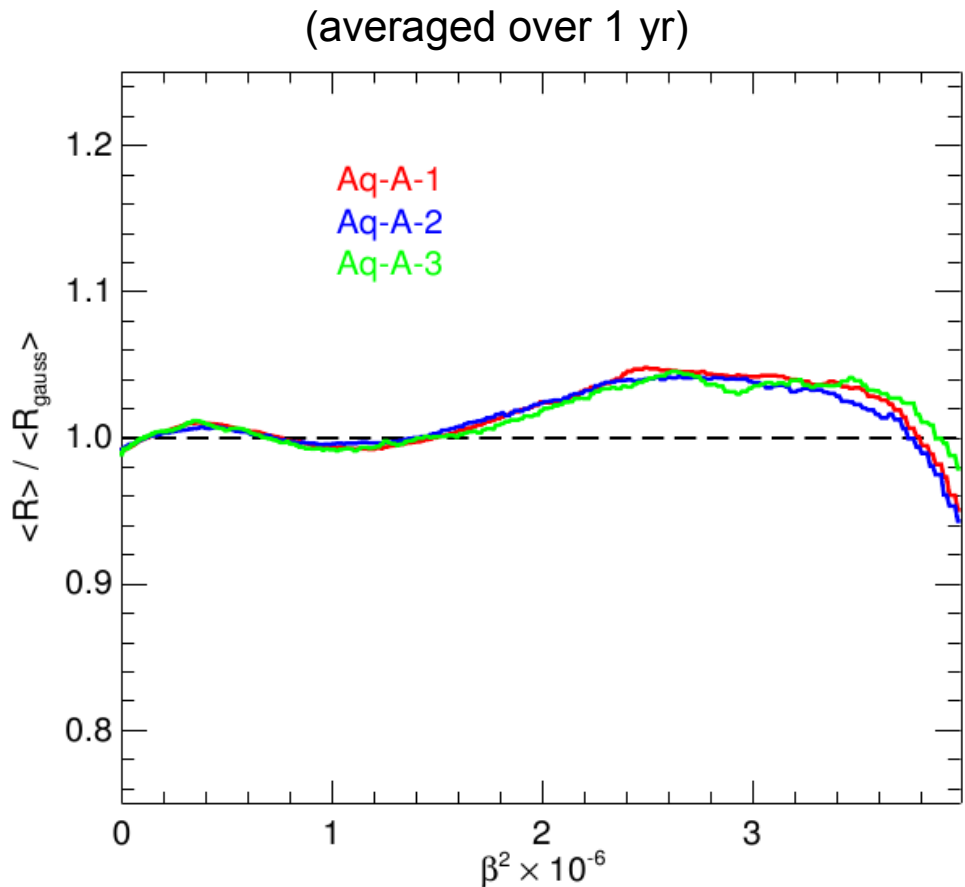
The velocity wiggles are generic and reflect the formation history of the halo

VELOCITY MODULUS IN THE SIX AQUARIUS HALOS



The non-Gaussian features in the velocity distribution imply ~10% corrections in the count rates of WIMP recoil searches

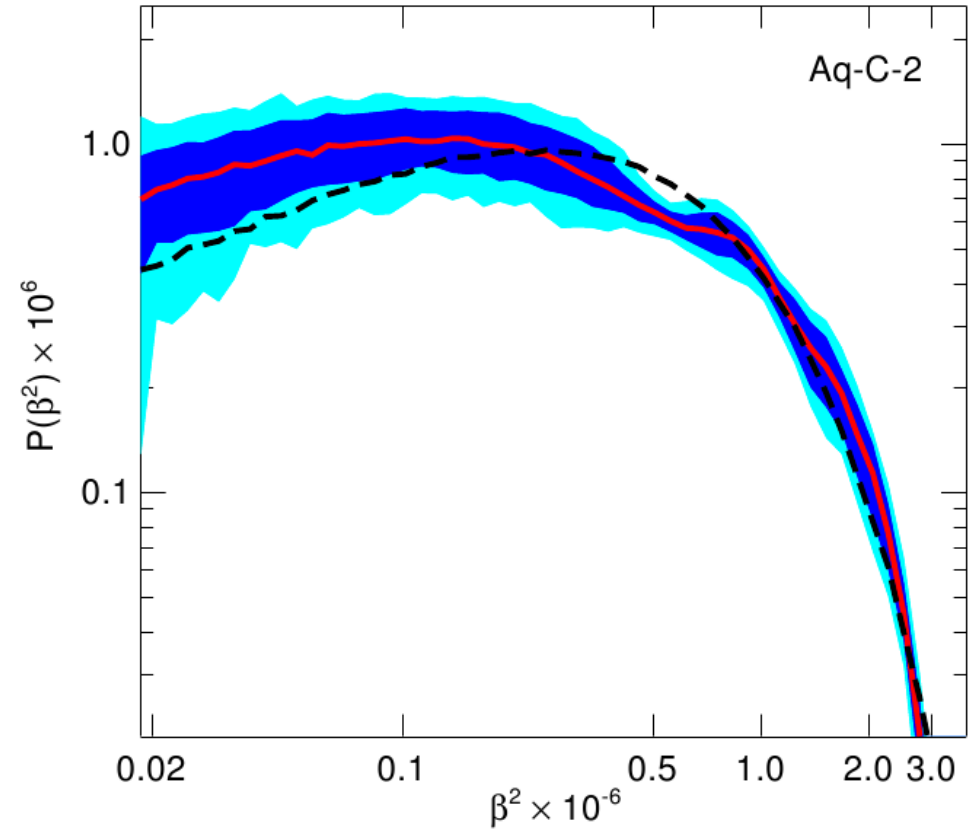
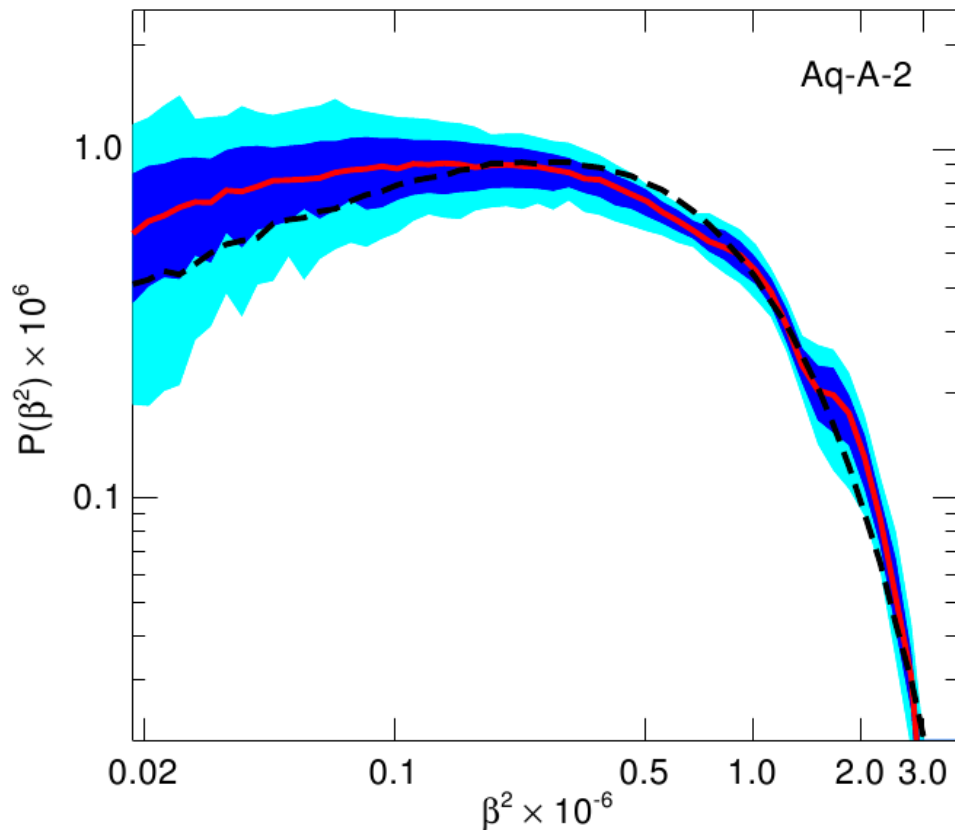
IMPACT ON THE COUNT RATES FOR TYPICAL DIRECT DETECTION EXPERIMENTS



$$R = \mathcal{R} \rho_0 T(E, t) \quad T(E, t) = \int_{v_{\min}}^{\infty} dv \frac{f_v(t)}{v} \quad v_{\min} = \left(\frac{E (m_\chi + m_A)^2}{2m_\chi^2 m_A} \right)^{1/2}$$

If dark matter consists of **axions**, their energy spectrum can be accurately measured – this would be **dark matter astronomy!**

PREDICTED CAVITY POWER AS A FUNCTION OF FREQUENCY

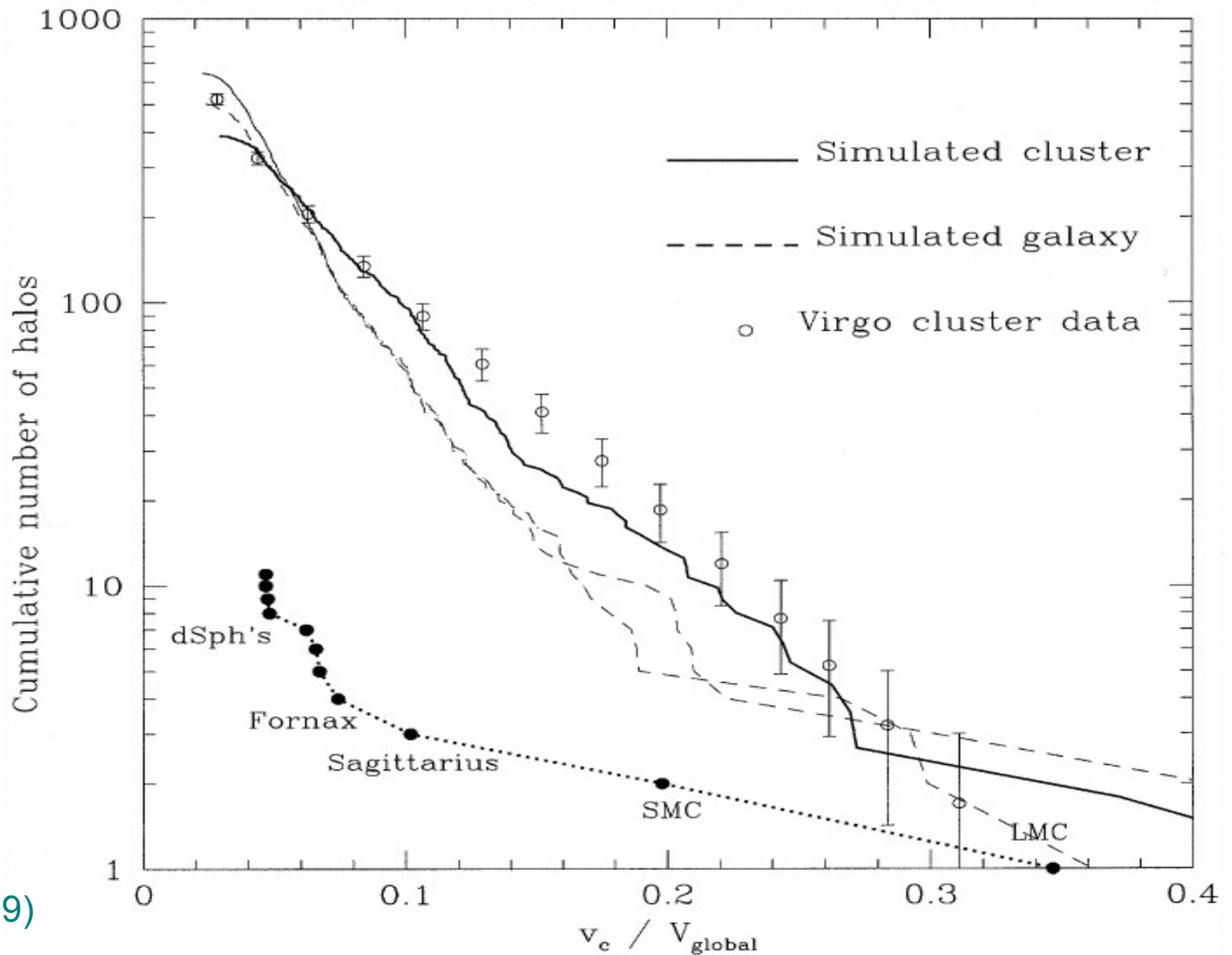


—▶ The non-Gaussian bumps and wiggles are in principle measurable and provide information about the formation history of the Milky Way

The satellite abundance issue

Taken at face value, the number of luminous satellites in the Milky Way is much smaller than the number of dark matter lumps

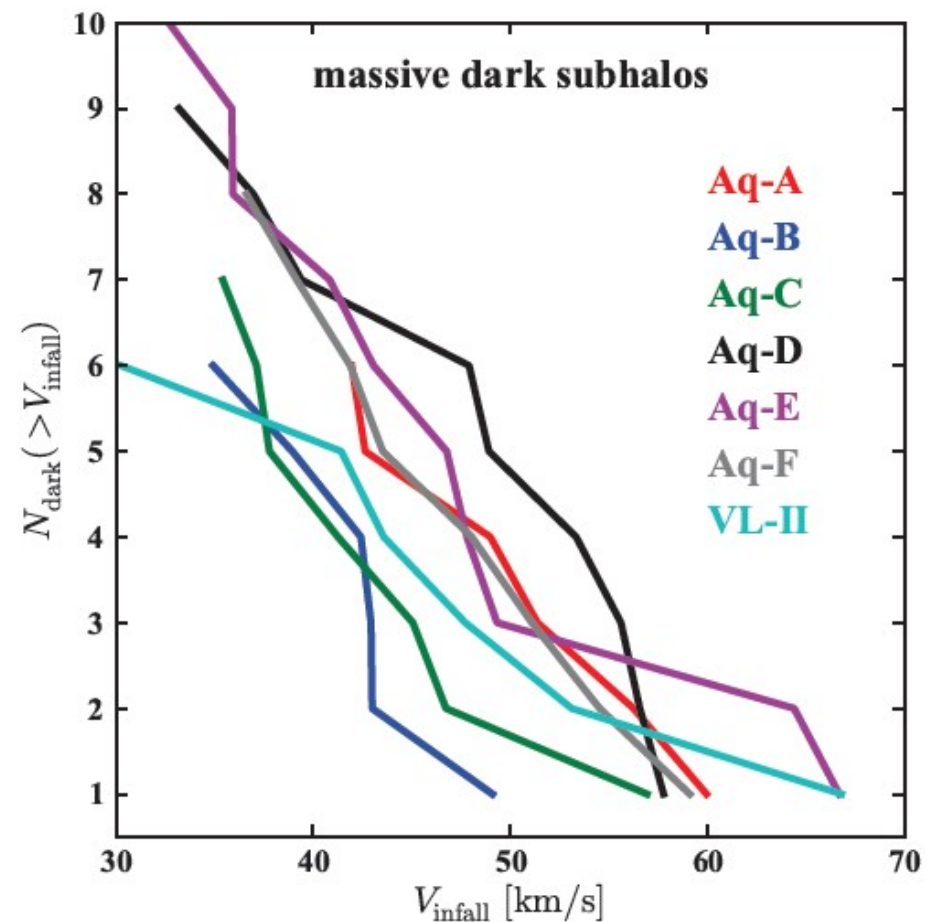
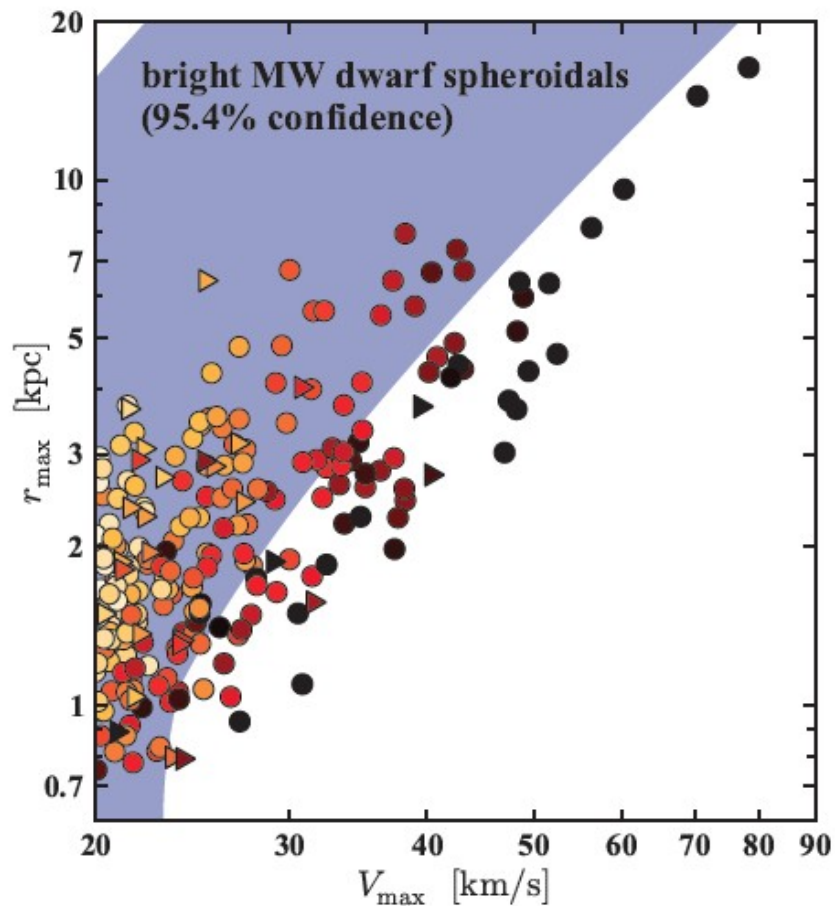
THE SATELLITE PROBLEM



Moore et al. (1999)

Relatively dense massive subhalos are predicted that apparently cannot host any of the luminous satellites of the Milky Way

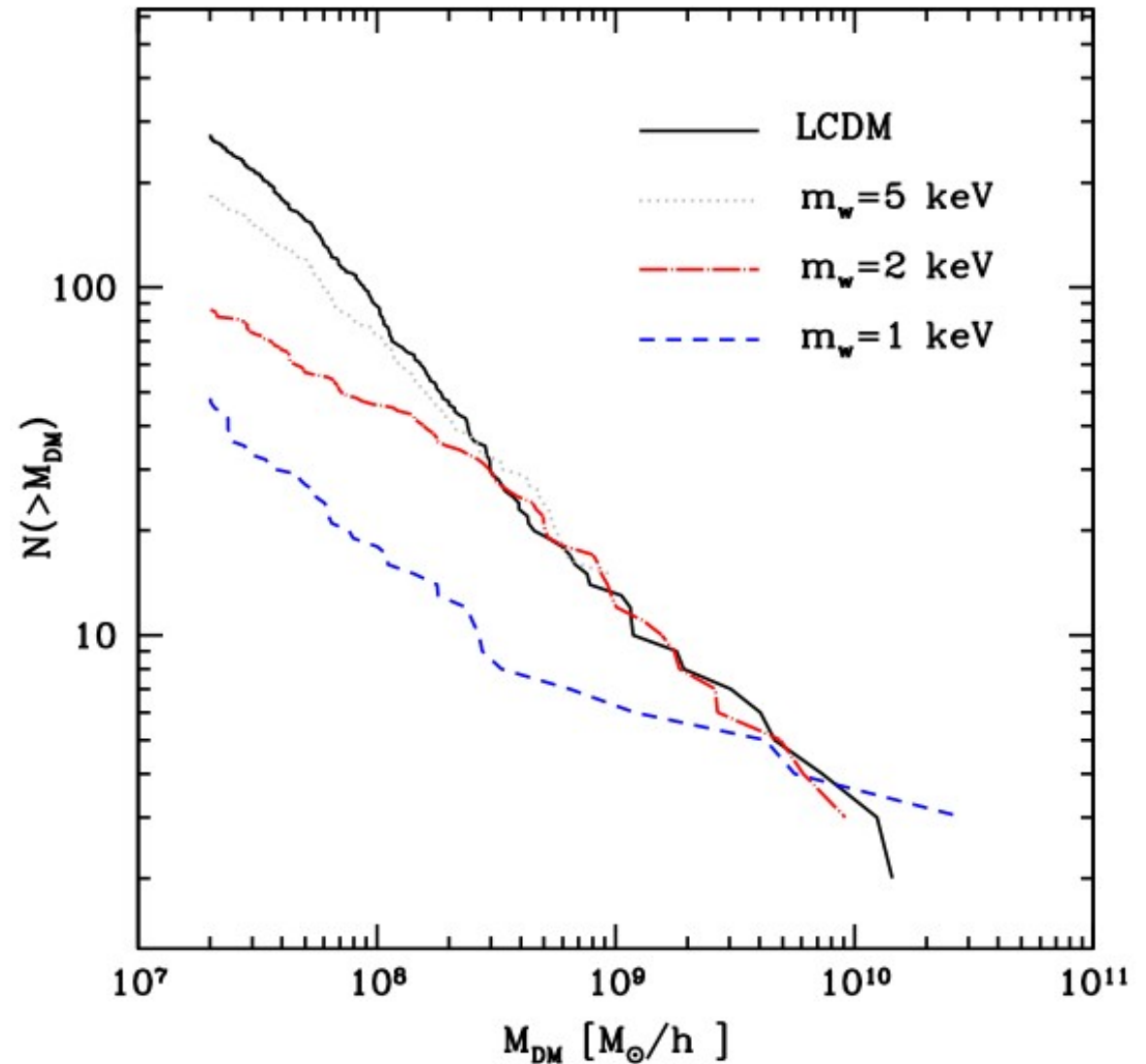
THE PUZZLING DARKNESS OF SOME OF THE LARGE DARK MATTER SATELLITES



Boylan-Kolchin, Bullock & Kaplinghat (2011)

Warm dark matter models also reduce the number of Milky Way satellites substantially – for 1 keV there are still enough

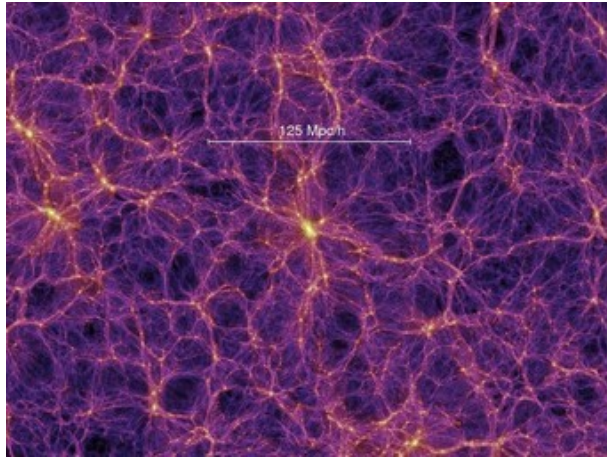
SATELLITE ABUNDANCE AS A FUNCTION OF DM PARTICLE MASS



Maccio & Fontanot (2010)

Basics of collisionless simulations

Why are **cosmological simulations** of structure formation useful for studying the dark universe?



Simulations are the theoretical tool of choice for calculations in the non-linear regime.

They connect the (simple) cosmological initial conditions with the (complex) present-day universe.

Predictions from N-body simulations:

- Abundance of objects (as a function of mass and time)
- Their spatial distribution
- Internal structure of halos (e.g. density profiles, spin)
- Mean formation epochs
- Merger rates
- Detailed dark matter distribution on large *and* fairly small scales
- Galaxy formation models
- Gravitational lensing
- Baryonic acoustic oscillations in the matter distribution
- Integrated Sachs-Wolfe effect
- Dark matter annihilation rate
- Morphology of large-scale structure (“cosmic web”)
-

The N-body approach to collisionless dynamics

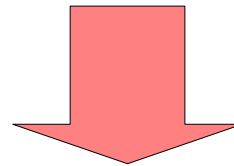
BASIC MONTE-CARLO IDEA

Collisionless
Boltzmann equation

Poisson-Vlasov System

$$\frac{df}{dt} = \frac{\partial f}{\partial t} + \frac{\partial f}{\partial \mathbf{x}} \cdot \mathbf{v} + \frac{\partial f}{\partial \mathbf{v}} \cdot \left(-\frac{\partial \Phi}{\partial \mathbf{x}} \right) = 0$$

$$\nabla^2 \Phi(\mathbf{x}, t) = 4\pi G \int f(\mathbf{x}, \mathbf{v}, t) d\mathbf{v}$$



N-body System

$$\ddot{\mathbf{x}}_i = -\nabla_i \Phi(\mathbf{x}_i)$$

$$\Phi(\mathbf{x}) = -G \sum_{j=1}^N \frac{m_j}{[(\mathbf{x} - \mathbf{x}_j)^2 + \epsilon^2]^{1/2}}$$

need large **N**

Several questions come up when we try to use the N-body approach for collisionless simulations

- How do we compute the gravitational forces efficiently and accurately?
- How do we integrate the orbital equations in time?
- How do we generate appropriate initial conditions?
- How do we parallelize the simulation?

$$\ddot{\mathbf{x}}_i = -\nabla_i \Phi(\mathbf{x}_i)$$

$$\Phi(\mathbf{x}) = -G \sum_{j=1}^N \frac{m_j}{[(\mathbf{x} - \mathbf{x}_j)^2 + \epsilon^2]^{1/2}}$$

Note: The naïve computation of the forces is an N^2 -task.

Initial conditions generation

In special cases, the distribution function for static solutions of the CBE can be constructed analytically

An integral of motion $I = I(\mathbf{x}(t), \mathbf{v}(t))$ is constant along orbits, i.e.: $\frac{dI}{dt} = 0$

————▶ Then I is a solution of the CBE.

Jeans theorem: Steady-state solutions of the CBE only depend on integrals of motion.

For a spherical mass distribution, a DF that only depends on energy can be constructed with **Eddington's formula**.

Example:

Hernquist halo:
$$\rho(r) = \frac{M}{2\pi} \frac{a}{r(r+a)^3}$$

$$f(E) = \frac{1}{\sqrt{2}(2\pi)^3 (GMa)^{3/2}} \frac{\sqrt{e}}{(1-e)^2} \left[(1-2e)(8e^2 - 8e - 3) + \frac{3 \sin^{-1}(\sqrt{e})}{\sqrt{e(1-e)}} \right]$$

where: $e = -\frac{aE}{GM}$ $E = \frac{\mathbf{v}^2}{2} + \Phi$

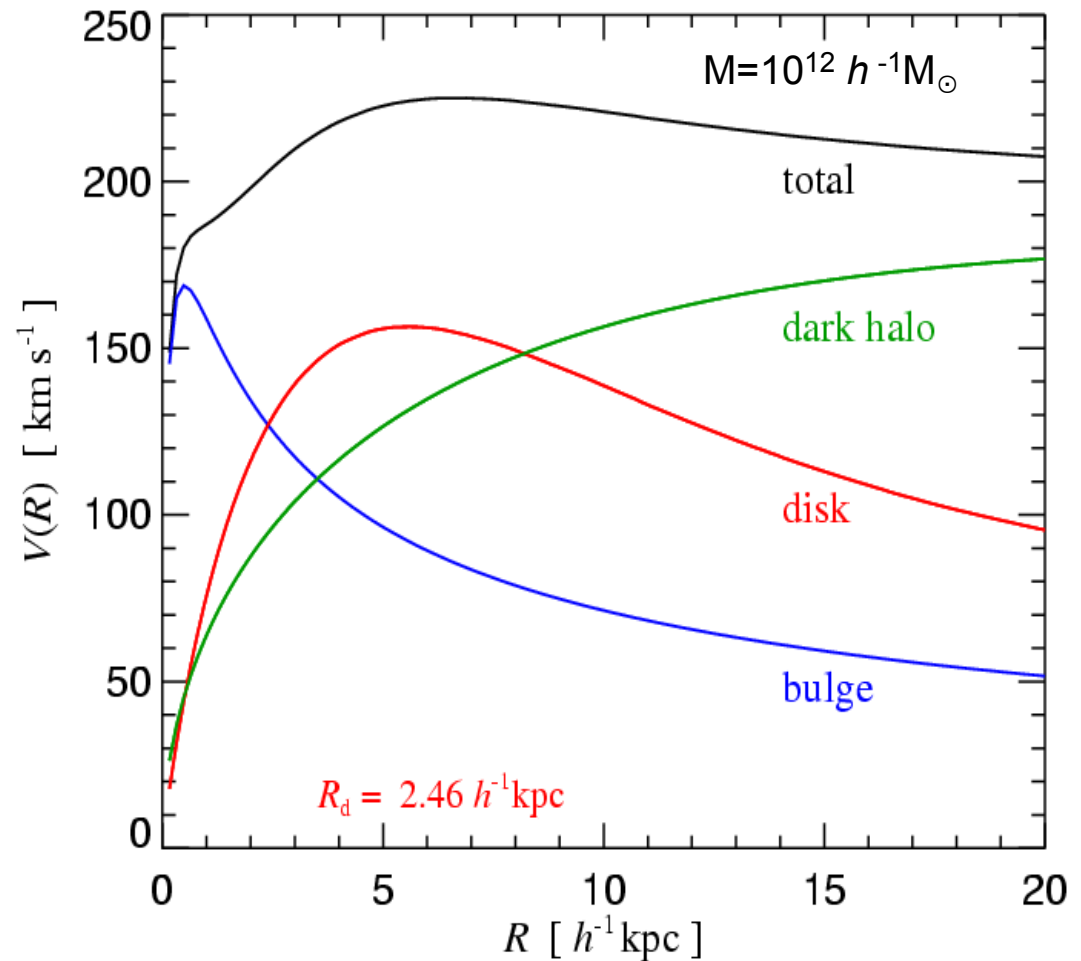
Construction of compound disk galaxies that are in dynamical equilibrium

STRUCTURAL PROPERTIES OF MODEL GALAXIES

Components:

- Dark halo (Hernquist profile matched to NFW halo)
- Stellar disk (exponential)
- Stellar bulge
- Gaseous disk (exponential)
- Central supermassive black hole

One approach: Compute the exact gravitational potential for the axisymmetric mass distribution and solve the **Jeans equations**



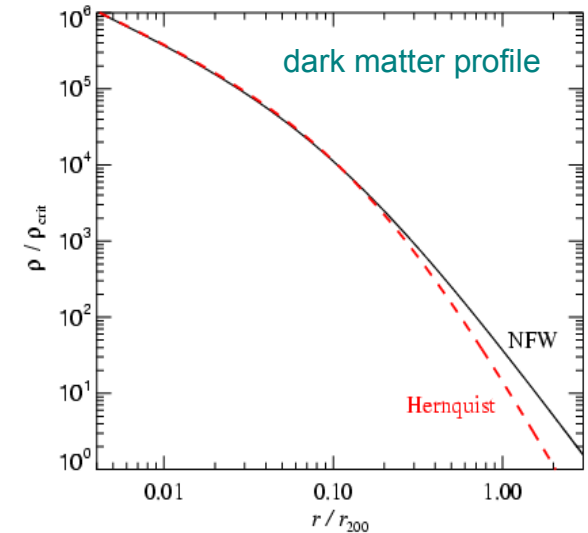
The first step in constructing an isolated galaxy model is the specification of the density structure of all mass components

DENSITY DISTRIBUTIONS OF DARK MATTER AND STARS IN BULGE AND DISK

Dark matter:

$$\rho_{\text{dm}}(r) = \frac{M_{\text{dm}}}{2\pi} \frac{a}{r(r+a)^3}$$

Hernquist or NFW profile



Stars in the disk:

$$\Sigma_{\star}(r) = \frac{M_{\star}}{2\pi h^2} \exp(-r/h)$$

“Isothermal sheet” with exponential profile

$$\rho_{\star}(R, z) = \frac{M_{\star}}{4\pi z_0 h^2} \text{sech}^2\left(\frac{z}{2z_0}\right) \exp\left(-\frac{R}{h}\right)$$

Disk scale length h determined by spin parameter of halo.

Stars in the bulge:

$$\rho_{\text{b}}(r) = \frac{M_{\text{b}}}{2\pi} \frac{b}{r(r+b)^3}$$

Bulge scale length b can be set to a fraction of the disk scale-length h .

Gas in the disk:

$$\Sigma_{\text{gas}}(r) = \frac{M_{\text{gas}}}{2\pi h^2} \exp(-r/h)$$

Vertical structure given by hydrostatic equilibrium.
Depends on the equation of state of the gas.

$$-\frac{1}{\rho_{\text{g}}} \frac{\partial P}{\partial z} - \frac{\partial \Phi}{\partial z} = 0$$

Solving the Jeans equations allows the construction of dynamically stable disk galaxy models

MOMENT EQUATIONS FOR THE VELOCITY STRUCTURE

We assume that the **velocity distribution function** of dark matter and stars can be approximated everywhere by a **triaxial Gaussian**.

Further, we assume axisymmetry, and that the distribution function depends only on E and L_z

Then cross-moments vanish:

$$\langle v_R v_z \rangle = \langle v_z v_\phi \rangle = \langle v_R v_\phi \rangle = 0$$
$$\langle v_R \rangle = \langle v_z \rangle = 0$$

The radial and vertical moments are given by:

$$\langle v_z^2 \rangle = \langle v_R^2 \rangle = \frac{1}{\rho} \int_z^\infty \rho(z', R) \frac{\partial \Phi}{\partial z'} dz'$$

The azimuthal dispersion fulfills a separate equation:

$$\langle v_\phi^2 \rangle = \langle v_R^2 \rangle + \frac{R}{\rho} \frac{\partial (\rho \langle v_R^2 \rangle)}{\partial R} + v_c^2$$

Circular velocity: $v_c^2 \equiv R \frac{\partial \Phi}{\partial R}$

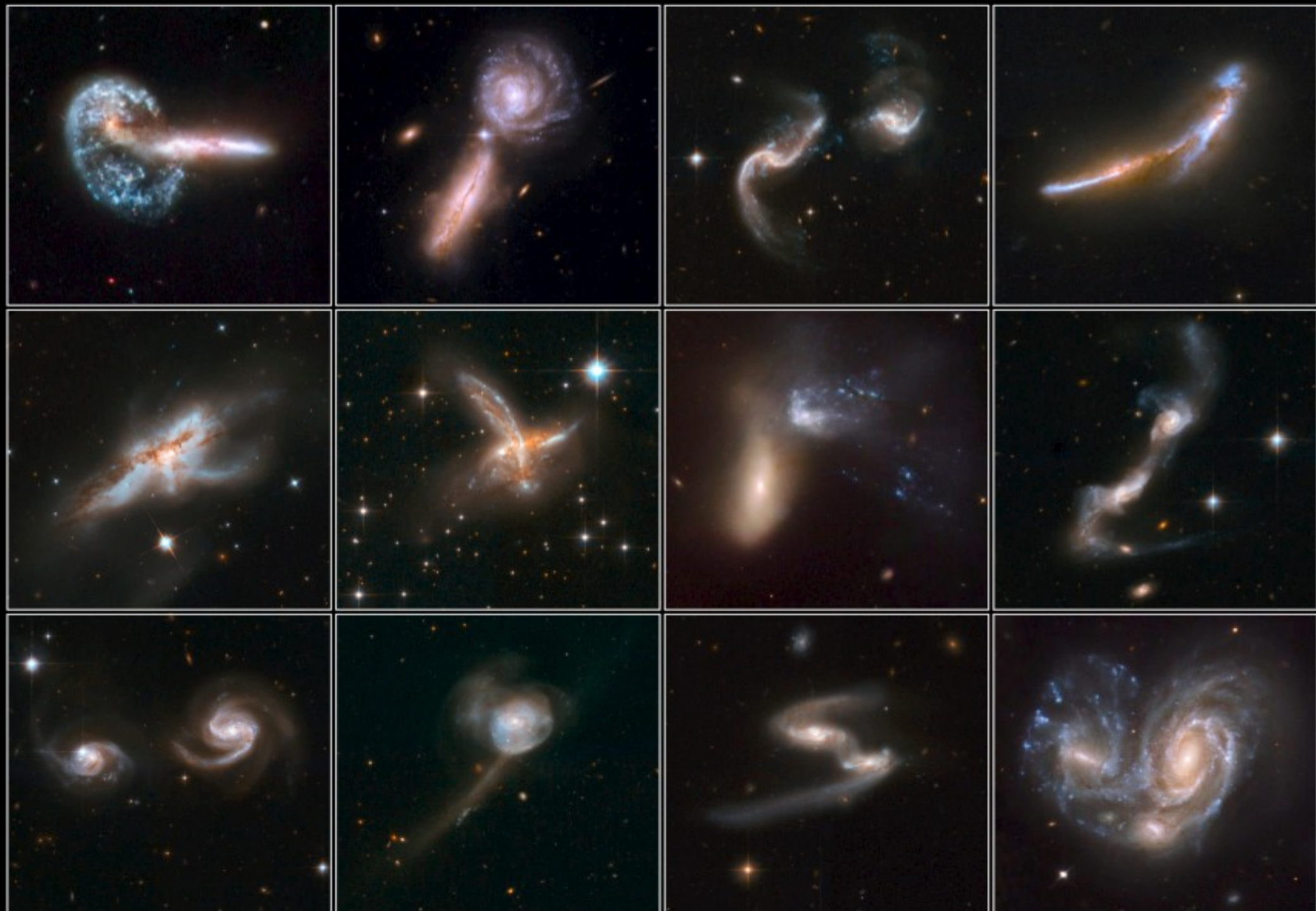
A remaining freedom lies in the azimuthal streaming $\langle v_\phi \rangle$, which is not determined by the above assumptions. For the dark matter, it can be set to zero, or to a value corresponding to a prescribed spin.

$$\sigma_\phi^2 = \langle v_\phi^2 \rangle - \langle v_\phi \rangle^2$$

Note: For the stellar disk, we instead use the epicycle theory to relate radial and vertical dispersions.

Interacting Galaxies

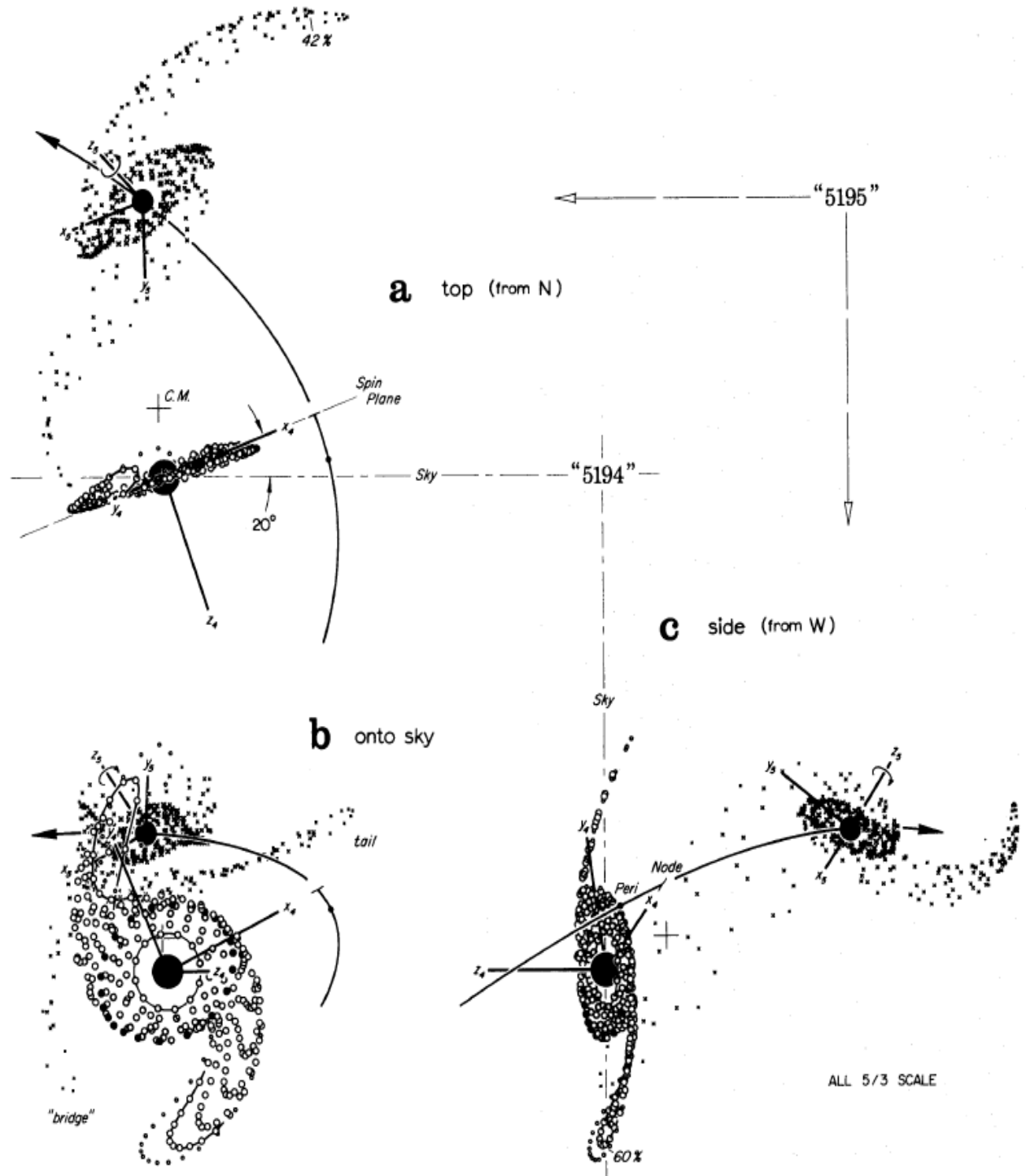
Hubble Space Telescope • ACS/WFC • WFPC2



The famous **merger hypothesis** conjectures that tidal features around galaxies occur in collisions which ultimately produce spheroidals

TOOMRE & TOOMRE (1972 !)

Restricted three-body simulations

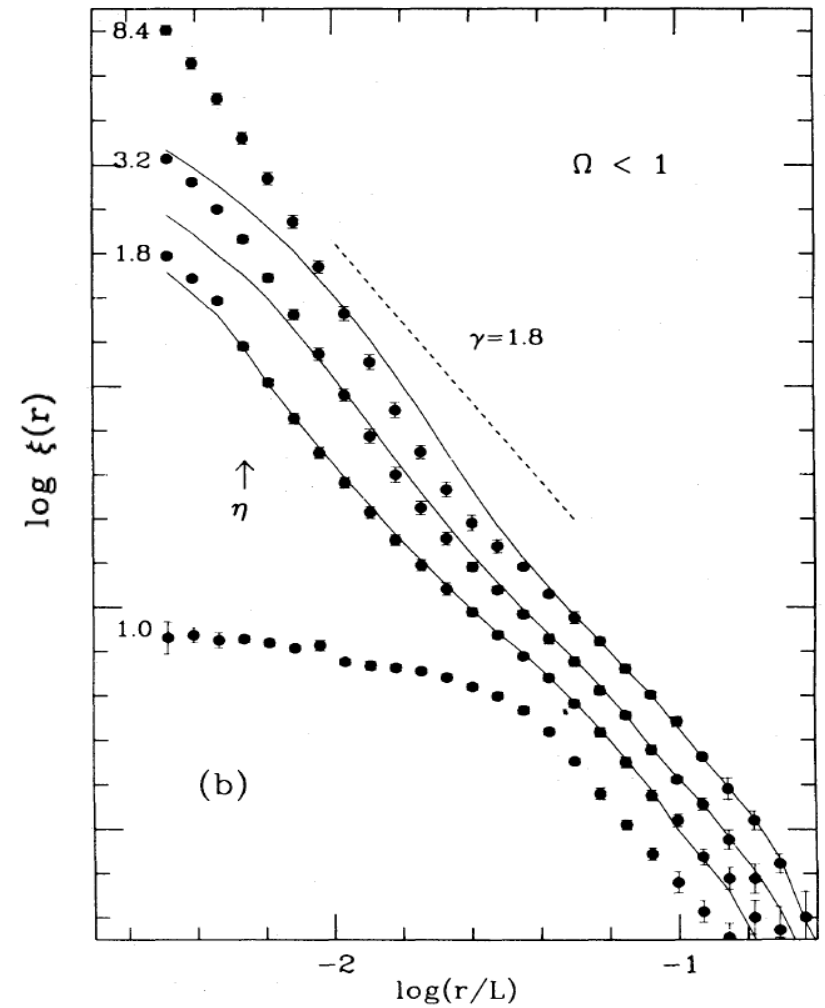
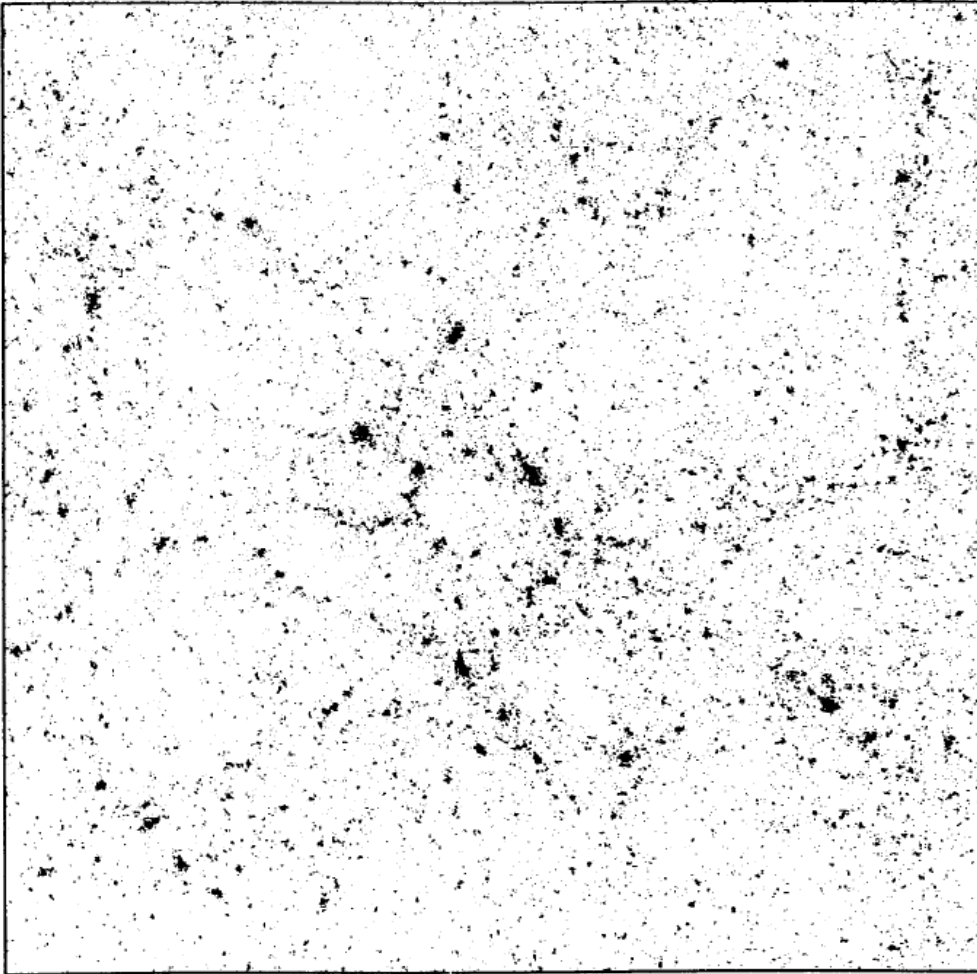


A model for the interaction of M51 and NGC 5195

More important than particle number is **physical insight and intuition**

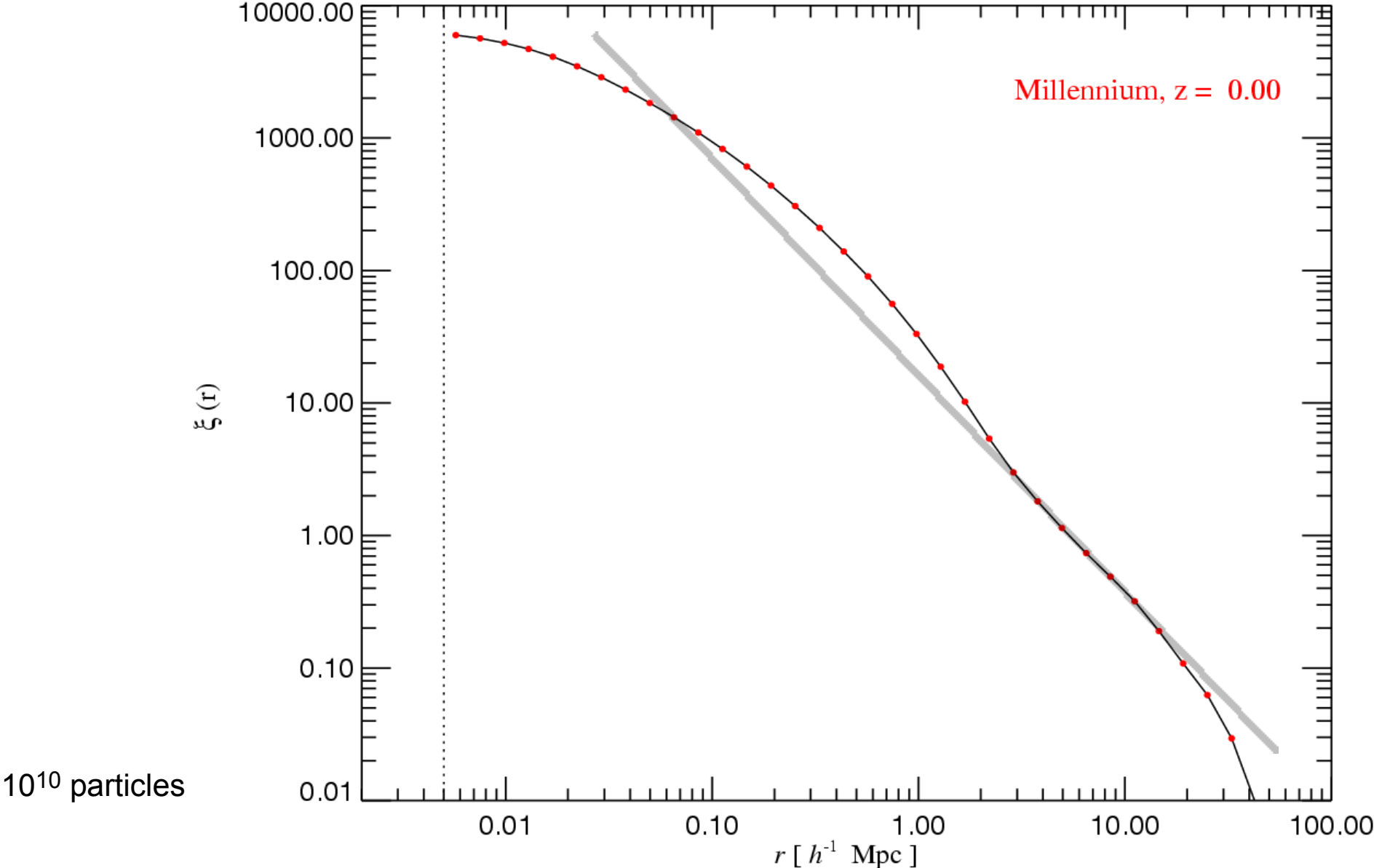
DAVIS, EFSTATHIOU, FRENK & WHITE (1985 !)

32³ particles – the first generation of CDM simulations



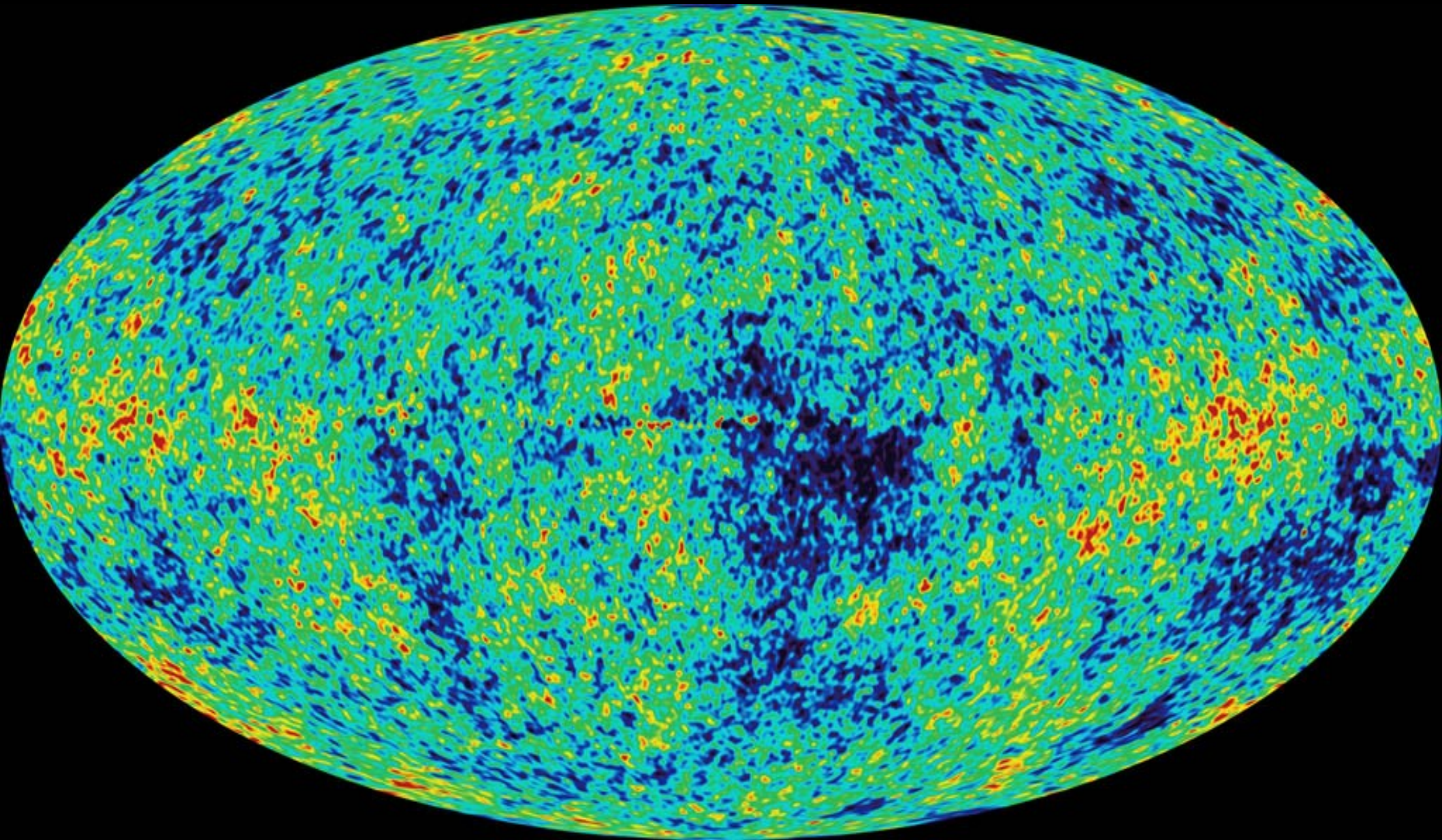
In modern simulations, the same dark matter autocorrelation function is measured, but more accurately

DARK MATTER TWO-POINT FUNCTION



The initial conditions for cosmic structure formation are directly observable

THE MICROWAVE SKY



WMAP Science Team (2003, 2006, 2008)

If the initial fluctuations are a Gaussian random field, we only need to know the power spectrum and the cosmological parameters to describe the ICs

DIFFERENT PROBES OF THE MASS POWER SPECTRUM

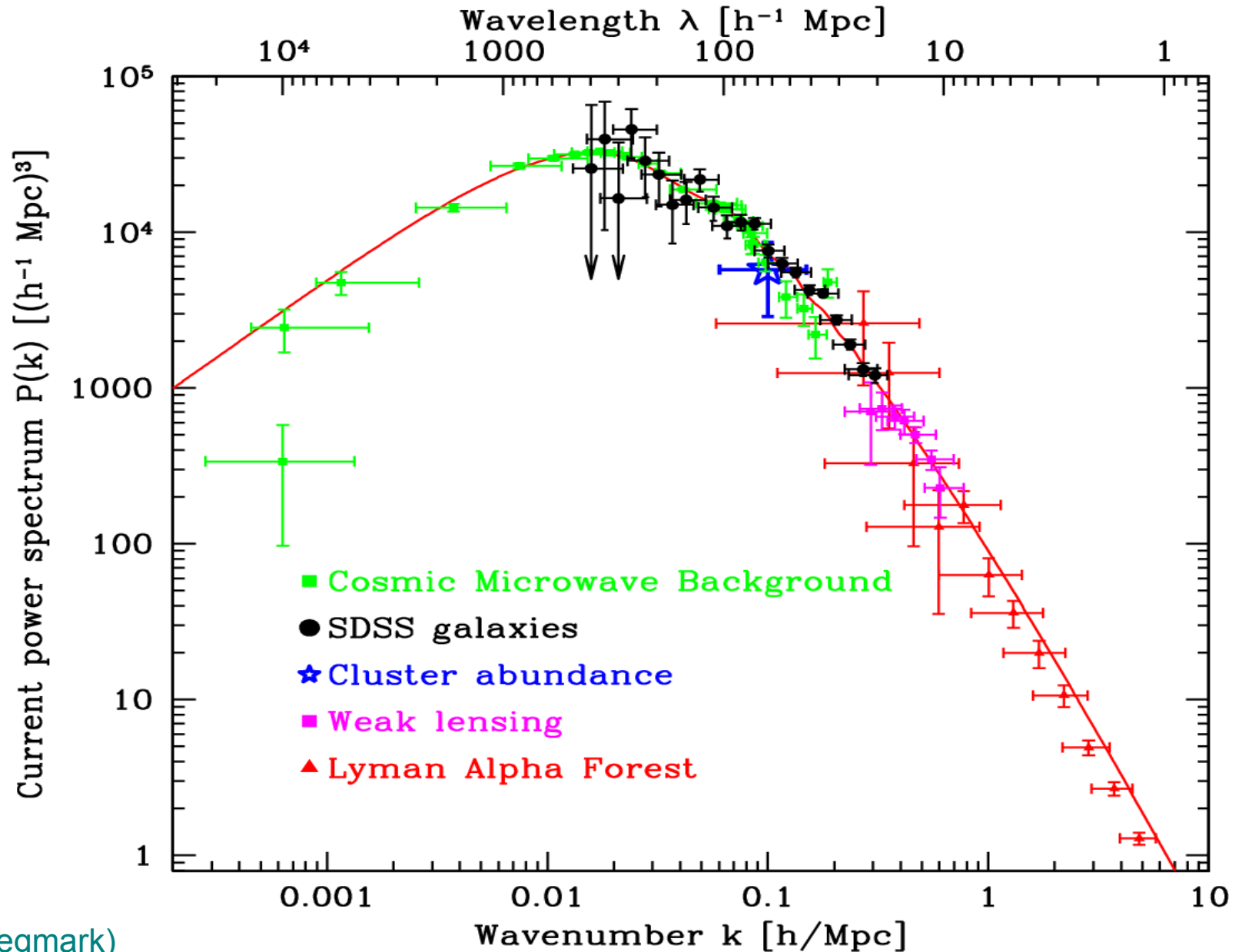
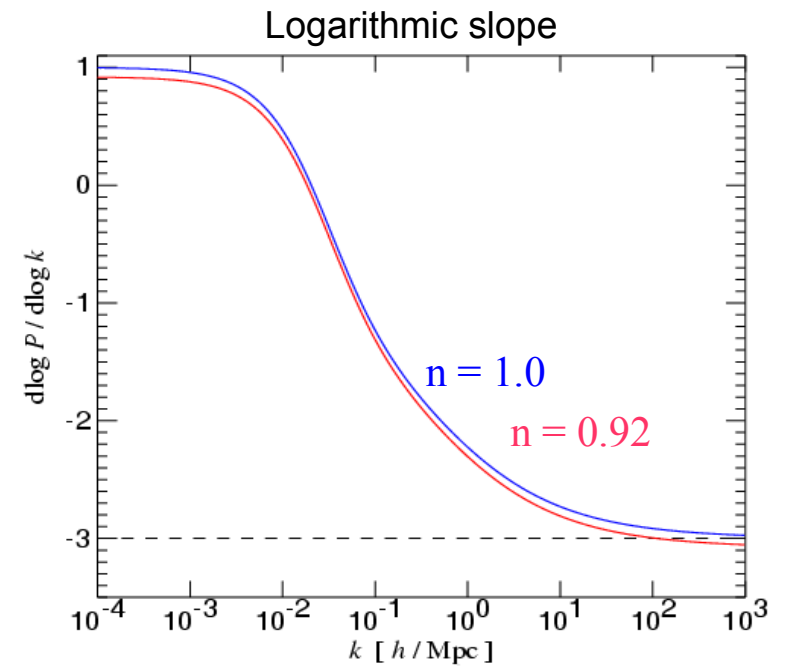
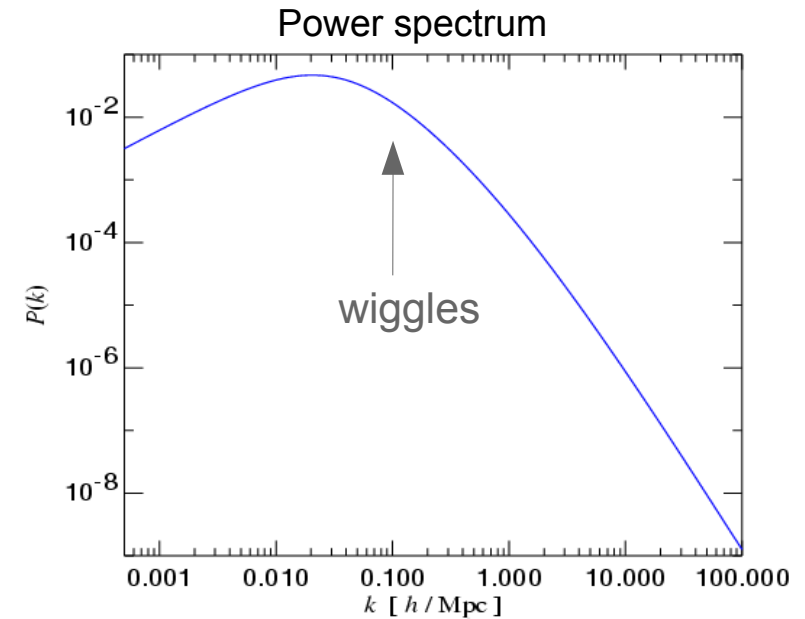
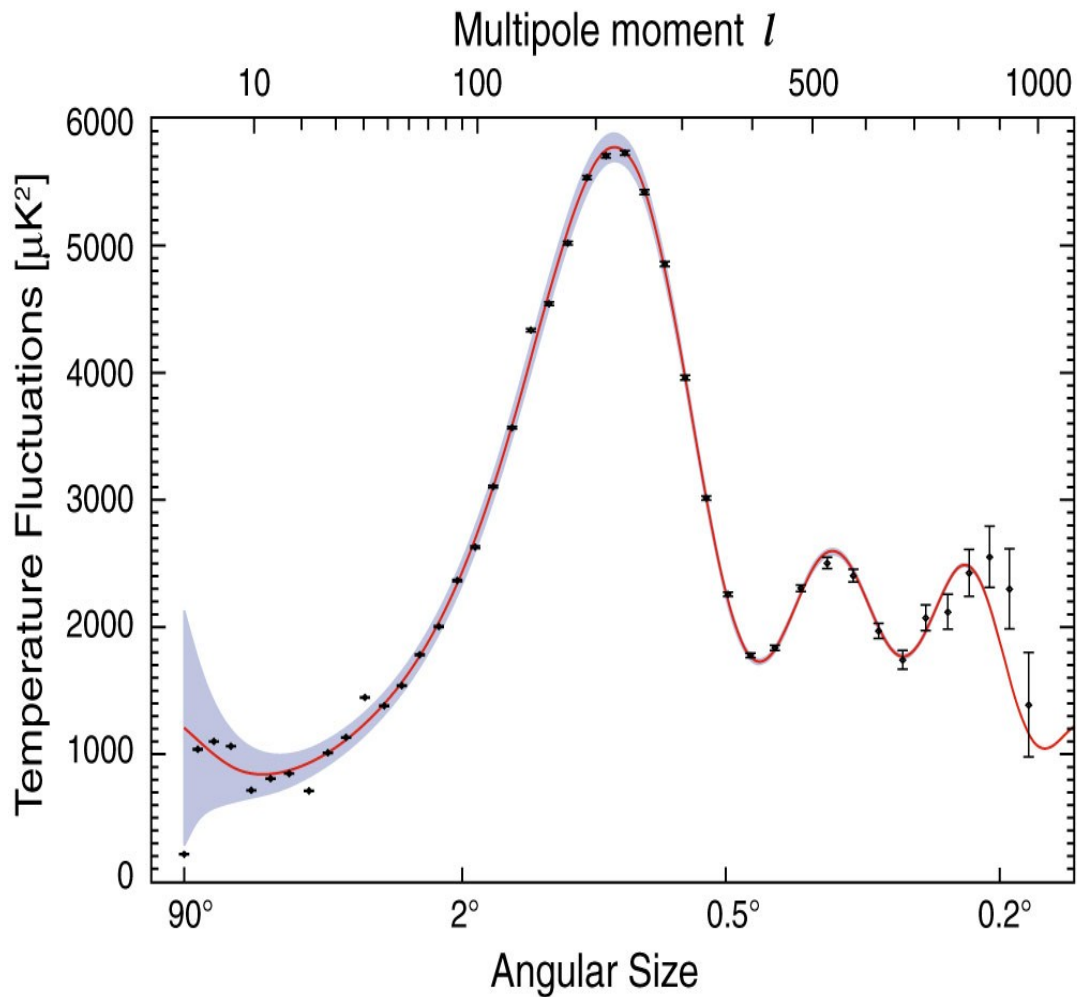


(figure from Max Tegmark)

The linear theory power spectrum can be computed accurately

THE LINEAR POWER SPECTRUM



To determine the power spectrum amplitude, we normalize the spectrum to observations of clustering (usually galaxy clusters)

FILTERED DENSITY FIELD AND THE NORMALIZATION OF THE POWER SPECTRUM

The filtered density field:
$$\sigma^2(M, z) = D^2(z) \int_0^\infty \frac{dk}{2\pi^2} k^2 P(k) \left[\frac{3j_1(kR)}{kR} \right]^2$$

Observational input:
$$\sigma_8 = 0.74 - 0.9 \quad R = 8 h^{-1} \text{Mpc}$$

Extrapolate back to the starting redshift with the growth factor $D(z)$

This depends on cosmology.

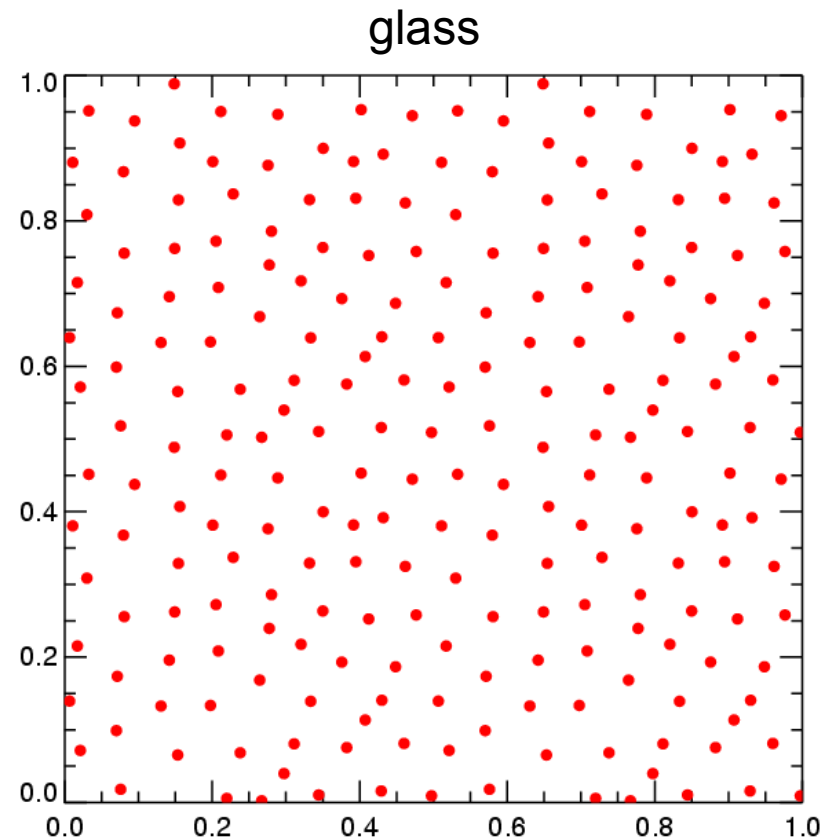
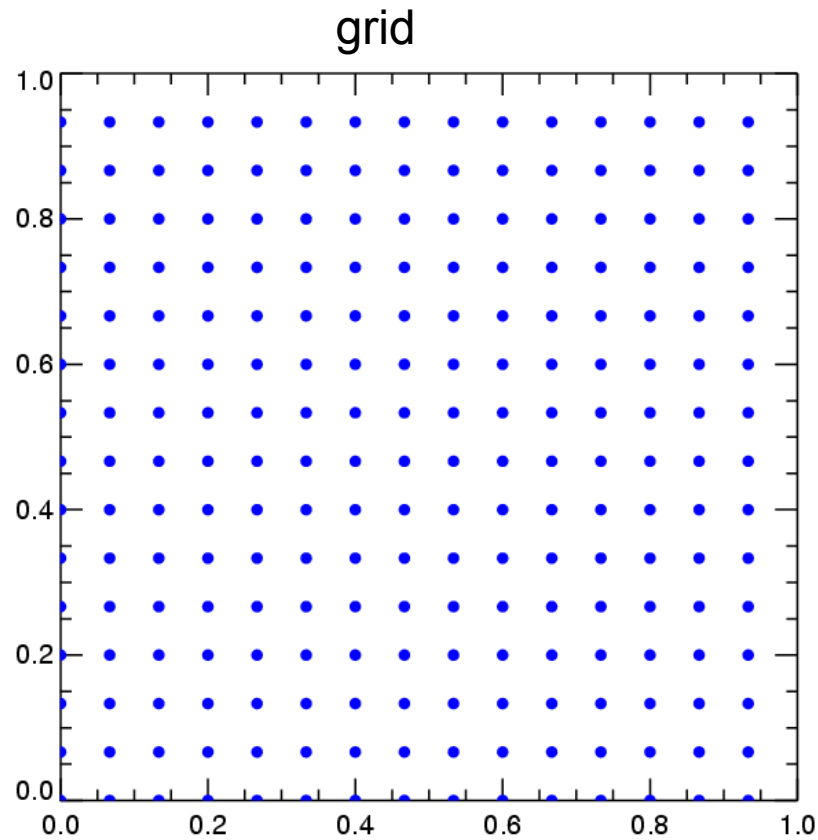
—————▶ fluctuation spectrum of initial conditions fully specified.

Aside:
$$P(k) \propto k^n \quad \rightarrow \quad \sigma^2(M) \propto M^{-(n+3)/3}$$

- Close to the critical slope, halos on very different mass scales form nearly simultaneously
- The multiplicity function of halos becomes essentially flat

To create a realization of the perturbation spectrum, a model for an unperturbed density field is needed

GLASS OR CARTESIAN GRID



For CDM, the initial velocity dispersion is negligibly small.

But there is a mean streaming velocity, which we need to imprint in initial conditions.

Using the Zeldovich approximation, density fluctuations are converted to displacements of the unperturbed particle load

SETTING INITIAL DISPLACEMENTS AND VELOCITIES

Particle displacements: $\mathbf{d}_i(t) = \mathbf{x}_i(t) - \mathbf{q}_i$

Density change due to displacements:

$$\rho(\mathbf{x}) = \frac{\rho_0}{\left| \frac{\partial \mathbf{x}}{\partial \mathbf{q}} \right|} = \frac{\rho_0}{\left| \delta_{ij} + \frac{\partial \mathbf{d}}{\partial \mathbf{q}} \right|}$$

For small displacements:

$$\left| \delta_{ij} + \frac{\partial \mathbf{d}}{\partial \mathbf{q}} \right| \simeq 1 + \nabla_{\mathbf{q}} \cdot \mathbf{d}$$

Resulting density contrast:

$$\delta(\mathbf{x}) = \frac{\rho(\mathbf{x}) - \rho_0}{\rho_0} = -\nabla_{\mathbf{q}} \cdot \mathbf{d}$$

During linear growth:

$$\begin{aligned} \delta(t) &= D(t) \delta_0 \\ \mathbf{d}(t) &= D(t) \mathbf{d}_0 \end{aligned} \quad \longrightarrow \quad \dot{\mathbf{x}} = \dot{\mathbf{d}} = \dot{a} \frac{dD}{da} \mathbf{d}_0 = \frac{\dot{a}}{a} \frac{a}{D} \frac{dD}{da} \mathbf{d}$$

Particle velocities:

$$\dot{\mathbf{x}} = H(a) f(\Omega) \mathbf{d} \quad f(\Omega) = \frac{d \ln D}{d \ln a} \simeq \Omega^{0.6}$$

Note: Particles move on straight lines in the Zeldovich approximation.

Displacement field:

$$\nabla^2 \phi = \delta \quad \mathbf{d} = -\nabla \phi$$

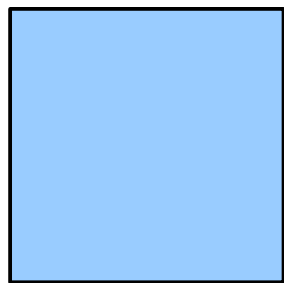
Fourier realization:

$$\phi_{\mathbf{k}} = -\frac{1}{k^2} \delta_{\mathbf{k}} \quad \mathbf{d}_{\mathbf{k}} = -i\mathbf{k} \phi_{\mathbf{k}} = \frac{i\mathbf{k}}{k^2} \delta_{\mathbf{k}} \quad \mathbf{d}_{\mathbf{k}} = -\nabla \phi = \sum_{\mathbf{k}} \frac{i\mathbf{k} \delta_{\mathbf{k}}}{k^2} \exp(i\mathbf{k}\mathbf{x})$$

One can assign random amplitudes and phases for individual modes in Fourier space

GENERATING THE FLUCTUATIONS IN K-SPACE

Simulation box



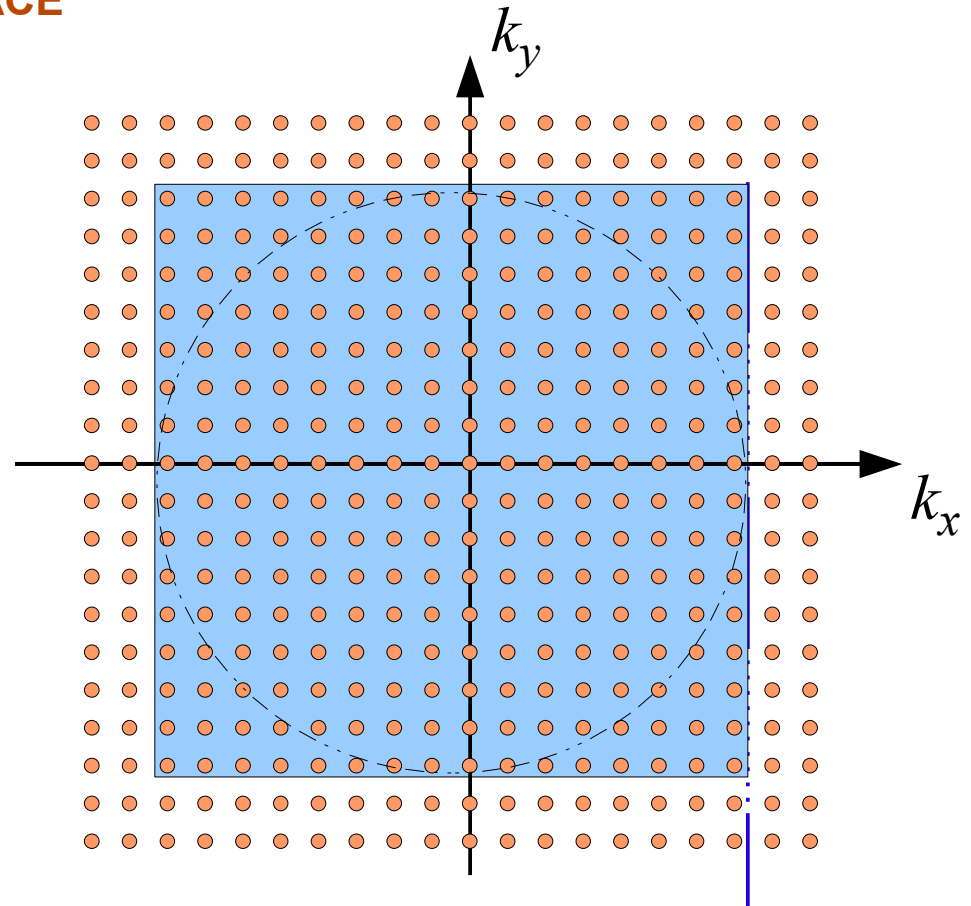
sampled with N^2 points

L

$$\delta_{\mathbf{k}} = B_{\mathbf{k}} \exp^{i\phi_{\mathbf{k}}}$$

For each mode, draw a random phase, and an amplitude from a Rayleigh distribution.

$$\langle \delta_{\mathbf{k}}^2 \rangle = P(k)$$



$$k_{\text{Nyquist}} = \frac{2\pi}{L} \frac{N}{2}$$

Calculating gravitational forces

Direct summation calculates the gravitational field **exactly**

FORCE ACCURACY IN COLLISIONLESS SIMULATIONS

Direct summation approach:

$$\ddot{\mathbf{x}}_i = -\nabla_i \Phi(\mathbf{x}_i)$$

$$\Phi(\mathbf{x}) = -G \sum_{j=1}^N \frac{m_j}{[(\mathbf{x} - \mathbf{x}_j)^2 + \epsilon^2]^{1/2}}$$

N^2 complexity

Are *approximate* force calculations sufficient?

Yes, provided the force errors are random and small enough.

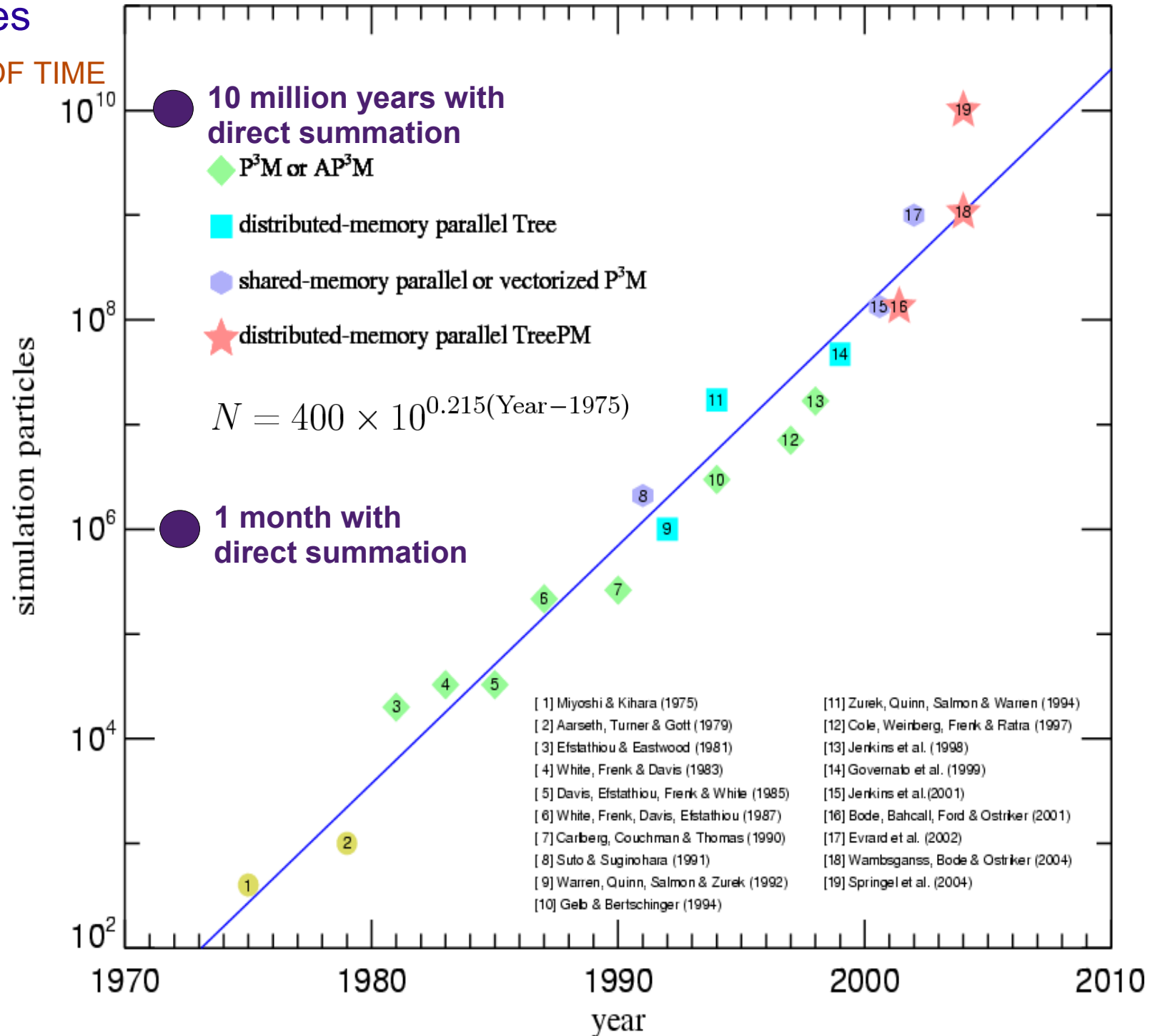
Since the N-body force field is noisy anyway, small random errors will only insignificantly reduce the relaxation time.

Systematic errors in the force, or error correlations are however very problematic.

Cosmological N-body simulations have grown rapidly in size over the last three decades

"N" AS A FUNCTION OF TIME

- ▶ Computers double their speed every 18 months (Moore's law)
- ▶ N-body simulations have doubled their size every 16-17 months
- ▶ Recently, growth has accelerated further.
The Millennium Run should have become possible in 2010 – we it was done in 2004.
It took ~350000 CPU hours, about a month on 512 cores.



The particle mesh (PM) force calculation

The particle-mesh method

Poisson's equation can be solved in real-space by a convolution of the density field with a Green's function.

$$\Phi(\mathbf{x}) = \int g(\mathbf{x} - \mathbf{x}') \rho(\mathbf{x}) d\mathbf{x}'$$

Example for
vacuum boundaries:

$$\Phi(\mathbf{x}) = -G \int \frac{\rho(\mathbf{x})}{|\mathbf{x} - \mathbf{x}'|} d\mathbf{x}' \quad g(\mathbf{x}) = -\frac{G}{|\mathbf{x}|}$$

In Fourier-space, the convolution becomes a simple multiplication!

$$\hat{\Phi}(\mathbf{k}) = \hat{g}(\mathbf{k}) \cdot \hat{\rho}(\mathbf{k})$$

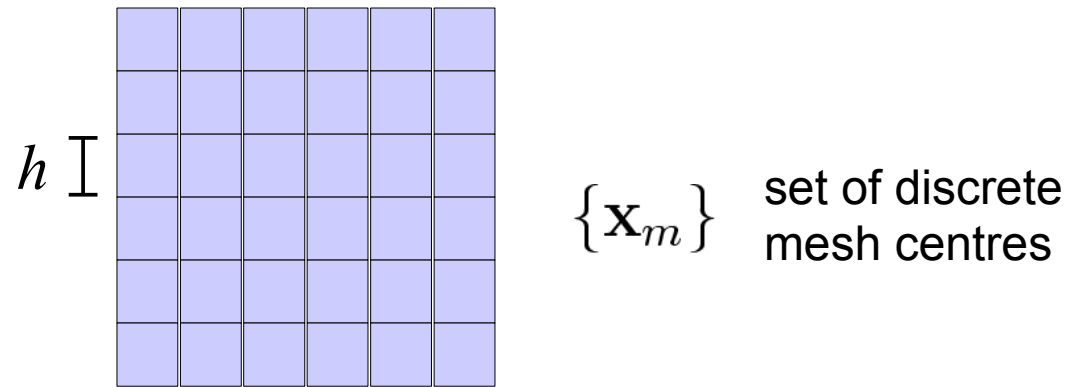
—► **Solve the potential in these steps:**

- (1) FFT forward of the density field
- (2) Multiplication with the Green's function
- (3) FFT backwards to obtain potential

The four steps of the PM algorithm

- (a) Density assignment
- (b) Computation of the potential
- (c) Determination of the force field
- (d) Assignment of forces to particles

Density assignment



Give particles a “shape” $S(\mathbf{x})$. Then to each mesh cell, we assign the fraction of mass that falls into this cell. The overlap for a cell is given by:

$$W(\mathbf{x}_m - \mathbf{x}_i) = \int_{\mathbf{x}_m - \frac{h}{2}}^{\mathbf{x}_m + \frac{h}{2}} S(\mathbf{x}' - \mathbf{x}_i) d\mathbf{x}' = \int \Pi \left(\frac{\mathbf{x}' - \mathbf{x}_m}{h} \right) S(\mathbf{x}' - \mathbf{x}_i) d\mathbf{x}'$$

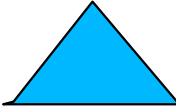
The assignment function is hence the convolution:

$$W(\mathbf{x}) = \Pi \left(\frac{\mathbf{x}}{h} \right) \star S(\mathbf{x}) \quad \text{where} \quad \Pi(x) = \begin{cases} 1 & \text{for } |x| \leq \frac{1}{2} \\ 0 & \text{otherwise} \end{cases}$$

The density on the mesh is then a sum over the contributions of each particle as given by the assignment function:

$$\rho(\mathbf{x}_m) = \frac{1}{h^3} \sum_{i=1}^N m_i W(\mathbf{x}_i - \mathbf{x}_m)$$

Commonly used particle shape functions and assignment schemes

Name	Shape function $S(\mathbf{x})$	# of cells involved	Properties of force
NGP Nearest grid point	 $\delta(\mathbf{x})$	$1^3 = 1$	piecewise constant in cells
CIC Clouds in cells	 $\frac{1}{h^3} \Pi\left(\frac{\mathbf{x}}{h}\right) \star \delta(\mathbf{x})$	$2^3 = 8$	piecewise linear, continuous
TSC Triangular shaped clouds	 $\frac{1}{h^3} \Pi\left(\frac{\mathbf{x}}{h}\right) \star \frac{1}{h^3} \Pi\left(\frac{\mathbf{x}}{h}\right)$	$3^3 = 27$	continuous first derivative

Note: For interpolation of the grid to obtain the forces, the same assignment function needs to be used to ensure momentum conservation. (In the CIC case, this is identical to tri-linear interpolation.)

Finite differencing of the potential to get the force field

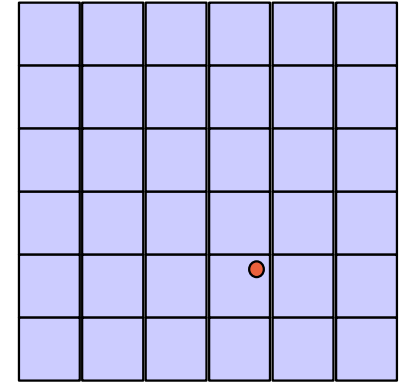
Approximate the force field $\mathbf{f} = -\nabla\Phi$ with finite differencing

2nd order accurate scheme:

$$f_{i,j,k}^{(x)} = -\frac{\Phi_{i+1,j,k} - \Phi_{i-1,j,k}}{2h}$$

4th order accurate scheme:

$$f_{i,j,k}^{(x)} = -\frac{4}{3} \frac{\Phi_{i+1,j,k} - \Phi_{i-1,j,k}}{2h} + \frac{1}{3} \frac{\Phi_{i+2,j,k} - \Phi_{i-2,j,k}}{4h}$$



Interpolating the mesh-forces to the particle locations

$$F(\mathbf{x}_i) = \sum_{\mathbf{m}} W(\mathbf{x}_i - \mathbf{x}_{\mathbf{m}}) f_{\mathbf{m}}$$

The interpolation kernel needs to be the same one used for mass-assignment to ensure force anti-symmetry.

Advantages and disadvantages of the PM-scheme

Pros: **SPEED** and simplicity

- Cons:**
- Spatial force resolution limited to mesh size.
 - Force errors somewhat anisotropic on the scale of the cell size



serious problem:

cosmological simulations cluster strongly and have a very large dynamic range

cannot make the PM-mesh fine enough and resolve internal structure of halos as well as large cosmological scales



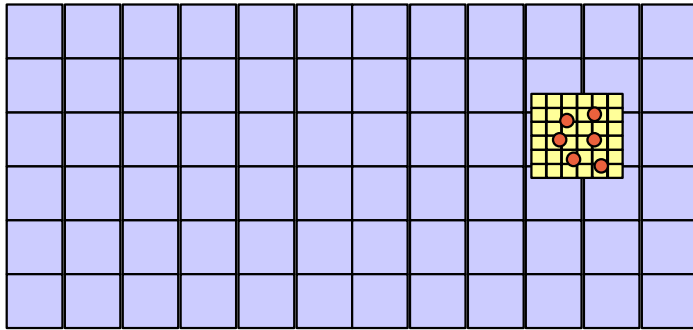
we need a method to increase the **dynamic range** available in the force calculation

Particle-Particle PM schemes (P³M)

Idea: Supplement the PM force with a direct summation short-range force at the scale of the mesh cells. The particles in cells are linked together by a chaining list.

Offers much higher dynamic range, but becomes slow when clustering sets in.

In AP³M, mesh-refinements are placed on clustered regions



Can avoid clustering slow-down, but has higher complexity and ambiguities in mesh placement

Codes that use AP³M: **HYDRA** (Couchman)

Iterative Poisson solvers can determine the potential directly on a (hierarchical grid)

Idea: Start with a trial potential and then iteratively relax the solution by updating with a finite difference approximation to the Laplacian.

$$\Phi'_{i,j,k} = \frac{1}{6} \left(\Phi_{i+1,j,k} + \Phi_{i-1,j,k} + \Phi_{i,j+1,k} + \Phi_{i,j-1,k} + \Phi_{i,j,k+1} + \Phi_{i,j,k-1} - 4\pi Gh^2 \rho_{i,j,k} \right)$$

This updating eliminates errors on the scale of a few grid cells rapidly, but longer-range fluctuations die out much more slowly.

In **multigrid methods**, a hierarchy of meshes is used to speed up convergence, resulting in a fast method that allows for locally varying resolution.

Examples for codes that use a real-space Poisson solver:

ART (Kravtsov)

MLAPM (Knebe)

On adaptive meshes, sometimes a combination of Fourier techniques and real-space solvers is used.

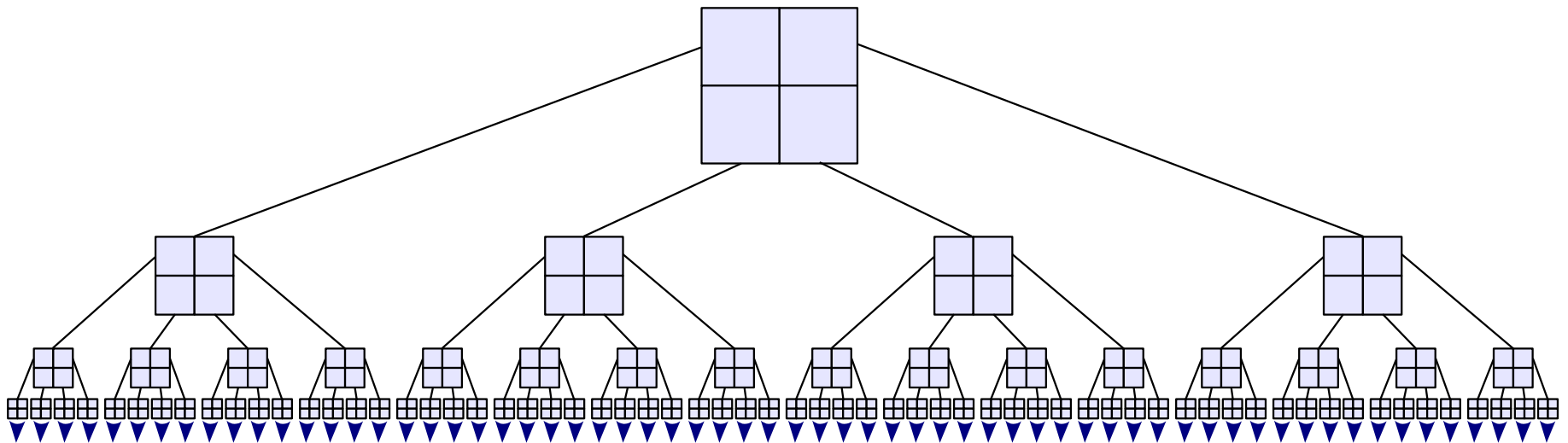
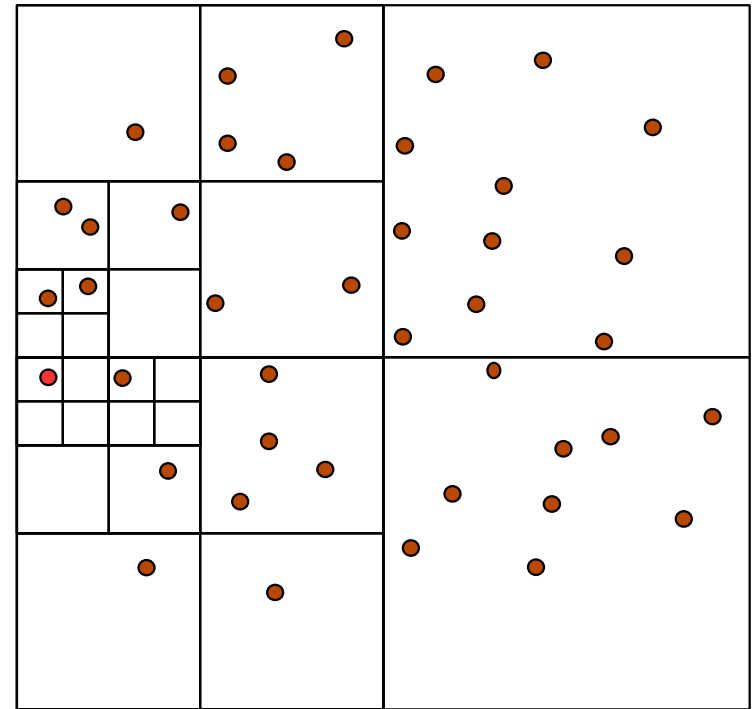
TREE algorithms

Tree algorithms approximate the force on a point with a multipole expansion

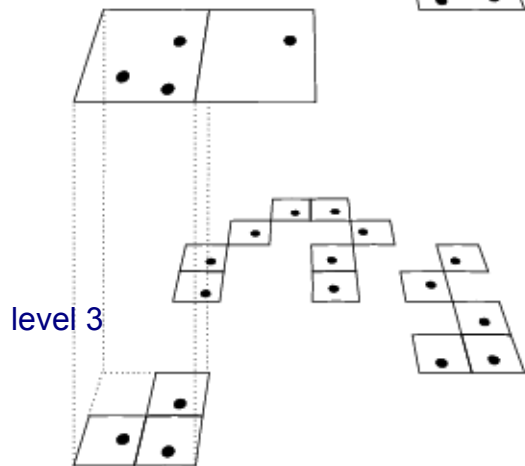
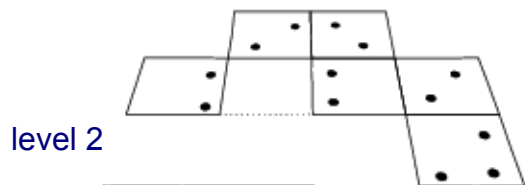
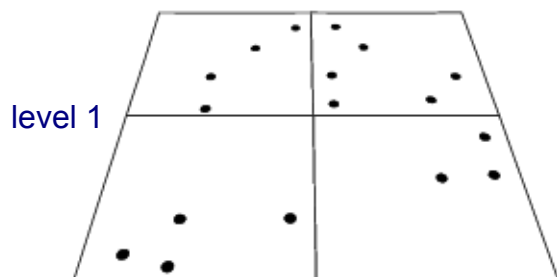
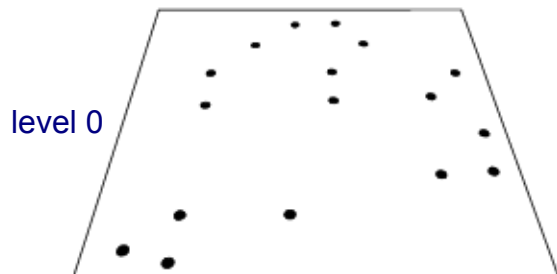
HIERARCHICAL TREE ALGORITHMS

Idea: Group distant particles together, and use their multipole expansion.

→ Only $\sim \log(N)$ force terms per particle.



Oct-tree in two dimensions



Tree algorithms

Idea: Use hierarchical multipole expansion to account for distant particle groups

$$\Phi(\mathbf{r}) = -G \sum_i \frac{m_i}{|\mathbf{r} - \mathbf{x}_i|}$$

We expand:

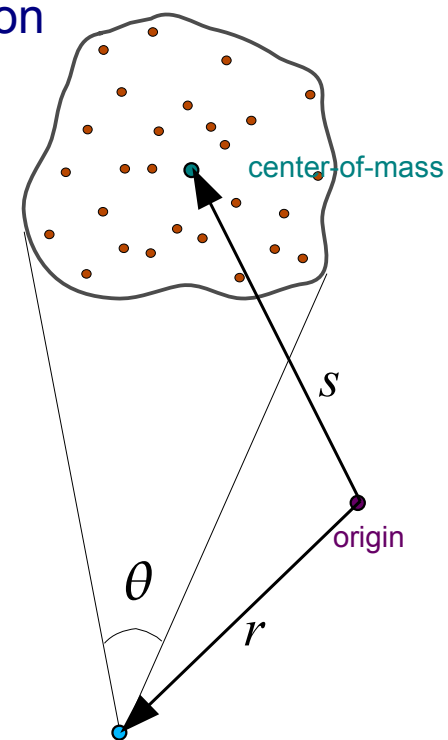
$$\frac{1}{|\mathbf{r} - \mathbf{x}_i|} = \frac{1}{|(\mathbf{r} - \mathbf{s}) - (\mathbf{x}_i - \mathbf{s})|}$$

for $|\mathbf{x}_i - \mathbf{s}| \ll |\mathbf{r} - \mathbf{s}|$ $\mathbf{y} \equiv \mathbf{r} - \mathbf{s}$

and obtain:

$$\frac{1}{|\mathbf{y} + \mathbf{s} - \mathbf{x}_i|} = \frac{1}{|\mathbf{y}|} - \frac{\mathbf{y} \cdot (\mathbf{s} - \mathbf{x}_i)}{|\mathbf{y}|^3} + \frac{1}{2} \frac{\mathbf{y}^T [3(\mathbf{s} - \mathbf{x}_i)(\mathbf{s} - \mathbf{x}_i)^T - \mathbf{I}(\mathbf{s} - \mathbf{x}_i)^2] \mathbf{y}}{|\mathbf{y}|^5} + \dots$$

the dipole term vanishes when summed over all particles in the group



The multipole moments are computed for each node of the tree

Monopole moment:

$$M = \sum_i m_i$$

Quadrupole tensor:

$$Q_{ij} = \sum_k m_k \left[3(\mathbf{x}_k - \mathbf{s})_i (\mathbf{x}_k - \mathbf{s})_j - \delta_{ij} (\mathbf{x}_k - \mathbf{s})^2 \right]$$

Resulting potential/force approximation:

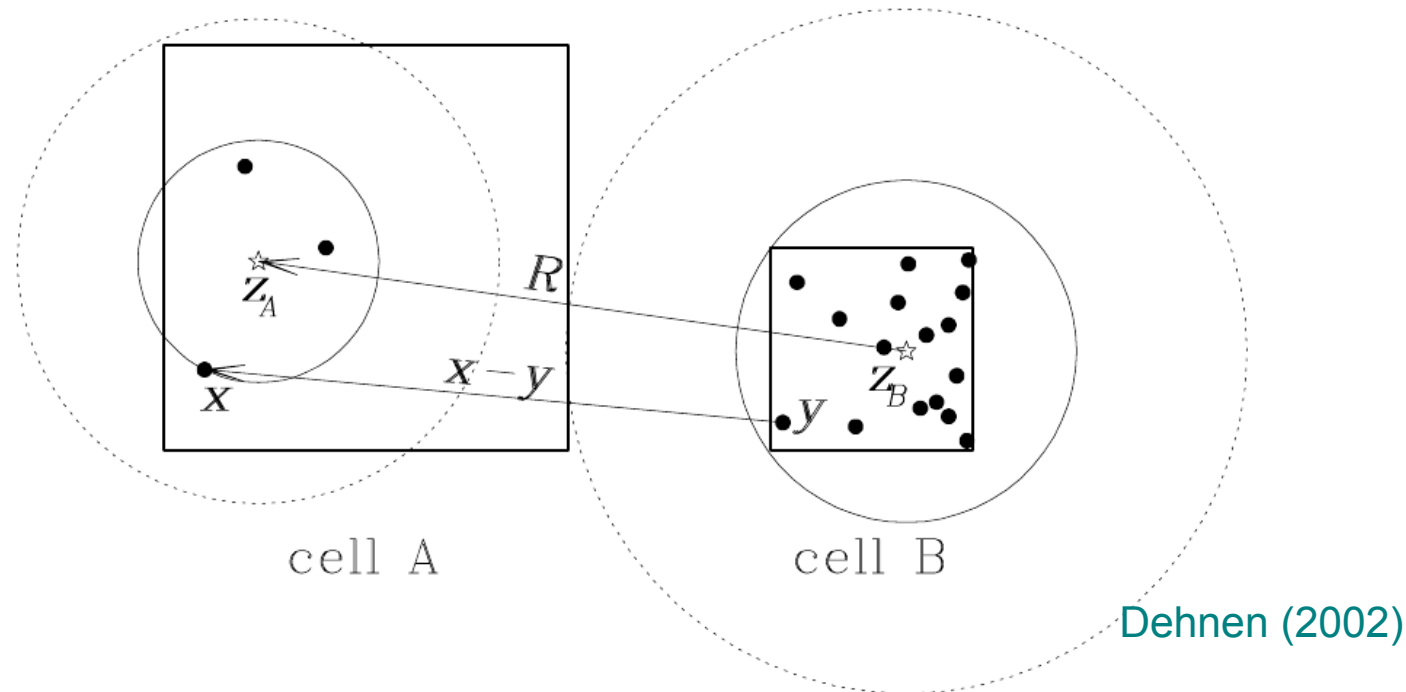
$$\Phi(\mathbf{r}) = -G \left[\frac{M}{|\mathbf{y}|} + \frac{1}{2} \frac{\mathbf{y}^T \mathbf{Q} \mathbf{y}}{|\mathbf{y}|^5} \right]$$

For a single force evaluation, not N single-particle forces need to be computed, but **only of order $\log(N)$ multipoles**, depending on the opening angle.

- The tree algorithm has no intrinsic restrictions for its dynamic range
- force accuracy can be conveniently adjusted to desired level
- the speed does depend only very weakly on clustering state
- geometrically flexible, allowing arbitrary geometries

The fast multipole method (FFM) generalizes the tree algorithm and expands the field symmetrically for each pair of interacting cells

Two interacting cells:



- Very fast
- Manifest momentum conservation

But:

- Doesn't work well with individual timesteps
- Difficult to parallelize for distributed memory machines

TreePM force calculation algorithm

Particularly at high redshift, it is expensive to obtain accurate forces with the tree-algorithm

THE TREE-PM FORCE SPLIT

Periodic peculiar potential

$$\nabla^2 \phi(\mathbf{x}) = 4\pi G[\rho(\mathbf{x}) - \bar{\rho}] = 4\pi G \sum_{\mathbf{n}} \sum_i m_i \left[\tilde{\delta}(\mathbf{x} - \mathbf{x}_i - \mathbf{n}L) - \frac{1}{L^3} \right]$$

Idea: Split the potential (of a single particle) in Fourier space into a long-range and a short-range part, and compute them separately with PM and TREE algorithms, respectively.

Poisson equation in Fourier space:

$$\phi_{\mathbf{k}} = -\frac{4\pi G}{\mathbf{k}^2} \rho_{\mathbf{k}} \quad (\mathbf{k} \neq 0)$$

$$\phi_{\mathbf{k}}^{\text{long}} = \phi_{\mathbf{k}} \exp(-\mathbf{k}^2 r_s^2)$$

Solve with PM-method

- CIC mass assignment
- FFT
- multiply with kernel
- FFT backwards
- Compute force with 4-point finite difference operator
- Interpolate forces to particle positions

$$\phi_{\mathbf{k}}^{\text{short}} = \phi_{\mathbf{k}} \left[1 - \exp(-\mathbf{k}^2 r_s^2) \right]$$

FFT to real space

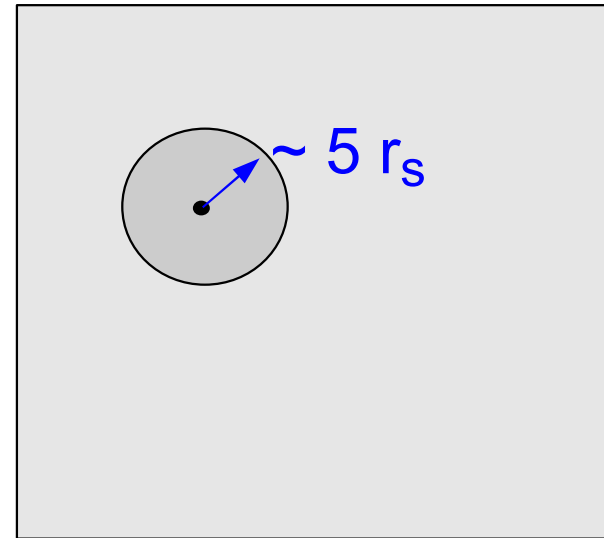
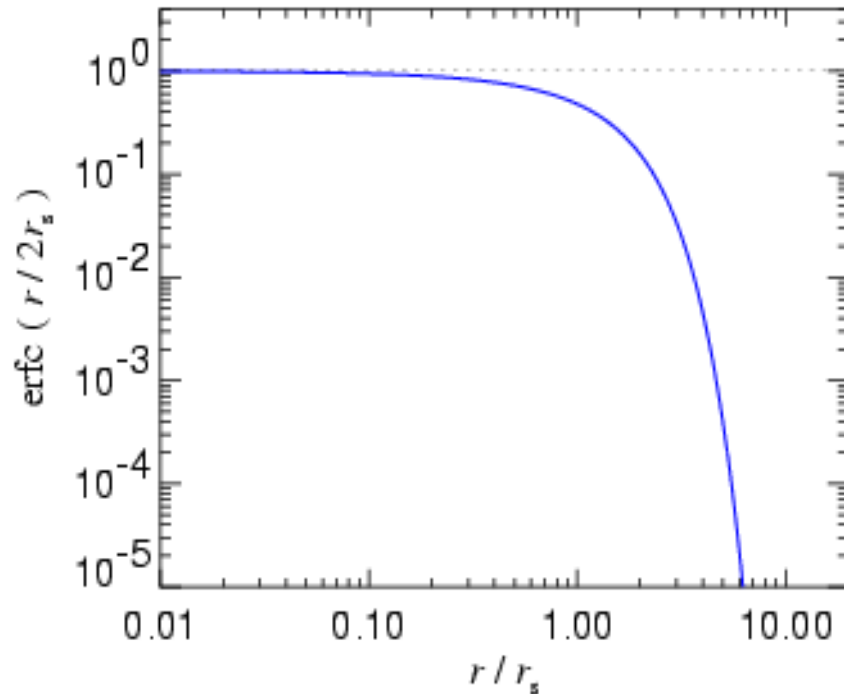
$$\phi(r) = -\frac{Gm}{r} \operatorname{erfc}\left(\frac{r}{2r_s}\right)$$

Solve in real space with TREE

In the TreePM algorithm, the tree has to be walked only locally

PERFORMANCE GAIN DUE TO LOCAL TREE WALK

$$\phi(r) = -\frac{Gm}{r} \operatorname{erfc}\left(\frac{r}{2r_s}\right)$$

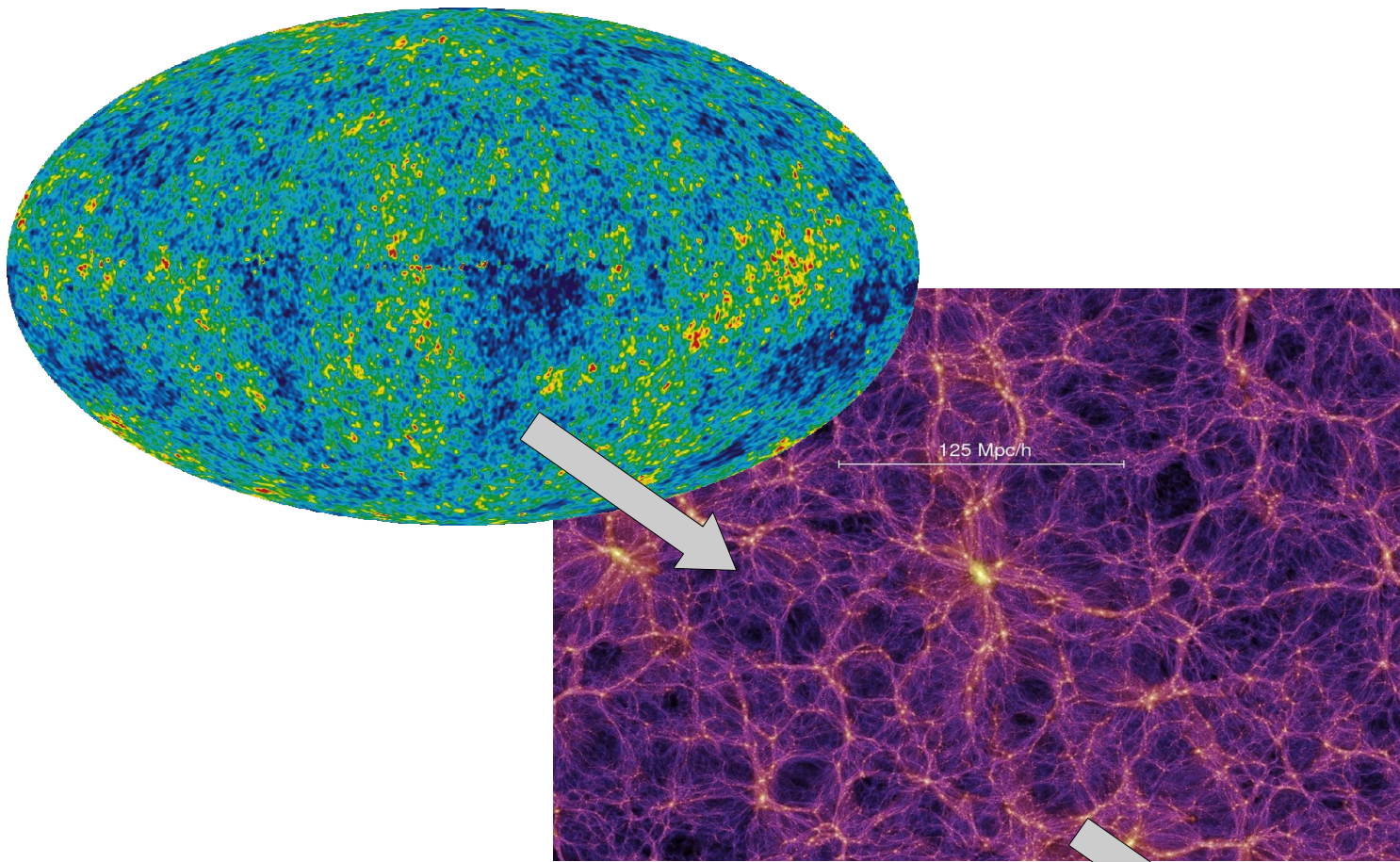


Advantages of TreePM include:

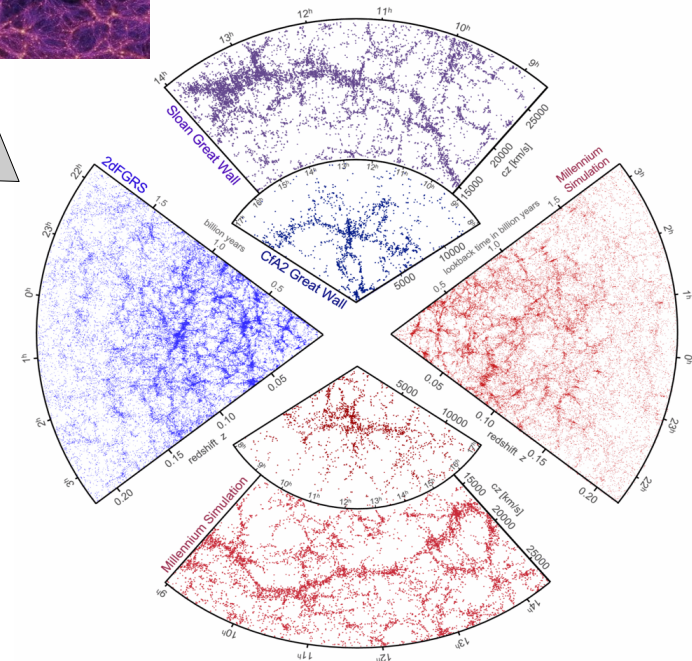
- Accurate and fast long-range force
- No force anisotropy
- Speed is largely insensitive to clustering (as for tree algorithm)
- No Ewald correction necessary for periodic boundary conditions

Using zero-padding and a different Greens-Function, the long-range force can also be computed for vacuum boundaries using the FFT.
(Implemented in Gadget-2)

Modelling the galaxy distribution



How do we get from the structure in the dark matter to the large-scale distribution of galaxies ?



Semi-analytic models are currently the most powerful technique to study **galaxy formation**

MOST IMPORTANT INPUT PHYSICS

Hierarchical growth of dark matter halos

→ *understood with high accuracy*

Radiative cooling of gas within halos (dissipation)

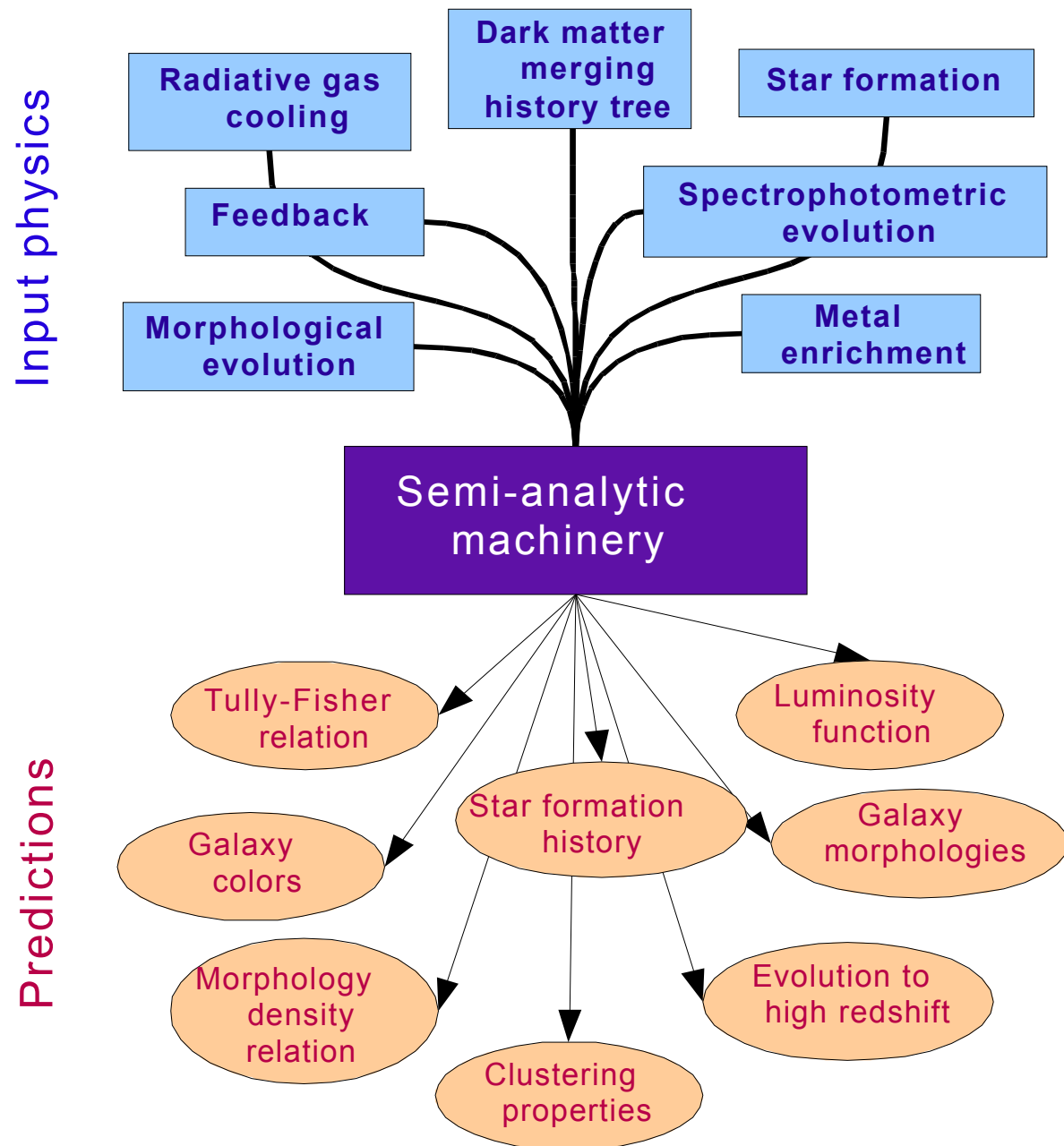
→ *in principle well within reach of current simulations, yet plagued with numerical difficulties*

Star formation and associated feedback processes

→ *highly uncertain physics, numerically extremely difficult*

Spectrophotometric modeling of stellar populations

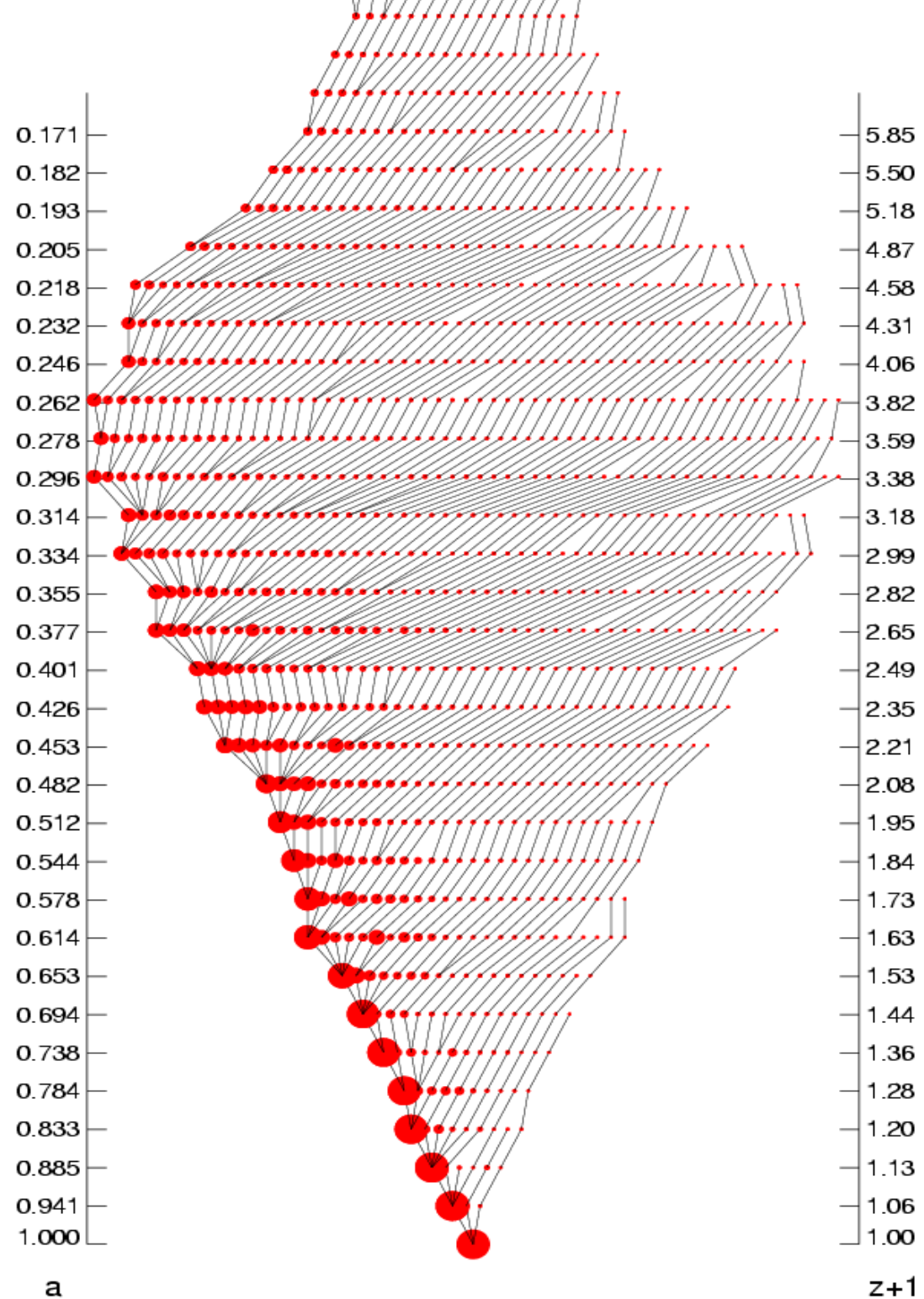
→ *some uncertainties, but no/small coupling to gas dynamics*



Analysis of many simulation outputs allows a measurement of the hierarchical build up of dark matter halos

FOLLOWING DARK MATTER IN TIME

Merger tree of a cluster
(only progenitors above a minimum mass are shown)

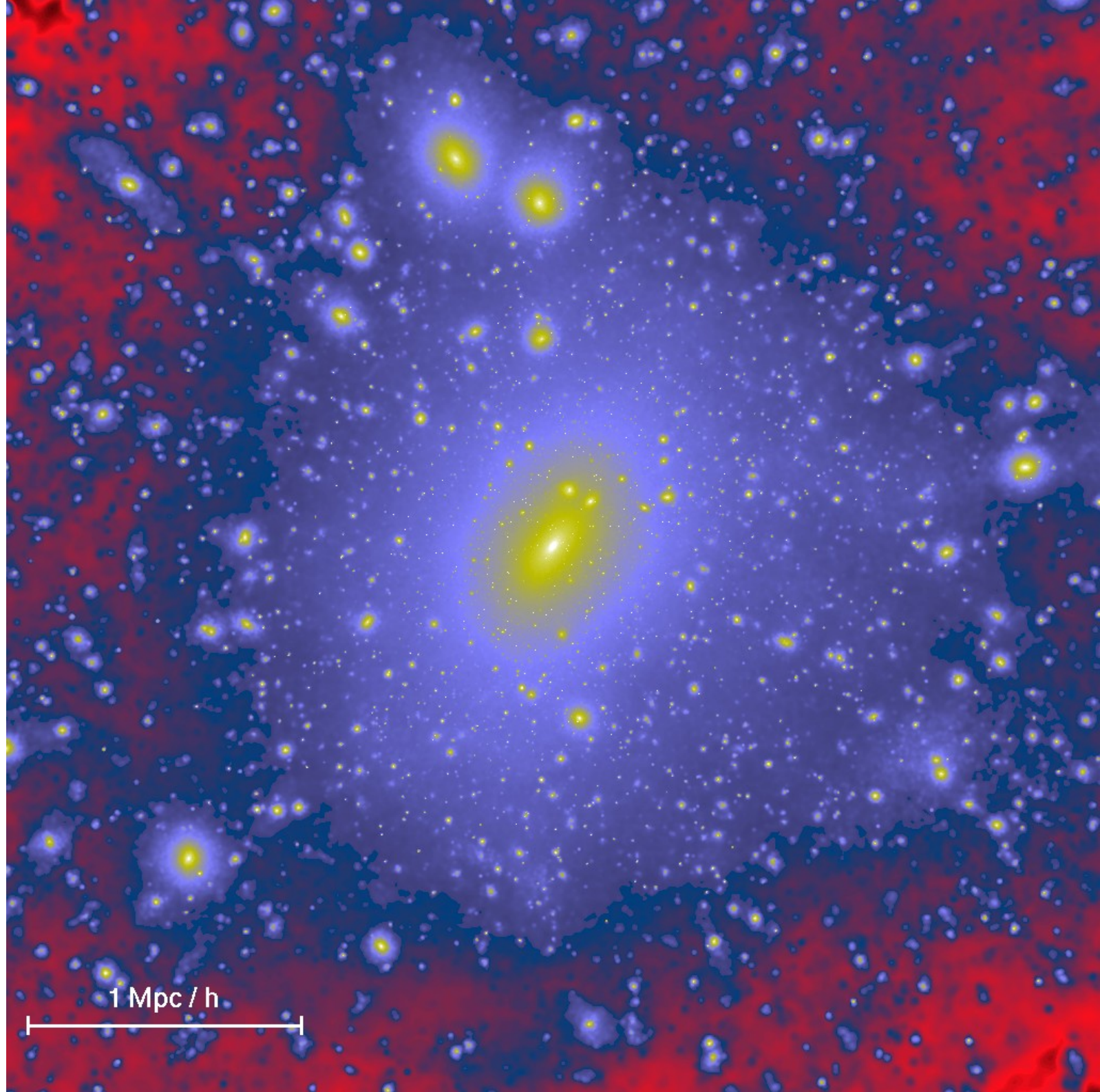


Halos formed in
high-resolution
simulations of
cold dark matter
show rich
substructure

SUBHALOS IN A RICH CLUSTER

~ 20 million
particles within
virial radius of
cluster

Springel, White,
Kauffmann,
Tormen (2000)



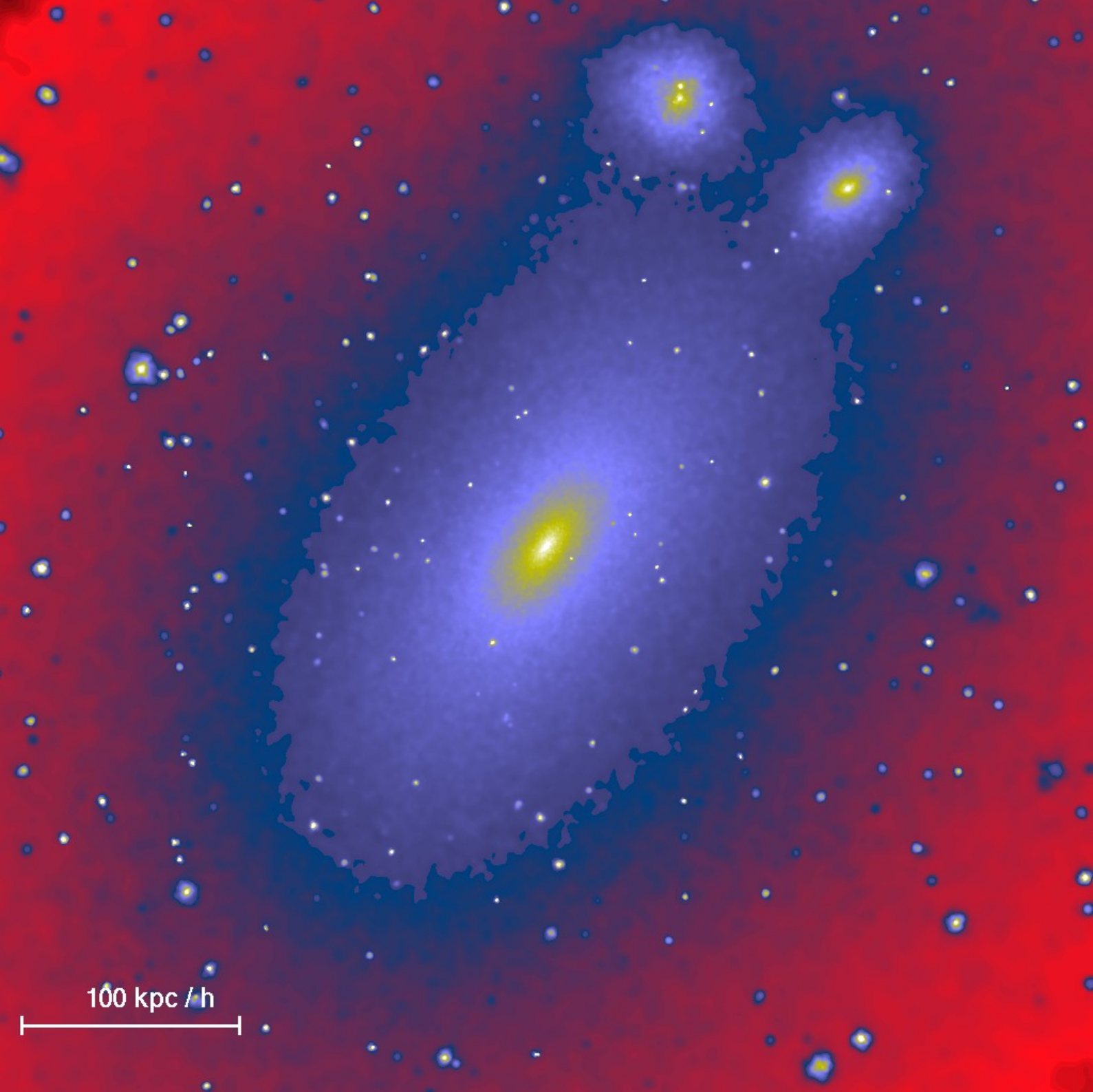
1 Mpc / h

Even in the central regions, substructures can still be found

SUBHALOS AROUND A CLUSTER CENTRE

~ 20 million particles within virial radius of cluster

Springel, White, Kauffmann, Tormen (2000)



100 kpc / h

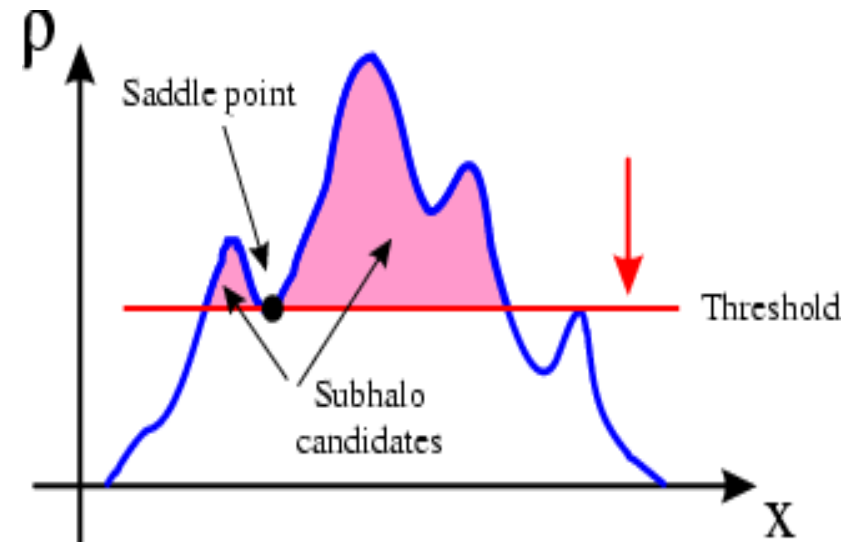
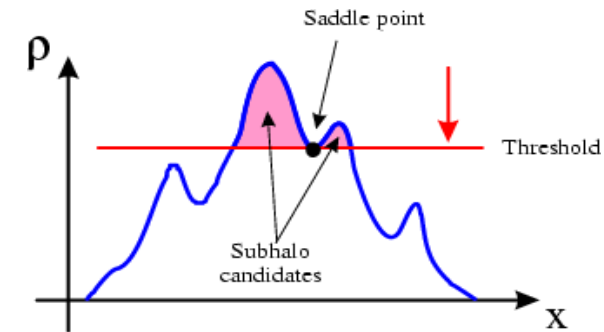
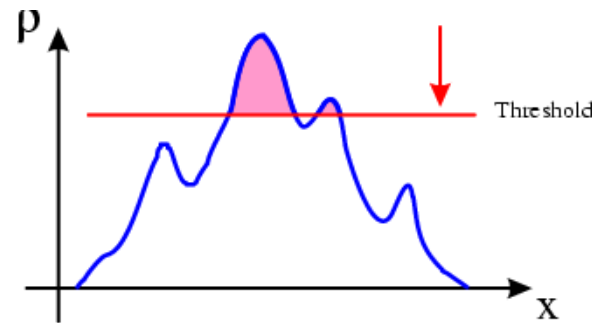
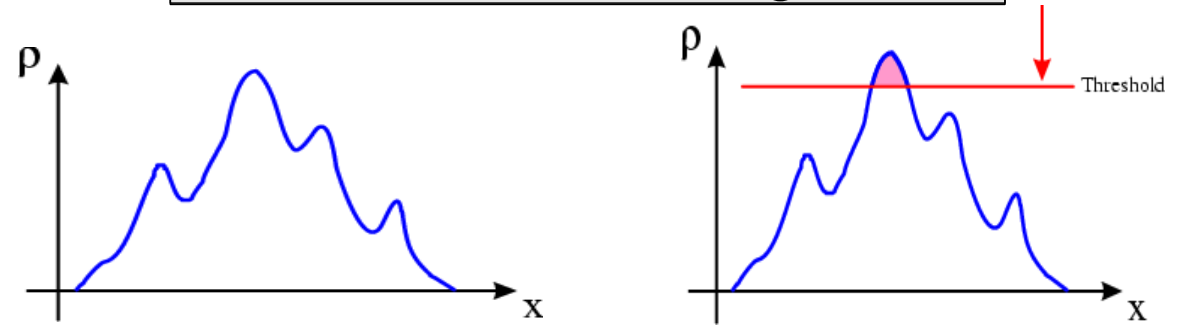
Finding dark matter satellites in simulations is a non-trivial task

AN ALGORITHMIC TECHNIQUES FOR SUBHALO IDENTIFICATION

SUBFIND

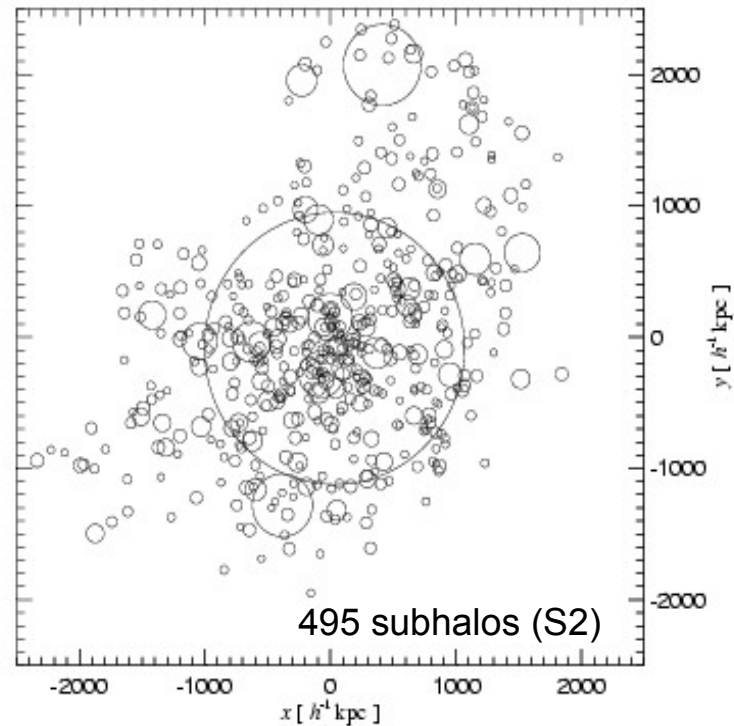
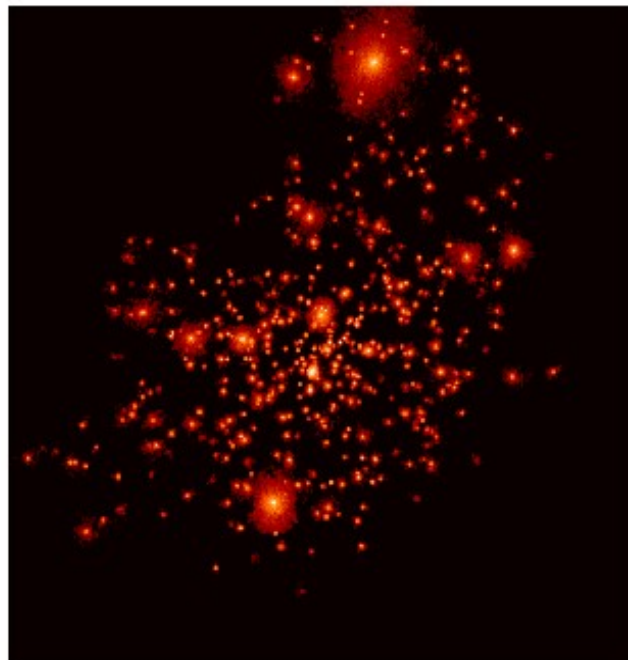
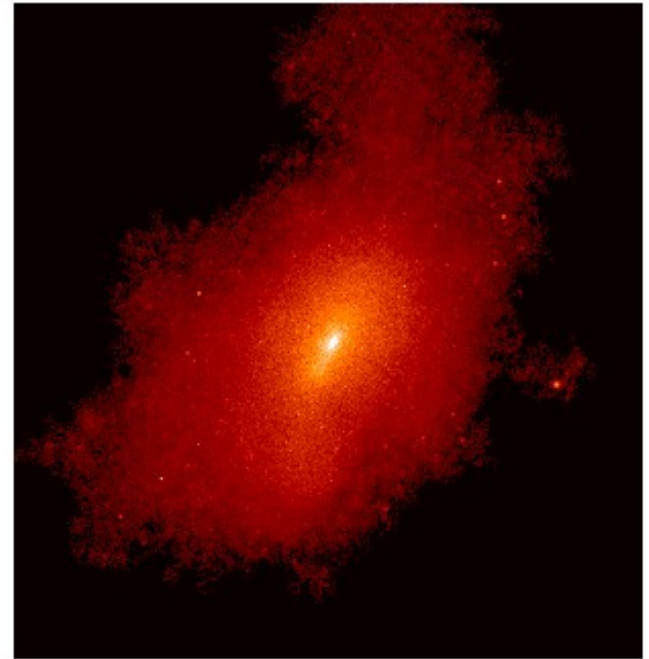
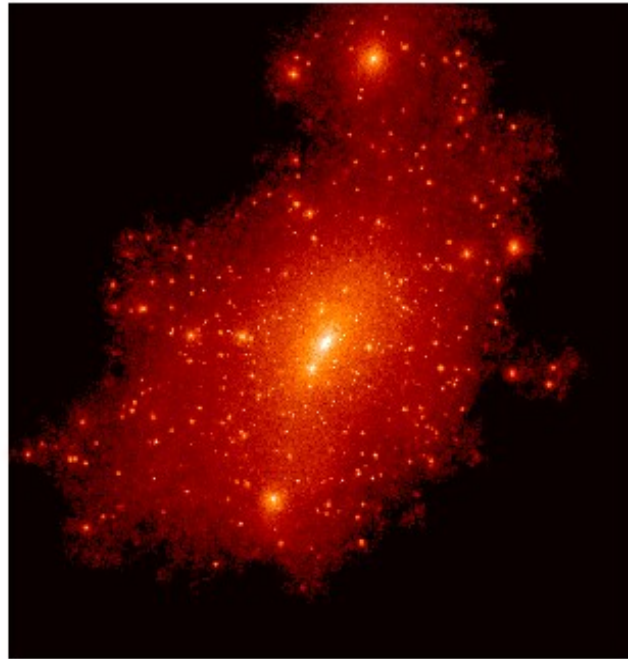
- (1) Estimate local DM density field
- (2) Find locally overdense regions with topological method
- (3) Subject each substructure candidate to a gravitational unbinding procedure

Subhalo finding



Halos formed in high-resolution simulations of cold dark matter show rich substructure

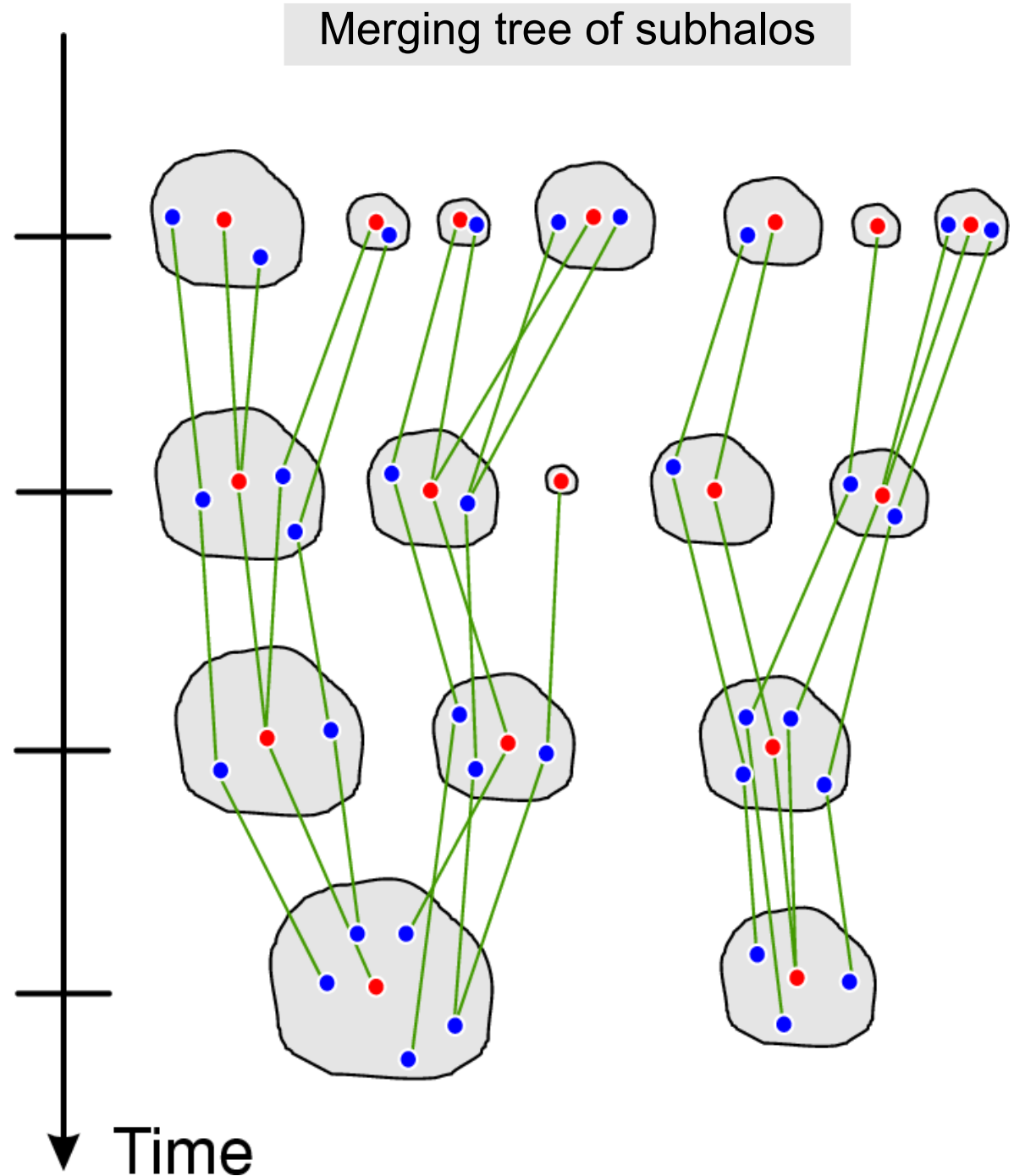
SUBHALOS IN THE S2 CLUSTER IDENTIFIED WITH SUBFIND



Tracking the fate of satellite galaxies in simulations is computationally and 'logistically' complicated

A SKETCH OF A SUBHALO MERGING TREE

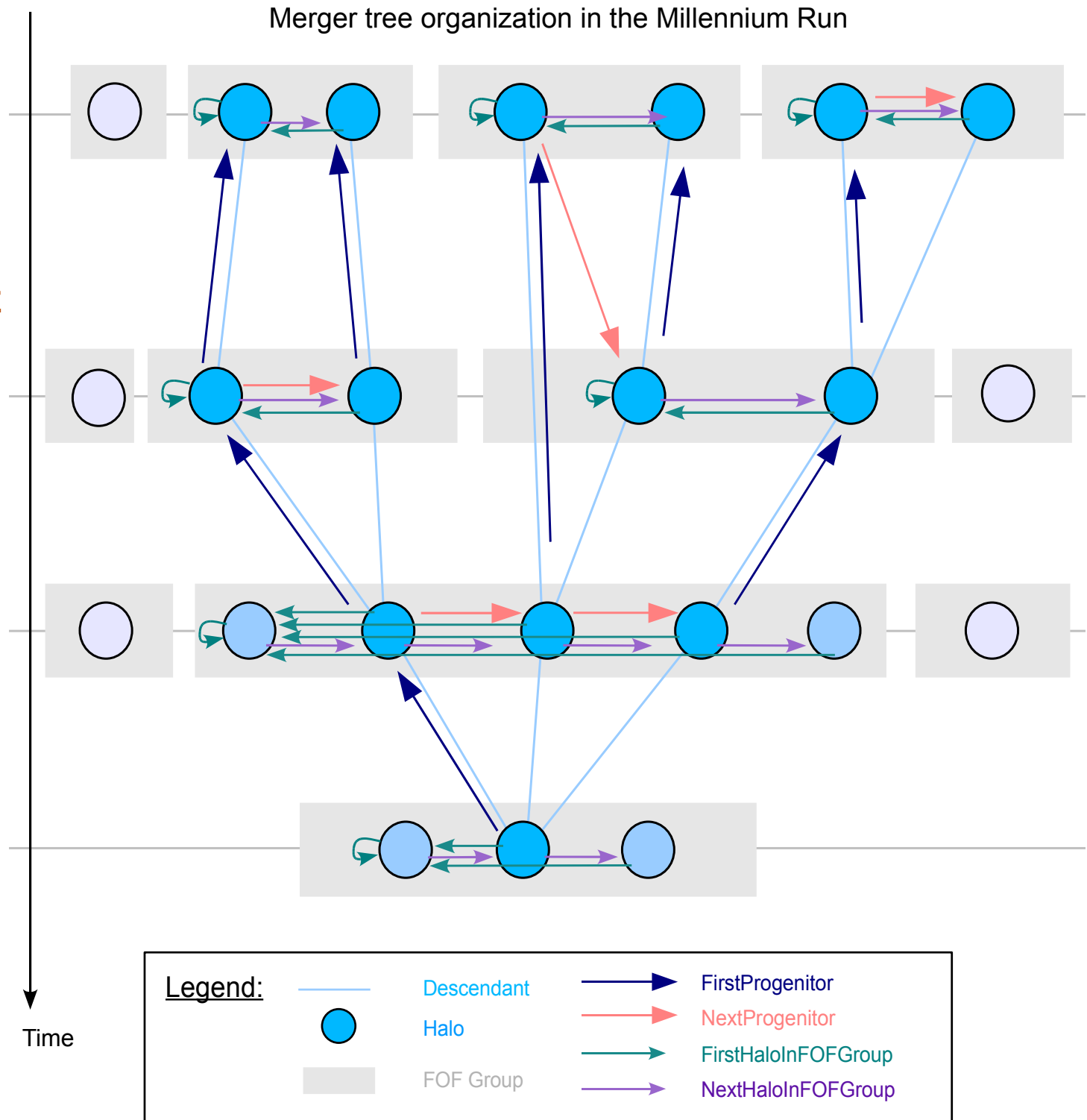
How do we manage to compute this for a simulation with more than 10^{10} particles, and more than 20 million halos?



The semi-analytic merger-tree in the Millennium Run connects about 800 million subhalos

SCHEMATIC MERGER TREE

- The trees are stored as self-contained objects, which are the input to the semi-analytic code
- Each tree corresponds to a FOF halo at $z=0$ (not always exactly)
- The collection of all trees (a whole forest of them) describes all the structures/galaxies in the simulated universe



Documentation

CREDITS/Acknowledgments

Registration

News

Public Databases

- DGalaxies
- DHalotrees
- MField
- millimil
- MMSnapshots
- MPAGalaxies
- MPAHaloTrees
- MPAMocks

Private (MyDB) Databases

- vspringel_db (rw) (context)



Welcome Volker Springel.

Streaming queries return unlimited number of rows in CSV format and are cancelled after 420 seconds.

Browser queries return maximum of 1000 rows in HTML format and are cancelled after 30 seconds.

```
select PROG.*
  from millimil..MPAHalo PROG,
       millimil..MPAHalo DES
 where DES.haloId = 1
       and PROG.haloId between DES.haloId and DES.lastprogenitorId
```

Query (stream)

Query (browse)

Help

Maximum number of rows to return to the query form:

Demo queries: click a button and the query will show in the query window.

Holding the mouse over the button will give a short explanation of the goal of the query. These queries are also available on [this page](#).

Mainly Halos:

Mainly Galaxies:

Metadata queries: The SQL statements under these buttons provide examples for querying and managing the state of a private database. Holding the mouse over the button will give a short explanation of the goal of the statement.